

SCALE EFFECTS ON HYBRID  
ROCKET ENGINE PERFORMANCE

By

Alexander Velliaris

Bachelor of Engineering, Ryerson University (2015)

A thesis

Presented to Ryerson University

In partial fulfillment of the  
Requirements for the degree of

Master of Applied Science

in the program of

Aerospace Engineering

Toronto, Ontario, Canada, 2017

©Alexander Velliaris 2017

## Author's Declaration

I hereby declare that I am the sole author of this thesis. This is a true copy of the thesis, including any required final revisions, as accepted by my examiners.

I authorize Ryerson University to lend this thesis to other institutions or individuals for the purpose of scholarly research.

I further authorize Ryerson University to reproduce this thesis by photocopying or by other means, in total or in part, at the request of other institutions or individuals for the purpose of scholarly research. I understand that my thesis may be made electronically available to the public.

# SCALE EFFECTS ON HYBRID ROCKET ENGINE PERFORMANCE

Alexander Velliaris

Master of Applied Science, Aerospace Engineering, Ryerson University  
(2017)

## Abstract

In the current study, the effects of scaling up a hybrid rocket engine (HRE) in size has on its performance is investigated. A HRE design from a past RU study is selected as the base model to be progressively increased in size while geometric scale is maintained, up to ten times the original's size. A computer program employing a quasi-steady convective heat feedback burn rate model is used to conduct simulated engine firings. One finding from this study is that the drop-off in performance for this engine, in going up in size, is not as much as expected. This can be attributed to a conservative oxidizer injection temperature setting in the model, and an oxidizer-fuel ratio mixture influence for this engine that is more impactful. The results presented here however do, to some degree, concur with established trends, with respect to thrust prediction, as the reference HRE is scaled up in size.

## Acknowledgements

First and foremost, I would like to thank my supervisor, Professor David Greatrix. Dr. Greatrix openly welcomed me into his team, and without his immeasurable knowledge and experience, this thesis would in no way have been possible. Advice, suggestions, and direction by Dr. Greatrix throughout my Master's program at Ryerson University were my priceless guidance and support. I would also like to acknowledge Dr. Greatrix's previous work on HRE regression rate and ballistics modelling, along with other past researchers at Ryerson University, as their work made mine possible.

And of course, I thank my mom, who has always been my guiding light and best friend...and who also put up with a sometimes stressed out graduate student. Thank you for always being there to encourage me.

Roger, who has always been by my side. Your support throughout my entire university adventure, and my life, will always be an inspiration for me to always try to live up to.

And, to my grandma, who may not be with us anymore, but who always encouraged me to pursue my education, dreams, and engineering goals. I wouldn't have gotten to where I am today without you, my second parent. Thanks grandma.

## Contents

Author's Declaration .....	ii
Abstract .....	iii
Acknowledgements .....	iv
List of Tables .....	vii
List of Figures .....	viii
List of Appendices .....	xi
Nomenclature .....	xii
1. Introduction .....	1
1.1 Some Background on Hybrid Rocket Engines .....	3
1.2 Objectives of this Study .....	5
2. Hybrid Rocket Engine Performance Modelling .....	6
2.1 Basics of Rocket Engine Performance .....	6
2.1.1 Impulse and Thrust .....	6
2.1.2 Hybrid Rocket Engines: Classical Regression Rate Models .....	9
2.1.3 Hybrid Rocket Engines: Gtratrix Regression Rate Model and Ballistics .....	12
3. Engine Scale Study .....	20
3.1 Methodology .....	20
3.1.1 IAC Rocket .....	21
3.2 Sizing the Nozzle .....	22
3.3 Firing Results .....	23
3.3.1 IAC HRE .....	23
3.3.2 125% Scale Up .....	26
3.3.3 150% Scale Up .....	28
3.3.4 200% Scale Up .....	31
3.3.5 400% Scale Up .....	35
3.3.6 600% Scale Up .....	37
3.3.7 800% Scale Up .....	41
3.3.8 1000% Scale Up .....	44
3.3.9 Combined Results for all Scales .....	47
4. Discussion of Results .....	50

4.1 Pressure-Time Curves and Required Oxidizer Mass Flow Rate .....	50
5. Conclusion .....	53
5.1 Concluding Remarks and Recommendations for Future Work .....	53
Appendices.....	54
Appendix A: Performance Results for all Scales up to Propellant Burn-Out .....	54
IAC HRE Full Firing Charts .....	54
125% HRE Scale Up Full Firing Charts .....	56
150% HRE Scale Up Full Firing Charts .....	58
200% HRE Scale Up Full Firing Charts .....	60
400% HRE Scale Up Full Firing Charts .....	62
600% HRE Scale Up Full Firing Charts .....	64
800% HRE Scale Up Full Firing Charts .....	66
1000% HRE Scale Up Full Firing Charts .....	68
Appendix B: Nozzle Scaling Calculator (for Matlab R2015b) .....	70
References .....	71

## List of Tables

Table 1: IAC HRE Parameters [15].....	21
Table 2: IAC HRE Post-Firing Performance Values of Interest, for 40% Fuel Burn .....	25
Table 3: Parameters for 125% HRE Scale Up .....	26
Table 4: 125% Scale-Up HRE Post-Firing Performance Values of Interest, for 40% Fuel Burn ....	28
Table 5: Parameters for 150% HRE Scale Up .....	28
Table 6: 150% Scale-Up HRE Post-Firing Performance Values of Interest, for 40% Fuel Burn ....	31
Table 7: Parameters for 200% HRE Scale Up .....	31
Table 8: 200% Scale-Up HRE Post-Firing Performance Values of Interest, for 40% Fuel Burn ....	34
Table 9: Parameters for 400% HRE Scale Up .....	35
Table 10: 400% Scale-Up HRE Post-Firing Performance Values of Interest, for 40% Fuel Burn ..	37
Table 11: Parameters for 600% HRE Scale Up .....	37
Table 12: 600% Scale-Up HRE Post-Firing Performance Values of Interest, for 40% Fuel Burn ..	41
Table 13: Parameters for 800% HRE Scale Up .....	41
Table 14: 800% Scale-Up HRE Post-Firing Performance Values of Interest, for 40% Fuel Burn ..	44
Table 15: Parameters for 1000% HRE Scale Up .....	44
Table 16: 1000% Scale-Up HRE Post-Firing Performance Values of Interest, for 40% Fuel Burn	46
Table 17: Error percentage table for calculated versus required oxidizer mass flow rates and chamber pressure at 40% fuel consumption relative to reference HRE, for all HREs.....	51

## List of Figures

Figure 1: Robert Goddard next to the First Modern Liquid-Propellant Rocket. Courtesy of NASA. .....	3
Figure 2: Simplified Illustration of the Main Components of a Hybrid Rocket Engine.....	4
Figure 3: Simplified illustration of a diffusion flame zone within the turbulent boundary layer in a HRE combustion process [13] .....	10
Figure 4: Predictive and Experimental Results for Regression Rate as a Function of Mass Flux Using HTPB/GOX Fuel-Oxidizer Combination at Different Fuel Port Diameters [11].....	16
Figure 5: Predictive and Experimental Results for Regression Rate as a Function of Mass Flux, for Different Propellants and HRE Sizes [11].....	17
Figure 6: Schematic Diagram of the IAC N <sub>2</sub> O/HTPB HRE [15].....	21
Figure 7: Chamber Pressure vs. Time for IAC HRE for 40% Fuel Consumption .....	23
Figure 8: Thrust (Sea Level) vs. Time for IAC HRE for 40% Fuel Consumption .....	24
Figure 9: Regression Rate vs. Time, at the Head-End Fuel Port, for IAC HRE for 40% Fuel Consumption.....	24
Figure 10: Stoichiometric Length vs. Time for IAC HRE for 40% Fuel Consumption .....	25
Figure 11: Chamber Pressure vs. Time for 125% Scale Up HRE for 40% Fuel Consumption.....	26
Figure 12: Thrust (Sea Level) vs. Time for 125% Scale Up HRE for 40% Fuel Consumption.....	27
Figure 13: Regression Rate vs. Time, at the Head-End Fuel Port, for 125% Scale Up HRE for 40% Fuel Consumption .....	27
Figure 14: Stoichiometric Length vs. Time for 125% Scale Up HRE for 40% Fuel Consumption ..	28
Figure 15: Chamber Pressure vs. Time for 150% Scale Up HRE for 40% Fuel Consumption.....	29
Figure 16: Thrust (Sea Level) vs. Time for 150% Scale Up HRE for 40% Fuel Consumption.....	29
Figure 17: Regression Rate vs. Time, at the Head-End Fuel Port, for 150% Scale Up HRE for 40% Fuel Consumption .....	30
Figure 18: Stoichiometric Length vs. Time for 150% Scale Up HRE for 40% Fuel Consumption ..	30
Figure 19: Chamber Pressure vs. Time for 200% Scale Up HRE for 40% Fuel Consumption.....	31
Figure 20: Thrust (Sea Level) vs. Time for 200% Scale Up HRE for 40% Fuel Consumption.....	32
Figure 21: Regression Rate vs. Time, at the Head-End Fuel Port, for 200% Scale Up HRE for 40% Fuel Consumption .....	33
Figure 22: Stoichiometric Length vs. Time for 200% Scale Up HRE for 40% Fuel Consumption ..	34
Figure 23: Chamber Pressure vs. Time for 400% Scale Up HRE for 40% Fuel Consumption.....	35
Figure 24: Thrust (Sea Level) vs. Time for 400% Scale Up HRE for 40% Fuel Consumption.....	36
Figure 25: Regression Rate vs. Time, at the Head-End Fuel Port, for 400% Scale Up HRE for 40% Fuel Consumption .....	36
Figure 26: Stoichiometric Length vs. Time for 400% Scale Up HRE for 40% Fuel Consumption ..	37
Figure 27: Chamber Pressure vs. Time for 600% Scale Up HRE for 40% Fuel Consumption.....	38
Figure 28: Thrust (Sea Level) vs. Time for 600% Scale Up HRE for 40% Fuel Consumption.....	38
Figure 29: Regression Rate vs. Time, at the Head-End Fuel Port, for 600% Scale Up HRE for 40% Fuel Consumption .....	39

Figure 30: Stoichiometric Length vs. Time for 600% Scale Up HRE for 40% Fuel Consumption ..	40
Figure 31: Chamber Pressure vs. Time for 800% Scale Up HRE for 40% Fuel Consumption .....	42
Figure 32: Thrust (Sea Level) vs. Time for 800% Scale Up HRE for 40% Fuel Consumption.....	42
Figure 33: Regression Rate vs. Time, at the Head-End Fuel Port, for 800% Scale Up HRE for 40% Fuel Consumption .....	43
Figure 34: Stoichiometric Length vs. Time for 800% Scale Up HRE for 40% Fuel Consumption ..	43
Figure 35: Chamber Pressure vs. Time for 1000% Scale Up HRE for 40% Fuel Consumption.....	44
Figure 36: Thrust (Sea Level) vs. Time for 1000% Scale Up HRE for 40% Fuel Consumption.....	45
Figure 37: Regression Rate vs. Time, at the Head-End Fuel Port, for 1000% Scale Up HRE for 40% Fuel Consumption .....	45
Figure 38: Stoichiometric Length vs. Time for 1000% Scale Up HRE for 40% Fuel Consumption	46
Figure 39: Chamber Pressure vs. Time for All HRE Scales for 40% Fuel Consumption.....	47
Figure 40: Thrust (Sea Level) vs. Time for all HRE Scales for 40% Fuel Consumption .....	47
Figure 41: Regression Rate vs. Time, at the head-end fuel port, for all HRE Scales for 40% Fuel Consumption, here shown for the first 20 seconds of firing to better show trends.....	48
Figure 42: Stoichiometric Length vs. Time, for all HRE Scales for 40% Fuel Consumption .....	49
Figure 43: Chamber Pressure vs. Time for IAC HRE Up to Burn-Out .....	54
Figure 44: Thrust (Sea Level) vs. Time for IAC HRE Up to Burn-Out.....	54
Figure 45: Regression Rate vs. Time, at the Head-End Fuel Port, for IAC HRE Up to Burn-Out...	55
Figure 46: Stoichiometric Length vs. Time for IAC HRE Up to Burn-Out .....	55
Figure 47: Chamber Pressure vs. Time for 125% Scale Up HRE Up to Burn-Out.....	56
Figure 48: Thrust (Sea Level) vs. Time for 125% Scale Up HRE Up to Burn-Out.....	56
Figure 49: Regression Rate vs. Time, at the Head-End Fuel Port, for 125% Scale Up HRE Up to Burn-Out .....	57
Figure 50: Stoichiometric Length vs. Time for 125% Scale Up HRE Up to Burn-Out.....	57
Figure 51: Chamber Pressure vs. Time for 150% Scale Up HRE Up to Burn-Out.....	58
Figure 52: Thrust (Sea Level) vs. Time for 150% Scale Up HRE Up to Burn-Out.....	58
Figure 53: Regression Rate vs. Time, at the Head-End Fuel Port, for 150% Scale Up HRE Up to Burn-Out .....	59
Figure 54: Stoichiometric Length vs. Time for 150% Scale Up HRE Up to Burn-Out.....	59
Figure 55: Chamber Pressure vs. Time for 200% Scale Up HRE Up to Burn-Out.....	60
Figure 56: Thrust (Sea Level) vs. Time for 200% Scale Up HRE Up to Burn-Out.....	60
Figure 57: Regression Rate vs. Time, at the Head-End Fuel Port, for 200% Scale Up HRE Up to Burn-Out .....	61
Figure 58: Stoichiometric Length vs. Time for 200% Scale Up HRE Up to Burn-Out.....	61
Figure 59: Chamber Pressure vs. Time for 400% Scale Up HRE Up to Burn-Out.....	62
Figure 60: Thrust (Sea Level) vs. Time for 400% Scale Up HRE Up to Burn-Out.....	62
Figure 61: Regression Rate vs. Time, at the Head-End Fuel Port, for 400% Scale Up HRE Up to Burn-Out .....	63
Figure 62: Stoichiometric Length vs. Time for 400% Scale Up HRE Up to Burn-Out.....	63
Figure 63: Chamber Pressure vs. Time for 600% Scale Up HRE Up to Burn-Out.....	64

Figure 64: Thrust (Sea Level) vs. Time for 600% Scale Up HRE Up to Burn-Out..... 64

Figure 65: Regression Rate vs. Time, at the Head-End Fuel Port, for 600% Scale Up HRE Up to Burn-Out ..... 65

Figure 66: Stoichiometric Length vs. Time for 600% Scale Up HRE Up to Burn-Out ..... 65

Figure 67: Chamber Pressure vs. Time for 800% Scale Up HRE Up to Burn-Out..... 66

Figure 68: Thrust (Sea Level) vs. Time for 800% Scale Up HRE Up to Burn-Out..... 66

Figure 69: Regression Rate vs. Time, at the Head-End Fuel Port, for 800% Scale Up HRE Up to Burn-Out ..... 67

Figure 70: Stoichiometric Length vs. Time for 800% Scale Up HRE Up to Burn-Out ..... 67

Figure 71: Chamber Pressure vs. Time for 1000% Scale Up HRE Up to Burn-Out..... 68

Figure 72: Thrust (Sea Level) vs. Time for 1000% Scale Up HRE Up to Burn-Out..... 68

Figure 73: Regression Rate vs. Time, at the Head-End Fuel Port, for 1000% Scale Up HRE Up to Burn-Out ..... 69

Figure 74: Stoichiometric Length vs. Time for 1000% Scale Up HRE Up to Burn-Out..... 69

## List of Appendices

Appendix A: Performance Results for all Scales up to Propellant Burn-Out .....	54
Appendix B: Nozzle Scaling Calculator (for Matlab R2015b).....	70

## Nomenclature

- $A$  = local core flow cross-sectional area,  $m^2$   
 $A_e$  = nozzle exit plane cross-sectional area,  $m^2$   
 $A_p$  = port cross-sectional area,  $m^2$   
 $A_s$  = fuel burning surface area,  $m^2$   
 $A_t$  = nozzle throat cross-sectional area,  $m^2$   
 $\alpha$  = coefficient of mass-flux-dependent burning rate,  $m/s-(kg/s\ m^2)^n$   
 $C_f$  = thrust coefficient, N  
 $C_p$  = gas specific heat,  $J/kg-K$   
 $C_s$  = fuel specific heat (solid phase),  $J/kg-K$   
 $c^*$  = characteristic exhaust velocity,  $m/s$   
 $d_p$  = fuel port (or hydraulic) diameter,  $m$   
 $e_s$  = surface ablation rate,  $m/s$   
 $f$  = Darcy-Weisbach friction factor  
 $G$  = mass flux,  $kg/m^2-s$   
 $G_o$  = oxidizer mass flux,  $kg/m^2-s$   
 $h$  = effective convective heat transfer coefficient,  $W/m^2-K$   
 $\Delta H_s$  = quasi-steady net surface heat of reaction,  $J/kg$   
 $k$  = gas thermal conductivity,  $W/m-K$   
 $L$  = length of the fuel grain,  $m$   
 $L_{st}$  = stoichiometric length,  $m$   
 $M$  = gas molecular mass,  $amu$   
 $Ma$  = Mach number (and  $Ma$  of local flow inside the fuel grain port)  
 $Ma_e$  = Mach number at the nozzle exit  
 $Ma_t$  = Mach number at the nozzle throat  
 $\dot{m}$  = total mass flow rate,  $kg/s$   
 $\dot{m}_f$  = fuel mass flow rate,  $kg/s$   
 $\dot{m}_o$  = oxidizer mass flow rate,  $kg/s$

$n$  = burning rate exponent  
 $Pr$  = Prandtl number  
 $p$  = local static pressure, Pa  
 $p_c$  = chamber pressure, Pa  
 $p_e$  = nozzle exit pressure, Pa  
 $p_\infty$  = far field pressure, Pa  
 $R$  = specific gas constant, J/kg-K  
 $Re_d$  = Reynolds number (with respect to pipe diameter)  
 $r$  = oxidizer/fuel mixture ratio  
 $r_b$  = fuel regression rate, m/s  
 $r_{st}$  = stoichiometric mixture ratio  
 $T$  = local flow temperature, K  
 $T_{ds}$  = decomposition gas temperature resulting from ablation, K  
 $T_f$  = flame temperature (gas phase), K  
 $T$  = fuel initial temperature (solid phase), K  
 $T_s$  = fuel burning surface temperature, K  
 $T_\infty$  = local central core gas temperature, K  
 $u$  = local axial velocity, m/s  
 $x$  = longitudinal distance along the fuel grain port, m  
 $\varepsilon$  = fuel surface roughness height, m  
 $\gamma$  = gas ratio of specific heats  
 $\mu$  = gas absolute viscosity, kg/m-s  
 $\rho$  = gas density, kg/m<sup>3</sup>  
 $\rho_s$  = fuel density (solid phase), kg/m<sup>3</sup>  
 $\rho_\infty$  = core flow gas density, kg/m<sup>3</sup>

### **Subscripts and Superscripts**

$p$  = subscript for particulate parameters

$x$  = subscript for axial direction

$\infty$  = subscript for values evaluated in the core flow; or, indicating far field value

$*$  = superscript indicating zero-transpiration case

$comp$  = subscript for compressible flow regime

$incomp$  = subscript for incompressible flow regime

## 1. Introduction

Hybrid rocket engines (HREs) have been found to have several performance and safety characteristics that have warranted their consideration for some flight vehicle applications that traditionally employ a chemical rocket propulsion system. One main benefit of hybrid rocket engines is their inherently safe design, whereby the propellant and oxidizer are separated and are in different phases, thus mitigating the risk of accidental ignition that one commonly associates with solid-propellant rocket motors (SRMs). In the HRE configuration, usually the oxidizer is a pressurized gas or liquid, whereas the fuel is a solid in a separate section (the combustion chamber) of the vehicle. HREs can also be throttled through valving of the liquid or gas oxidizer coming out of storage, as another advantage over SRMs. In hybrid rocket engines, the fuel grain is usually configured with a single port or, if needed, multiple ports to encourage a higher oxidizer mass flow rate [1,2]. Through this arrangement, the fuel acts as an engine casing insulator, thus alleviating the need to cool the surrounding combustion chamber walls.

As might be expected, there are drawbacks to the hybrid rocket engine configuration, the mitigation of which are still under investigation to this day. Of these are characteristically slow regression rates compared to SRMs of similar scale, which leads to lower relative thrust. Other potential issues include: lower mixing combustion efficiencies, low volumetric loading, higher fuel residuals (especially in multiple-port configurations), a dynamic effective fuel-oxidizer mixture ratio, and acoustic (pressure wave) vibrations that can seriously diminish performance. Mitigations to these issues have been explored over the years, and in general, some approaches alleviate some of these issues [3]. For example, researchers [4] have shown that pre- and post-combustion chambers can help stabilize the turbulent diffusion flame zones. It has also been shown that a proper choice of oxidizer injector configuration, can help stabilize the internal combustion and flow system [5].

Much research work has been done towards effectively increasing HRE overall mass flow rates, especially of interest for larger engines. Multiple port configurations, with the goal of increasing fuel surface area and burning rate, have been tested, and show some promise; however, unfavourably large unburned fuel residuals can be a problem. Adding a tangential flow component to the oxidizer injection, called swirl, has been explored, and has shown favourable increases with respect to fuel regression rates. There may be some advantage as to the choice of fuel, for example, [6,7]. Findings by Cantwell et al [8,9,10] have suggested that adding metallic particles to the fuels of hybrid rocket engines can help increase specific impulse ( $I_{sp}$ ) and regression rate values.

For over a decade now, research work at Ryerson University has been put into improving our knowledge and understanding of hybrid rocket engine performance. For example, there has been the development of a more accurate fuel burning rate model [11,12], which is explained in detail in chapter 2. A program (QSHYB) that simulates the quasi-steady internal ballistics of hybrid rocket engines has been created [12]. The QSHYB program provides performance predictions for thrust, chamber pressure, and burning rate history for a variety of hybrid rocket configurations. The program has shown good agreement with experimental data in a number of cases [11,12].

## 1.1 Some Background on Hybrid Rocket Engines



*Figure 1: Robert Goddard next to the First Modern Liquid-Propellant Rocket. Courtesy of NASA.*

The genesis of modern liquid rocket engine (LRE) development is attributed to Robert Goddard. On March 16<sup>th</sup>, 1926, after years of painstaking, isolated work with little to no support, Goddard successfully launched the first liquid-propellant rocket. The appropriately named “Goddard 1” flew just over 12 meters above the ground for 2.5 seconds through the combustion of liquid oxygen and gasoline [13], giving the field of rocketry a major step forward.

Solid rocket motors are nominally simpler in design when compared to LREs, and have been around for hundreds of years, in various forms. A solid propellant, composed of both a fuel and oxidizer, is ignited, and then burns until consumption. Because of this, their design is relatively simple, cheap, can be stored for decades in some cases, and can offer very high thrust

relative to weight. As a disadvantage, because of their “fire and forget” nature, so to speak, they cannot in general be throttled, and are potentially risky with respect to unintentional ignition.

The purpose of creating a hybrid rocket engine was to open up a new dimension of versatility and provide potential advantages over LREs and SRMs, whereby components of solid rocket motors and liquid rocket engines could be combined. The most common arrangement of a hybrid rocket engine is to have either a gaseous or liquid oxidizer fed to a solid fuel grain. The reverse case, though uncommon, has been done. Serious development of hybrid rocket engines began in the late 1940’s, during which most U.S. rocket propulsion companies, as well as some European ones, were experimenting with HREs [13]. Naturally, a fusion of solid and liquid fuel rockets will create a system that will show characteristics of both systems, leaving the engineer with a number of design opportunities and performance characteristics to examine.

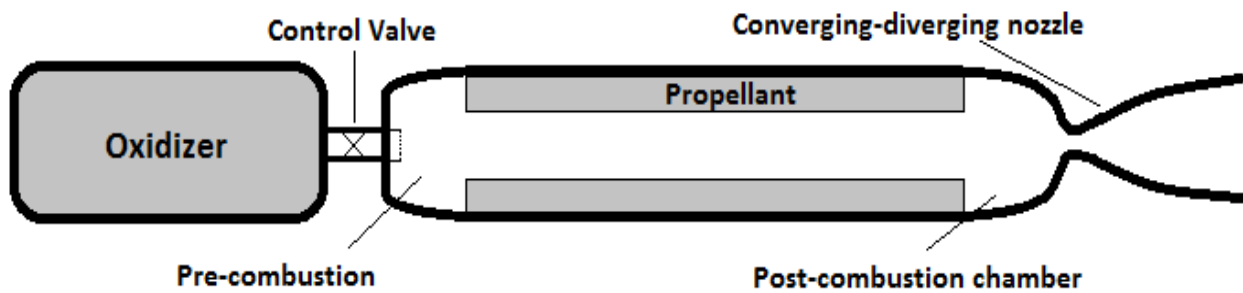


*Figure 2: Simplified Illustration of the Main Components of a Hybrid Rocket Engine*

## 1.2 Objectives of this Study

Several studies have, and presently are, being conducted that look into the behaviour of HRE parameters on a largely individual basis. For example, there is a large focus on increasing the regression rate of the HRE fuel during combustion, with many experimental examples [6,14]. While this is an important parameter, there are other things to consider. For example, the size of the engine, as one goes bigger, is a common concern. Indeed, fuel regression rate, and engine size, are linked. A common design choice encountered, depending on the thrust level desired: will a multi-port configuration be needed, above a certain engine size threshold? Of course, the answer depends, at least in part, on the fuel regression rate. And, of course, the fuel regression rate depends, at least in part, on port diameter.

To further advance HRE technology, a better understanding of how engine sizing affects performance is required. The main objective of this thesis is to study, in some detail and using a more accurate burning rate model, the effect engine size has on internal ballistic performance. Specifically, the goal is to observe changes in thrust, specific impulse, stoichiometric length, and chamber pressure, versus firing time, as the engine model is scaled up in size. The RU computer program, called QSHYB, will be used for modelling the engine and conducting simulated firings. The reference rocket for this study is a  $N_2O$ /HTPB (nitrous-oxide/hydroxyl-terminated polybutadiene) hybrid rocket engine from a paper by Bockelt and Greatrix [15]. As a comparison baseline, the initial quasi-steady chamber pressure of all model variants is to be kept the same, and the scaled up oxidizer mass flow rate is held constant (i.e., no throttling) for a given engine's firing time. The major contribution this thesis therefore aims to offer to the field of HRE research is a sizing study that incorporates Dr. Greatrix's HRE regression rate model and supporting equations at its core [16].

## 2. Hybrid Rocket Engine Performance Modelling

This chapter will cover the equations necessary for obtaining performance metrics needed for the study of hybrid rocket engines of various sizes. Section 2.1.1 provides the basic equations for parameters relative to this thesis' performance study: thrust, specific impulse, total impulse, and mass flow rate through a choked nozzle throat. Section 2.1.2 covers historical HRE regression rate models briefly, and section 2.1.3 goes over Dr. Greatrix's HRE burn rate model in detail, as it is the one used in this thesis.

### 2.1 Basics of Rocket Engine Performance

#### 2.1.1 Impulse and Thrust

A chemical rocket, at its most basic level, is the manifestation of Newton's Third Law. In some shape or form, a fuel and oxidizer are combined and combusted, the resulting gas accelerated to supersonic speeds (in an ideal case) through a converging-diverging nozzle, and expelled out one end of the vehicle. Thus, for the action of the gases being exhausted out of the rocket at high speeds, and when not in a vacuum, also against the external atmospheric pressure, a reaction force is imposed on the vehicle. As one can imagine, there are many ways to make a rocket of various shapes and sizes. One simple performance parameter that is ultimately used to compare them is total and specific impulse. Total impulse is defined as the thrust force  $F$  of a rocket integrated over the firing time  $t_b$ :

$$I_t = \int_0^{t_b} F dt, \quad \text{N} \cdot \text{s} \quad (1)$$

whereas average specific impulse is defined as:

$$\bar{I}_{sp} = \frac{\int_0^{t_b} F dt}{g_o \int \dot{m} dt}, \quad \text{s} \quad (2)$$

More widely used is the *instantaneous specific impulse*,  $I_{sp}$ , which is defined as follows:

$$I_{sp} = \frac{F}{\dot{m}g_o}, \quad \text{s} \quad (3)$$

Specific impulse, due to how the underlying units cancel out, is in units of seconds. Whereas specific impulse is more applicable since it is in the context of burn time (a rocket that makes a lot of thrust for one second may not be as useful for certain applications), thrust is still an important measure of performance especially when sizing up similar systems. As rockets are devices that expel mass at high velocities to produce thrust, the thrust is obviously the result of a momentum change. In this thesis, the rocket in question expels mass from one end, namely the end of a converging-diverging nozzle. One simple expression for rocket thrust  $F$  can be given as:

$$F = C_F p_c A_t, \text{ N} \quad (4)$$

where  $A_t$  is the nozzle throat area, the thrust coefficient  $C_F = f(\gamma, p_c, p_e)$ , where  $p_e$  is the static pressure at the nozzle exit plane. A more involved equation incorporating the momentum of the exiting gas can be provided as a standard one-dimensional thrust equation [16], stated below, as:

$$F = \frac{dm}{dt} u_e + (p_e - p_\infty) A_e = \dot{m}_e u_e + (p_e - p_\infty) A_e \quad (5)$$

where  $u_e$  is the x-component of the exhaust gas velocity,  $p_\infty$  is the far field air pressure, and  $A_e$  is the area of the nozzle exit plane. This early in the process, one can already see that mass flow rate and flow velocity out of the rocket play the majority contribution for rocket thrust.

One equation commonly used to compare the relative performance of different rocket designs, including ones of larger relative size, is the characteristic exhaust velocity  $c^*$  [13]:

$$c^* = \frac{p_c A_t}{\dot{m}_t}, \text{ m/s} \quad (6)$$

The characteristic exhaust velocity relates to the efficiency of a rocket's combustion and is a commonly used comparison metric in the rocket community as it can easily be determined from data (both measured experimentally or given by a simulation). Assuming choked flow through the nozzle of the rocket, the overall mass flow rate of a rocket with one converging-diverging exhaust nozzle can be modelled as:

$$\dot{m}_t = \dot{m}_e = \left[ \frac{\gamma}{R_{sp} T_F} \left( \frac{2}{\gamma + 1} \right)^{\frac{\gamma+1}{\gamma-1}} \right]^{1/2} A_t p_c, \text{ kg/s} \quad (7)$$

where  $T_F$  is the flame temperature in the combustion chamber,  $p_c$  is the chamber pressure, and  $A_t$  is the nozzle throat area. For this thesis, the specific gas constant above,  $R_{sp}$  uses the average molecular mass of the combustion products in its calculation:

$$R_{sp} = \frac{8314}{M_{gas}}, \quad \text{J/kmol} \cdot \text{k} \quad (8)$$

The term in brackets in equation (7) is another form, in this case the inverse, of the characteristic exhaust velocity ( $c^*$ ); as this thesis is scaling up in size based on one reference HRE, this value would always be the same for all sizes of that engine. One commonly provided measure of performance in the HRE community is the combustion efficiency  $\eta_c$ , a ratio of actual (experimental) and theoretical characteristic exhaust velocity, which is defined as [13]:

$$\eta_c = \frac{c_{act}^*}{c_{theo}^*} < 1 \quad (9)$$

Furthermore, equation (7) can be substituted into equation (5), and an equation for rocket thrust with a choked nozzle can be written:

$$F = C_{F,v} \left[ 1 - \left( \frac{P_e}{P_c} \right)^{\frac{\gamma-1}{\gamma}} \right]^{1/2} A_t p_c + (p_e - p_\infty) A_e \quad (10)$$

where  $C_{F,v}$ , the vacuum thrust coefficient, is expressed as:

$$C_{F,v} = \left[ \frac{2\gamma^2}{\gamma-1} \left( \frac{2}{\gamma+1} \right)^{\frac{\gamma+1}{\gamma-1}} \right]^{1/2} \quad (11)$$

and the nozzle exit plane static pressure can be provided via:

$$p_e = p_c \left[ 1 + \frac{\gamma-1}{2} Ma_e^2 \right]^{\frac{-\gamma}{\gamma-1}} \quad (12)$$

The equations for parameters provided in this chapter are typically for instantaneous estimates. Over the course of a firing, parameters can be plotted and an average gained by integrating them over the length of the firing time. As will be shown in the next sections, the fuel burning rate in hybrid rocket engines is a major contribution, understandably, to mass generation and flow rate, in conjunction, of course, with the oxidizer mass flow input. A lower oxidizer-fuel mixture ratio  $r$  means a stronger fuel burning rate contribution.

### 2.1.2 Hybrid Rocket Engines: Classical Regression Rate Models

Serious interest in modelling the combustion characteristics, and with that, the ballistics of hybrid rocket engines began in the late 1950's. Pioneering work into the understanding of how hybrid rockets burned fuel was spearheaded in those early years by, among others, Gerald A. Marxman, C.E. Wooldridge, and R. J. Muzzy [17-20]. Marxman specifically created a model that took into account heat and mass transfer along with chemical reactions, and ended up with a model that agreed well with some experimental data available at the time [21,22]. It was understood that for HREs, combustion took place within a narrow diffusion flame zone at the bottom of a turbulent boundary layer. This flame zone, through convective and radiative heat transfer, vaporizes the fuel below which is then convected away into the flame zone where it is mixed and combusted with oxidizer from the core flow [19,21].

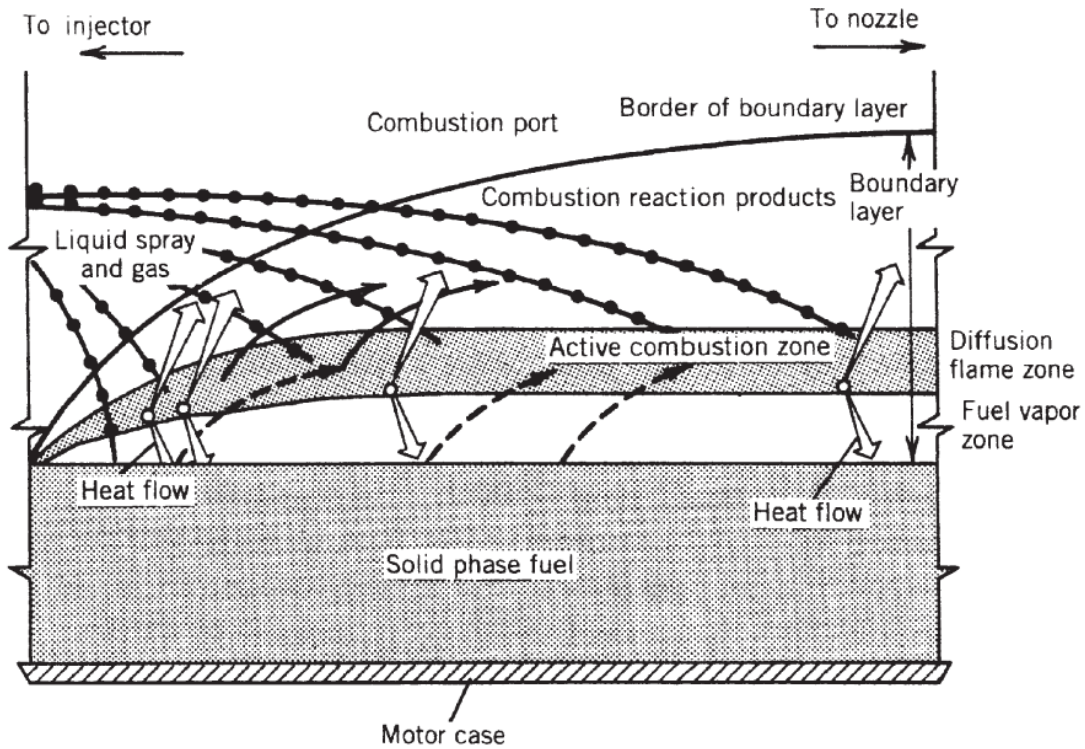


Figure 3: Simplified illustration of a diffusion flame zone within the turbulent boundary layer in a HRE combustion process [13]

For conventional head-end injection cylindrical single-port hybrid rocket engines, the solid fuel regression rate has been found to be predominantly a function of local axial mass flux ( $G = \rho u_x = \dot{m}/A_p$ ), as opposed to pressure as observed in SRMs, above the surface of the fuel. Knowing the regression rate of the fuel is required to find the mass flow rate of fuel  $\dot{m}_f$  being generated from the combustion and, in some cases, non-combustive ablation of the fuel being removed from the fuel grain. With a known oxidizer mass flow rate  $\dot{m}_{ox}$  being set, originating from one or more injectors, a combined mass flow rate of oxidizer and fuel can be attained, giving an overall mass flow rate  $\dot{m}$ . This total gas flow increases as one moves down the fuel port axially, as more fuel reacts with the remaining oxidizer in the core flow stream via the active combustion zone. Of course, being able to predict how fast the fuel will burn, and thus contribute to mass flux and chamber pressure, is required in order to have any form of predictability in scaling up a HRE. A conventional combustion-based regression rate equation, for a local fuel grain station in a cylindrical port configuration, is based on axial mass flux  $G$  and empirical factors,  $a$  and  $n$ , of

which have been obtained from experimental firings. This basic equation commonly used by the HRE community is stated below as [16]:

$$r_b = aG^n, \quad 0.4 < n < 0.85 \quad (13)$$

It should be noted that the coefficient  $a$  is inversely proportional to fuel port diameter. As the total mass flow rate within the fuel port relies on the amount of fuel entering the core flow via combustion (and ablation, in some circumstances), several iterations are usually required for a more accurate value of fuel regression rate when using equation (13). On occasion, it has been observed that HRE regression rates tend to agree with an effectively constant mass flux. Therefore, one approximation to equation (13) is to use only the oxidizer mass flux ( $G_o = \dot{m}_o/A_p$ ), in place of the combined oxidizer and fuel mass flux:

$$r_b \approx aG_o^n \quad (14)$$

As port area  $A_p$  gets bigger with time into a firing,  $G_o$ , for a constant  $\dot{m}_o$ , will get smaller. Of course, equations (13) and (14) are very simple in nature and are, at best, useful to get a rough idea of HRE regression rates in an early design setting. Several efforts to quantify experimental data into a burning rate predictive model have been attempted in the past [16,18,19], all with varying degrees of success and accuracy. Whereas an empirical correlation for predicting the values of the  $a$  and  $n$  factors of one test HRE proved accurate, they would break down for other HREs of differing size, of which would need their own empirical correlations. For example, a more involved and recent equation for HRE fuel burning rate, provided by Sutton and Biblarz [13], is as follows:

$$r_b = 0.036 \frac{G^{0.8}}{\rho_s} \left(\frac{\mu}{x}\right)^{0.2} \left[ \frac{\rho_b r_b}{\rho_\infty u_\infty (f/8)} \right]^{0.23} \quad (15)$$

where  $x$  is the axial location along the combustion port,  $\mu$  is the combustion gas viscosity, and the terms with the  $\infty$  subscript refer to parameters evaluated in the core flow. Once again however, equation (15), like other HRE regression rate models in the past, is based on empirical factors and is applicable only within a narrow, restrictive range of turbulent flow regimes within the fuel port [6,7]. This reliability on empirical factors, and their ability to lose predictability when the test HRE they are based on changes geometrically, makes these regression models unreliable

and unpredictable in a scaling study. To test them, one would need to take the expensive route of constructing and firing scaled-up versions of an HRE, defeating the purpose of predicting HRE scale-up performance. However, this study employs the use of a verified regression rate model based on previous Ryerson University studies. The next section will go over this model in order to explain why it is desired to study how it performs when it is used to simulate scaled-up HREs and predict their performance.

### 2.1.3 Hybrid Rocket Engines: Greatrix Regression Rate Model and Ballistics

It is difficult to design and build a rocket engine when the models for its performance are empirical at their base. Being empirical makes it difficult to scale up a reference rocket with known performance data and predict how accurately it will perform with larger features. Past studies conducted for scaled up hybrid rocket engines resulted in mixed results: whereas some HREs followed one empirical model well as they were scaled up, for other HREs, one observed large deviations from the baseline predictions dependent on smaller engine information [7,23]. This lack of universality in being able to predict, at least to a reasonable degree, how a larger scale version of a test rocket will perform can be quite a detriment to a design team.

As the purpose of the study presented in this thesis is to record and present the effects in the scaling up of a HRE has on its performance, a more universal regression rate model is required. As discussed previously, the historic regression rate equations were based on experimental firings and would deviate from their predictions once the HRE in question was changed in size significantly; such is the case in this study, where the base HRE is scaled up to ten times its original size. Especially desired is a model that does not depend on empirical corrections and estimates, as these would defeat the purpose of prediction. One such predictive model is available.

For HREs that do not contain metal particulates in the fuel, as is the case in this study, it was highlighted in the previous section that HREs typically show an independence from pressure. It has been observed that the dominant mechanism in HRE fuel regression is through convective

heat transfer [17], which largely depends on axial mass flux [6,16]. For this reason, the Greatrix model for a conventional HRE can be applied:

$$r_b = \frac{h(T_F - T_S)}{\rho_s [C_s(T_S - T_i) - \Delta H_s]} \quad (16)$$

Dr. Greatrix's model for HRE regression rate is based on convective heat feedback theory. Through energy conservation, a balance between the energy entering the fuel burning surface from the combustion zone flame above it and the heat energy leaving the surface, via mass transfer out of the surface, can be established. The convective heat transfer component from the flame zone (above the fuel surface and within the turbulent boundary layer) to the burning surface is driven via the difference between the core flame temperature,  $T_F$ , and the fuel burning surface temperature,  $T_S$ . The mass transfer out of the burning surface (the fuel going from a solid, melting to a liquid, and ultimately becoming a gas [18]) is driven by a change from the initial solid fuel temperature  $T_i$  to its burning surface temperature. If significant, the net surface heat of reaction  $\Delta H_s$  can be included into the model to better account for all heat transfer effects. This heat of reaction difference term can either be positive (exothermic) or negative (endothermic), depending on the fuel-oxidizer combination, and the local pressure. It is not unusual to ignore the net surface heat of reaction contribution to the overall burn rate, as past studies using a quasi-steady approach to analysis have found [11,12,24]. Since this study also uses this approach, the  $\Delta H_s$  term in equation (16) has been set to zero for this paper.

It should be noted that, while other heat transfer mechanisms exist in a simple HRE, such as radiative heat transfer from the flame zone, its contribution to the overall burn rate is far outweighed by the convective heat transfer component, and therefore ignored. While there are cases where radiative heat transfer does come into effect, usually from metallic particles added to the fuel grain, the current study uses on HTPB as its fuel, and hence only the convective heat transfer component is included.

As a HRE is fired, the solid fuel, through heat transfer, undergoes a phase change from solid, to liquid, and then to a gas that evolves off of the burning surface. In this regard, the fuel surface is undergoing a mass transfer process, whereby gaseous fuel is "blowing" radially off of the fuel burning surface as it regresses. This mass transfer process is defined as transpiration,

and its contribution to the model is significant. As a mass flow is coming off of the fuel surface, it reduces the wall friction of the core flow, and hence reduces heat transfer to the surface (as the flow coming off of the fuel surface is effectively pushing against the core flow). Due to this property of HRE combustion, the heat transfer value for a transpired case is less than that of a non-transpired one, and therefore needs to be corrected, for a more accurate model.

The equations for correcting for transpiration are derived based on two-dimensional flow over a simplified case over a flat plate experiencing either suction (not applicable in this case) or blowing at its surface. Experiments carried out by Mickley et al [25,26] reinforced theoretical modelling by Mickley, of which is referred to as film theory. The theory approximates, to a good degree, flow characteristics within an ideal zone along the wall where transpiration takes place. This is a zone *within* the overall flow boundary layer, and should not be confused with it. Further simplifications to Mickley's thin film theory allow the flow within this zone to be assumed as laminar, further simplifying equations and derivations. A key parameter to Greatrix's model, equation (16), factors in the convective heat transfer coefficient under transpiration,  $h$ . However, finding the non-transpired case first,  $h^*$ , is generally required before estimating  $h$ . This zero-transpiration coefficient is derived via Reynolds' analogy equating shear stress to heat transfer for a turbulent flow:

$$h^* = \frac{k^{2/3} C_p^{1/3} G f^*}{\mu^{2/3} 8} \quad (17)$$

In this formula,  $h^*$  is the the zero-transpiration effective heat transfer coefficient of the axial mass flux of the combustion core gas. Equation (17) shows a direct dependence on axial mass flux  $G$ , however there is also dependence on  $f^*$ , the Darcy-Weisbach zero-transpiration friction factor. For a fully developed turbulent boundary layer, Colebrook's equation states [13]:

$$(f^*)^{-1/2} = -2 \log_{10} \left[ \frac{2.51}{\text{Re}_d (f^*)^{1/2}} + \frac{\varepsilon/d_p}{3.7} \right] \quad (18)$$

where  $\varepsilon$  is the fuel surface roughness height,  $d_p$  is the fuel port diameter, and  $\text{Re}_d$  is the Reynolds number. For the HRE in this study, specifically one with a cylindrical fuel port, the Reynolds number equation for turbulent flow in a pipe of circular cross section can be used, stated below as:

$$Re_d = \frac{\rho_{gas} u d_p}{\mu} \quad (19)$$

where  $u$  is the axial velocity of the gas. The density of the combustion gas,  $\rho_{gas}$ , in this study are assumed to follow an ideal gas relationship. Relating the combustion gas density to combustion flame temperature and chamber pressures gives:

$$\rho_{gas} = \frac{p_c}{R_{sp} T_f} \quad (20)$$

where the specific gas constant  $R$  comes from the universal gas constant, provided by equation (8). For the case where the flow is still developing, which in most cases is near the head-end fuel port, and the flow is within an applicable Reynolds number (on the order of 4000 or more), a commonly used empirical expression for Darcy-Weisbach zero-transpiration friction factor can be used [16]:

$$f^* = 4 \left[ 1.89 - 1.62 \log_{10} \left( \frac{\varepsilon}{\chi} \right) \right]^{-2.5} - 7.04 \left[ 1.89 - 1.62 \log_{10} \left( \frac{\varepsilon}{\chi} \right) \right]^{-3.5} \quad (21)$$

Additionally, if the core flow Mach number reaches a value which would make it compressible (i.e. above Mach 0.3), a correction for compressibility can be made by applying a correction to the friction factor:

$$f_{comp} = f_{incomp} / \left[ 1 + Pr^{1/3} \left( \frac{\gamma - 1}{2} \right) Ma_{port}^2 \right] \quad (22)$$

where  $Pr$  is the Prandtl number of the core gas flow. With these equations in mind, via film theory [16,25], a correction for transpiration can be given as:

$$h = \frac{\rho_s r_b C_p}{\exp \left( \frac{\rho_s r_b C_p}{h^*} \right) - 1} \quad (23)$$

By substituting equations (17), (18), and (23) into the Greatrix model, a solution for the regression rate of a simple HRE can be generated. For the case of head-end oxidizer injection, Greatrix's model for HRE fuel regression by substitution becomes [13,24]:

$$r_b = \frac{h^*}{\rho_s C_p} \ln \left[ 1 + \frac{C_p}{C_s} \frac{(T_F - T_S)}{(T_S - T_i - \Delta H_s / C_s)} \right] \quad (24)$$

This model has successfully been used in previous investigations by Ryerson University as a predictive fuel regression rate model for HREs employing a conventional setup with head-end oxidizer injection. To verify the accuracy and applicable range of this model, results from simulations employing this model were compared with several published studies. The studies explored HREs with various fuel and oxidizer combinations, and it was found that the HRE regression rate model incorporating the Greatrix HRE model agreed well with the published firing data, shown below in Figure 4 and Figure 5.

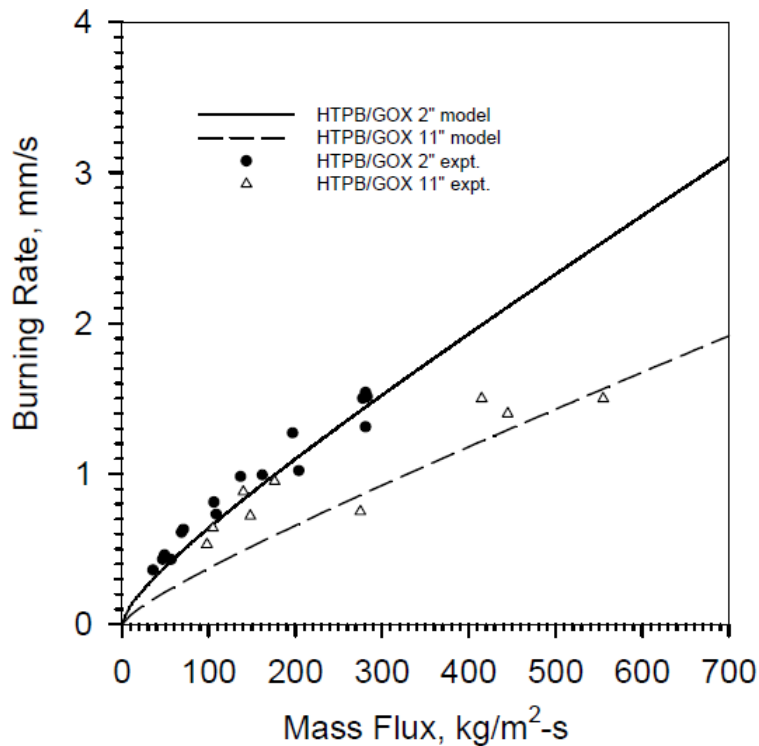


Figure 4: Predictive and Experimental Results for Regression Rate as a Function of Mass Flux Using HTPB/GOX Fuel-Oxidizer Combination at Different Fuel Port Diameters [11]

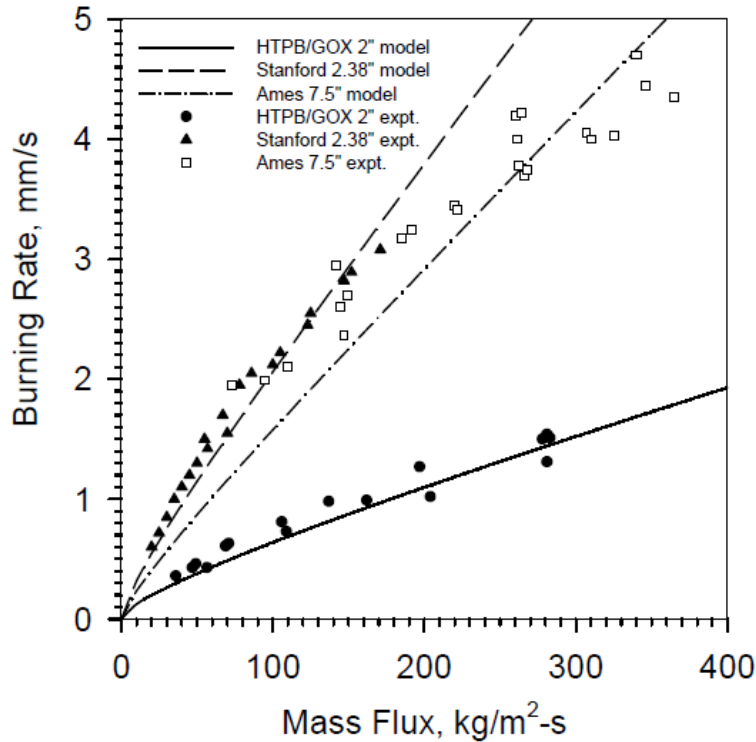


Figure 5: Predictive and Experimental Results for Regression Rate as a Function of Mass Flux, for Different Propellants and HRE Sizes [11]

Another parameter in HRE performance that must be observed, not just in scaling a HRE, but in viewing the overall performance of a HRE, is its stoichiometric length  $L_{st}$ . During the firing process, as one moves down the fuel port (relative to the head end), the oxidizer-fuel ratio  $r$  changes. Say one were to take an instantaneous snapshot of the HRE while it is being fired and observed the oxidizer-fuel ratio as a function of axial distance from the head-end,  $r(x)$ . In this case, as one moves down the fuel grain,  $r(x)$  decreases as more oxidizer has reacted with vaporized fuel in the active combustion zone. Likewise, looking at one station along the fuel grain as the firing progresses, the oxidizer-fuel ratio as a function of axial position and time,  $r(x, t)$  will increase as more fuel is burned away at the given fuel grain station. As these values change over the course of a firing, designers of HREs will commonly try to set a fuel grain length such that at some point in the firing, it will coincide with the stoichiometric oxidizer-fuel ratio for the given fuel and oxidizer being used. This fuel grain length is called the stoichiometric length,  $L_{st}$ . Using the Greatrix regression rate model, the stoichiometric length of a HRE can be provided:

$$L_{st} \approx \frac{G d_p}{4 \rho_s r_{st} r_b} \approx \frac{2 Pr^{2/3} d_p}{f^*(\ln[\beta_2])(r_{st})} \quad (25)$$

where  $\beta_2$  is the term in square parenthesis in equation (24). With a regression rate model that is suitable for predicting HRE performance for a wide range of configurations, a chamber pressure formula can be created. For subsonic fuel port Mach numbers below Mach 0.3, if one “knows”  $a$  and  $n$ , Greatrix [16, p.424] provides a quick estimate for chamber pressure for an HRE as:

$$p_c = c^* \cdot \frac{\dot{m}}{A_t} \approx \left[ \frac{\gamma}{RT_f} \left( \frac{2}{\gamma + 1} \right)^{\frac{\gamma+1}{\gamma-1}} \right]^{-1/2} \cdot \frac{\rho_s S a \left( \frac{\dot{m}_O}{A_p} \right)^n + \dot{m}_O}{A_t} \quad (26)$$

Equation (26) is provided here, as a reference, to show the reader which geometric parameters affect HRE chamber pressure, as they are relevant to the scaling up of a HRE (namely, nozzle throat and exit diameters, fuel port diameter, and burning surface area  $S$  which is connected to fuel port diameter and fuel grain length).

In this thesis, a one-dimensional numerical analysis (via the QSHYB program) is used to simulate HRE firings and measure their performance. The program uses quasi-steady (parameters not changing too rapidly in relative terms, such as the case when a pressure wave is present) one-dimensional ordinary differential equations described by Greatrix [27] that apply at a given time in the engine’s firing and at a given fuel grain location. The first set of equations for conservation of mass, linear momentum, and energy, apply to the core gas, going from the engine’s head-end injector towards the exhaust nozzle, respectively as:

$$\frac{d(\rho u)}{dx} = -\frac{1}{A} \frac{dA}{dx} \rho u + (1 - \alpha_p) \rho_s \frac{4r_b}{d} - \left( \frac{4r_b}{d} \right) \rho \quad (27)$$

$$\frac{d}{dx} (\rho u^2 + p) = -\frac{1}{A} \frac{dA}{dx} \rho u^2 - \left( \frac{4r_b}{d} \right) \rho u - \rho a_l - \frac{\rho_p}{m_p} D \quad (28)$$

$$\begin{aligned} \frac{d}{dx} (\rho u E + u p) = & -\frac{1}{A} \frac{dA}{dx} (\rho u E + u p) - \left( \frac{4r_b}{d} \right) \rho E + (1 - \alpha_p) \rho_s \frac{4r_b}{d} \left( C_p T_f + \frac{v_f^2}{2} \right) - \\ & \rho u a_l - \frac{\rho_p}{m_p} (u_p D + Q) \end{aligned} \quad (29)$$

The second set of equations for conservation of mass, linear momentum, and energy, apply to the monodisperse non-burning fuel particles entering the HRE core flow. These equations are:

$$\frac{d(\rho_p u_p)}{dx} = -\frac{1}{A} \frac{dA}{dx} \rho_p u_p + \alpha_p \rho_s \frac{4r_b}{d} - \left(\frac{4r_b}{d}\right) \rho_p \quad (30)$$

$$\frac{d(\rho_p u_p^2)}{dx} = -\frac{1}{A} \frac{dA}{dx} \rho_p u_p^2 - \left(\frac{4r_b}{d}\right) \rho_p u_p - \rho_p a_l + \frac{\rho_p}{m_p} D \quad (31)$$

$$\begin{aligned} \frac{d}{dx} (\rho_p u_p E_p) = & -\frac{1}{A} \frac{dA}{dx} (\rho_p u_p E_p) - \left(\frac{4r_b}{d}\right) \rho_p E_p + \alpha_p \rho_s \frac{4r_b}{d} \left(C_m T_f + \frac{v_f^2}{2}\right) \\ & - \rho_p u_p a_l + \frac{\rho_p}{m_p} (u_p D + Q) \end{aligned} \quad (32)$$

In the case of the local fuel location being larger than the stoichiometric length position,  $x > L_{st}$ , there is no more oxidizer remaining in the core flow gas, and therefore no combustion can occur. However, the core flow  $T_\infty$  is still hot enough to cause ablation of the fuel, and therefore regression still occurs at a slower rate, albeit with the ablated fuel gas entering the core flow at a lower effective temperature  $T_{ds}$ . The ablation rate  $e_s$  for the simplest of cases can be assumed to follow the convective energy feedback model outlined for the HRE combustion regression rate:

$$e_s = \frac{h^*}{\rho_s C_p} \ln \left[ 1 + \frac{C_p}{C_s} \frac{(T_\infty - T_{ds})}{[(T_{ds} - T_i) - \Delta H_s / C_s]} \right] \quad (33)$$

Once again, the net surface heat of reaction  $\Delta H_s$  will likely be even smaller than what it is in equation (24), since in this case there is no combustion occurring above the fuel. Using Graetz's quasi-steady equations, thrust can be calculated as outlined in section 2.1.1. In turn, with that information, specific impulse and characteristic velocity can be attained. As the analysis is quasi-steady, it also allows for the case of high Mach numbers in the aft section of the HRE, of which was a limiting case for the simplified regression rate models.

## 3. Engine Scale Study

### 3.1 Methodology

This study conducted HRE sizing by incrementally increasing the size of a reference IAC N<sub>2</sub>O/HTPB HRE (where N<sub>2</sub>O is the oxidizer and HTPB is the fuel), a motor designed for a small sounding rocket with variable thrust capability via command application of swirl [15]. In order to establish a proper benchmark of performance parameters, the HREs had to be increased in size while retaining a relative scale. Looking at the equations outlined in chapter 2, several physical parameters affecting performance were chosen to retain scale while increasing in size. After careful review and consideration, the parameters chosen were:

1. Fuel grain length,  $l_f$
2. Initial fuel port diameter,  $d_p$
3. Chamber wall diameter,  $d_{wall}$
4. Oxidizer mass flow rate,  $\dot{m}_o$
5. Nozzle throat area,  $A_t$
6. Nozzle exit area,  $A_e$

All six parameters were incrementally increased in value so as to retain scaling relative to the IAC HRE. One would not double only the fuel grain length while leaving everything else the same, as this would not truly be a larger version of the original engine, just a longer one. This detracted from a logical increase in size would hence leave performance results incomparable, and break any form of geometric similarity between the HREs. The expansion ratio for all nozzles was kept at a sensible 10:1 as all simulated firings were conducted at standard sea level and altitude conditions. For the main body of this study, all HREs were fired to an arbitrarily chosen 40% fuel consumption, and then terminated. The performance data in the following sections is recorded at the head end of the fuel. The data for firings up to propellant burn-out can be found in Appendix A; it should be noted that for this data, the regression rate ends early as the head end fuel port station is usually (unless otherwise specified) the first to be completely consumed.

### 3.1.1 IAC Rocket

The IAC N<sub>2</sub>O/HTPB HRE (shown below in Figure 6) is a convenient choice of a base HRE for this study. Being previously published for an earlier RU study, the IAC HRE is modelled and simulated in the RU QSHYB program. Provided below in Table 1 is a list of all specifications for the IAC HRE.

Parameter	Value
Fuel Grain Length (m)	0.24
Initial Fuel Port Diameter (m)	0.035
Chamber Wall Diameter (m)	0.127
Nozzle Throat Diameter (m)	0.01285
Nozzle Exit Diameter (m)	0.127
Oxidizer Mass Flow Rate (kg/s)	0.385
Expansion Ratio	10:1
Oxidizer	N <sub>2</sub> O
Fuel	HTPB
Stoichiometric Oxidizer-Fuel Ratio $r_{st}$	6.5
Initial Fuel Temperature (K)	294
Fuel Specific Heat (J/kg/K)	2100
n	0.33
Oxidizer Temperature and Head End Inlet (K)	2750
Flame Temperature (K)	2800
Burning Surface Temperature (K)	800
Gas Molecular Weight (AMU)	26
Gas Specific Heat (J/kg/K)	1920
Fuel Roughness Height (μm)	10

Table 1: IAC HRE Parameters [15]

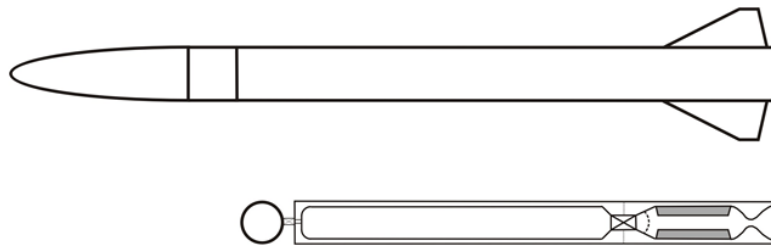


Figure 6: Schematic Diagram of the IAC N<sub>2</sub>O/HTPB HRE [15]

### 3.2 Sizing the Nozzle

It should be noted that the nozzle in this study was scaled differently versus the some of the other parameters. This was due to how nozzles are modelled in the simulation and the nature of how flows are modelled in a converging-diverging nozzle. For this study, a converging-diverging nozzle was modelled after classical isentropic flow relations under choked conditions. This equation can be provided as [16]:

$$\frac{A_t}{A_e} = \frac{Ma_e}{Ma_t} \left[ \frac{2 + (\gamma - 1)Ma_t^2}{2 - (\gamma - 1)Ma_e^2} \right]^{\frac{\gamma+1}{2(\gamma-1)}} \quad (34)$$

The QSHYB program takes into account the case where if the chamber pressures drops to the point that the nozzle throat no longer is choked, the firing terminates. Thus, unless specified in the results, the nozzle throat is choked with  $Ma_t$  equal to 1, and the specific heat ratio  $\gamma$  being that of the combustion gases. The derivation and basis of equation (34) stems from *area* ratios, and thus in order to maintain the same expansion ratio as the HRE was scaled up, the areas of the nozzle throat and exit were scaled up. This would not translate into a direct scaling of their diameters however, and so a small Matlab script was created in order to automate this process. The script can be found in Appendix B of this thesis.

### 3.3 Firing Results

This section provides the internal ballistic results plotted over time for the IAC HRE and subsequent scale-up HREs based on it.

#### 3.3.1 IAC HRE

The IAC HRE is the base model that is scaled up for all of the simulations reported later in this thesis. The graphs in this section are provided to show the baseline data, with the parameters provided in Table 1 from section 3.1.1.

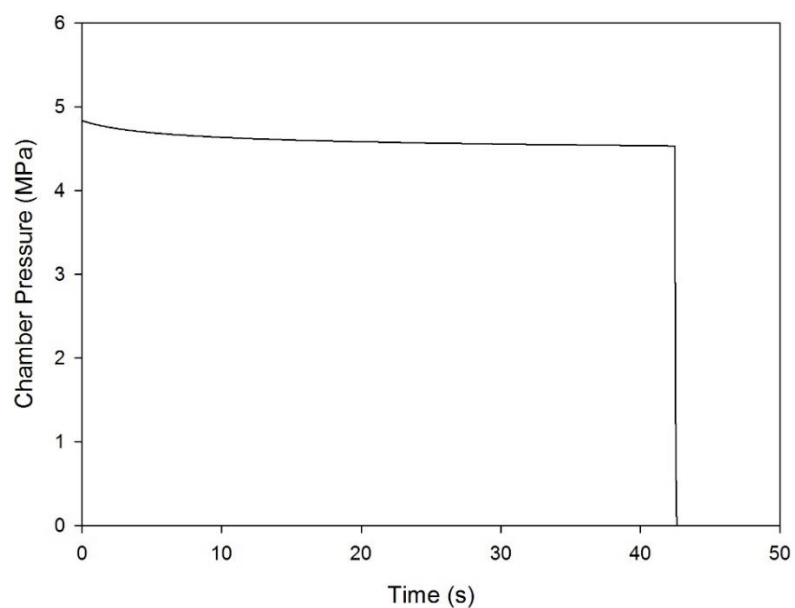


Figure 7: Chamber Pressure vs. Time for IAC HRE for 40% Fuel Consumption

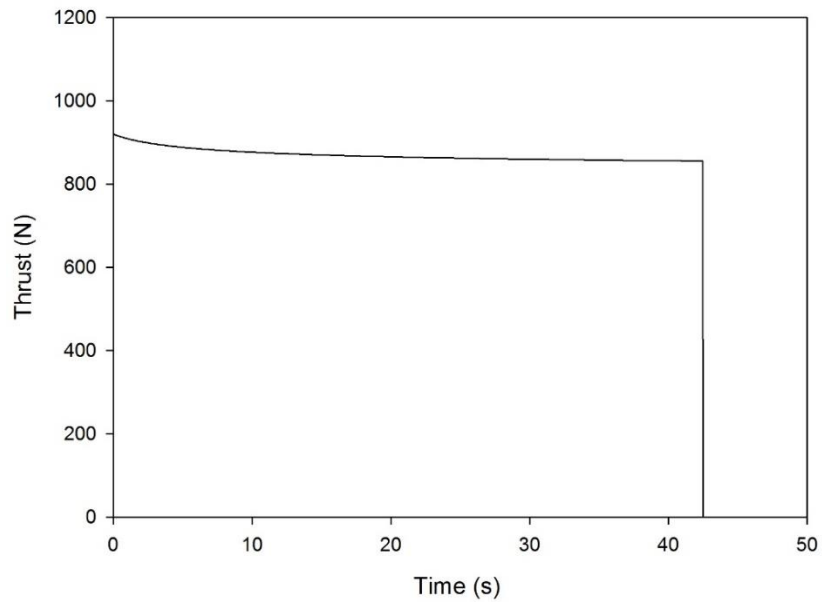


Figure 8: Thrust (Sea Level) vs. Time for IAC HRE for 40% Fuel Consumption

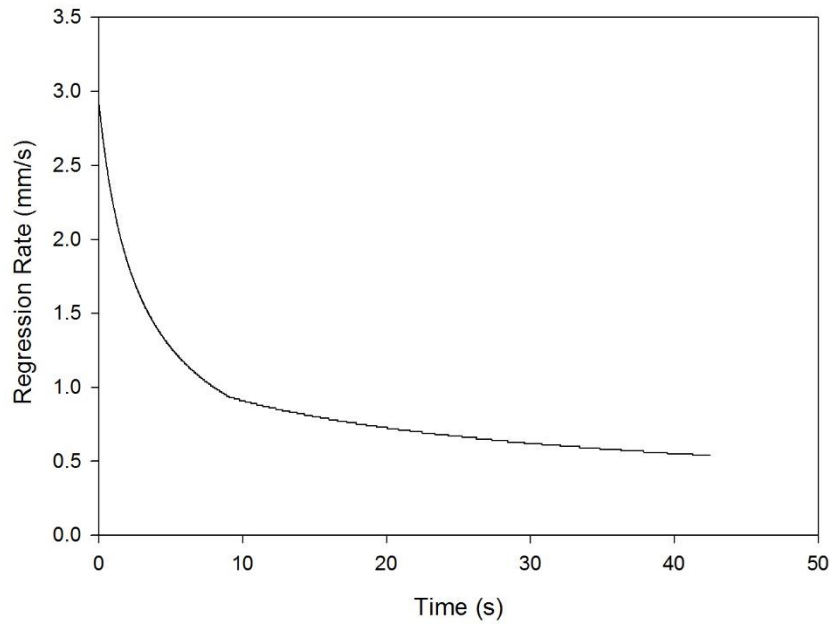


Figure 9: Regression Rate vs. Time, at the Head-End Fuel Port, for IAC HRE for 40% Fuel Consumption

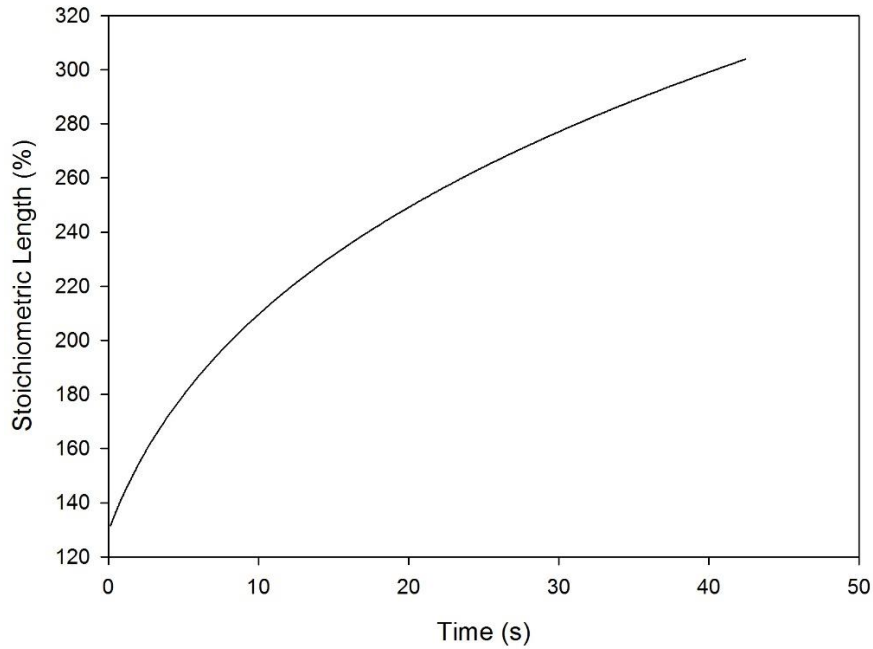


Figure 10: Stoichiometric Length vs. Time for IAC HRE for 40% Fuel Consumption

Parameter	Value
Mass of Unconsumed Fuel (kg)	1.5496
Total Impulse (N·s)	36947.1
Average Specific Impulse (s)	216.48
$c_{theo}^*$ (m/s)	1459.1
$c_{act}^*$ (m/s)	1457.5
Combustion Efficiency, $\eta_c$	99.8%

Table 2: IAC HRE Post-Firing Performance Values of Interest, for 40% Fuel Burn

It should be noted that the IAC HRE begins with a fuel grain length smaller than its stoichiometric length, by design (allows for interim command applications of swirl, which increases fuel burning rate and engine thrust, while shortening  $L_{st}$  during this swirl phase). In this case, under normal unthrottled operation, one would expect the stoichiometric length to increase as the firing progresses, as observed in Figure 10 above. In this case, equation (26) for stoichiometric length is not used, and instead an extrapolation is carried out within the QSHYB program to account for this case where the stoichiometric length is greater than 100%.

### 3.3.2 125% Scale Up

Parameter	Value
Fuel Grain Length (m)	0.3
Initial Fuel Port Diameter (m)	0.04375
Chamber Wall Diameter (m)	0.1587
Oxidizer Mass Flow Rate (kg/s)	0.4823
Nozzle Throat Diameter (m)	0.0144
Nozzle Exit Diameter (m)	0.0454

Table 3: Parameters for 125% HRE Scale Up

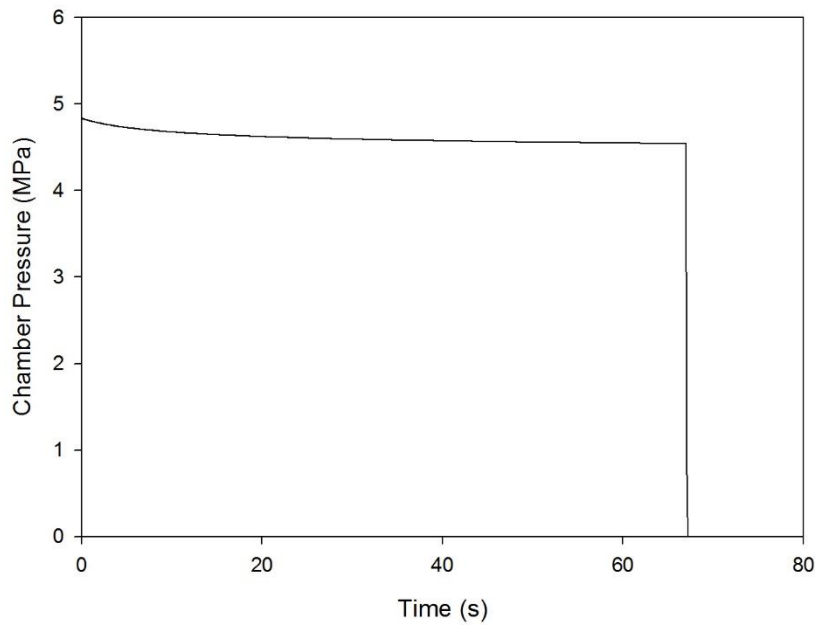


Figure 11: Chamber Pressure vs. Time for 125% Scale Up HRE for 40% Fuel Consumption

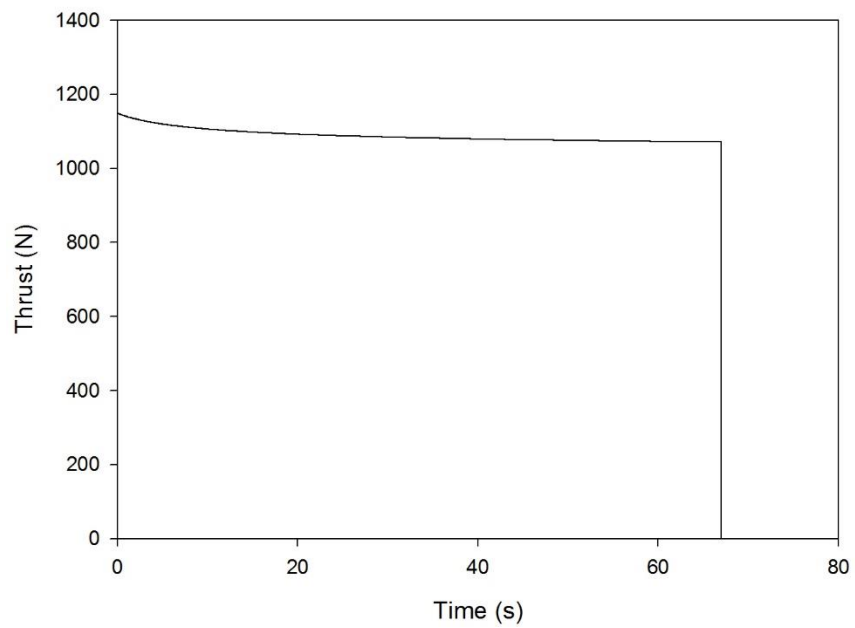


Figure 12: Thrust (Sea Level) vs. Time for 125% Scale Up HRE for 40% Fuel Consumption

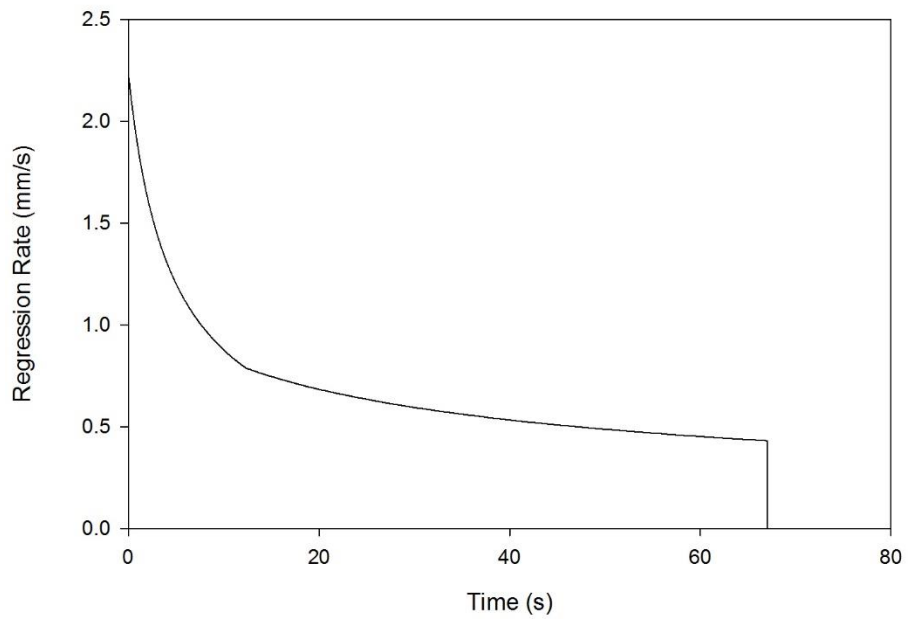


Figure 13: Regression Rate vs. Time, at the Head-End Fuel Port, for 125% Scale Up HRE for 40% Fuel Consumption

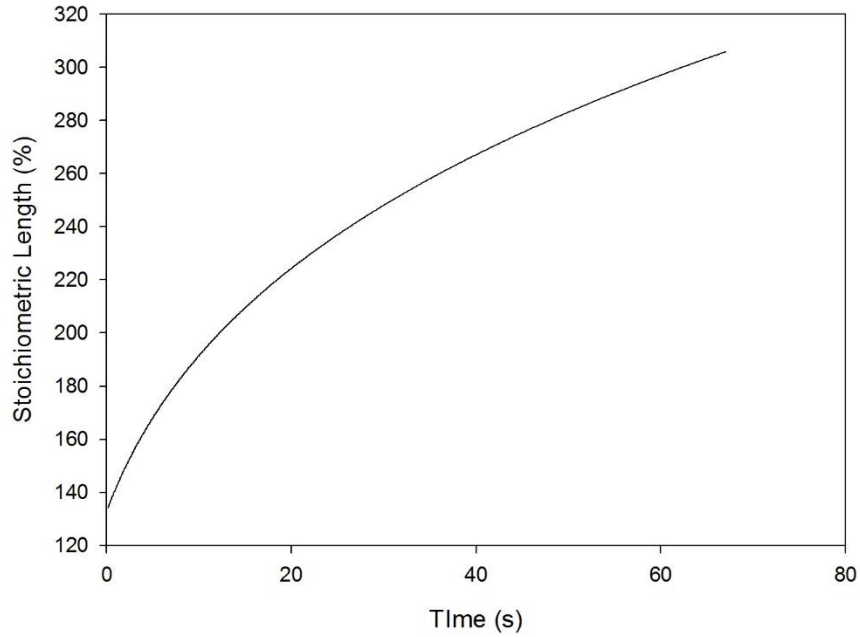


Figure 14: Stoichiometric Length vs. Time for 125% Scale Up HRE for 40% Fuel Consumption

Parameter	Value
Mass of Unconsumed Fuel (kg)	2.0174
Total Impulse (N·s)	72918.1
Average Specific Impulse (s)	216.48
$c_{theo}^*$ (m/s)	1459.1
$c_{act}^*$ (m/s)	1457.5
Combustion Efficiency, $\eta_c$	99.8%

Table 4: 125% Scale-Up HRE Post-Firing Performance Values of Interest, for 40% Fuel Burn

### 3.3.3 150% Scale Up

Parameter	Value
Fuel Grain Length (m)	0.36
Initial Fuel Port Diameter (m)	0.0525
Chamber Wall Diameter (m)	0.1905
Oxidizer Mass Flow Rate (kg/s)	0.5798
Nozzle Throat Diameter (m)	0.0157
Nozzle Exit Diameter (m)	0.0498

Table 5: Parameters for 150% HRE Scale Up

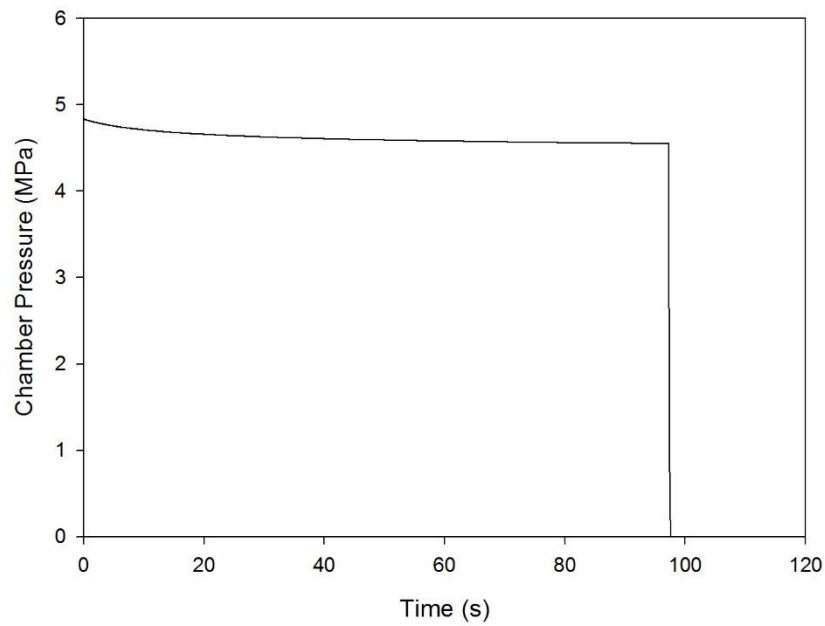


Figure 15: Chamber Pressure vs. Time for 150% Scale Up HRE for 40% Fuel Consumption

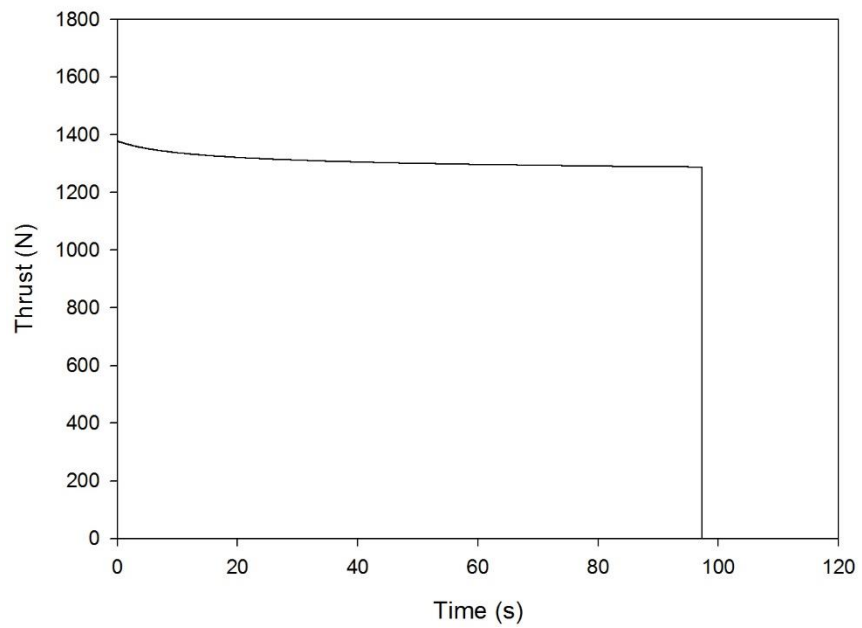


Figure 16: Thrust (Sea Level) vs. Time for 150% Scale Up HRE for 40% Fuel Consumption

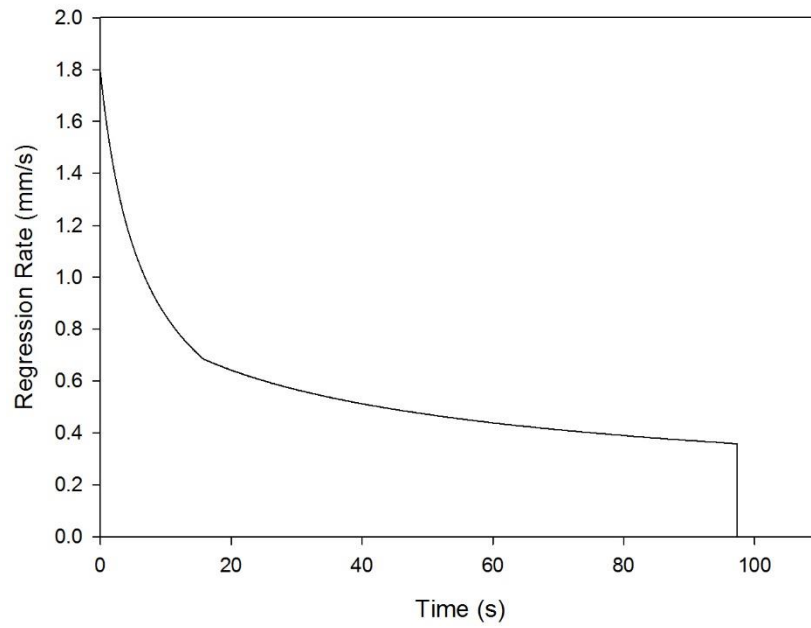


Figure 17: Regression Rate vs. Time, at the Head-End Fuel Port, for 150% Scale Up HRE for 40% Fuel Consumption

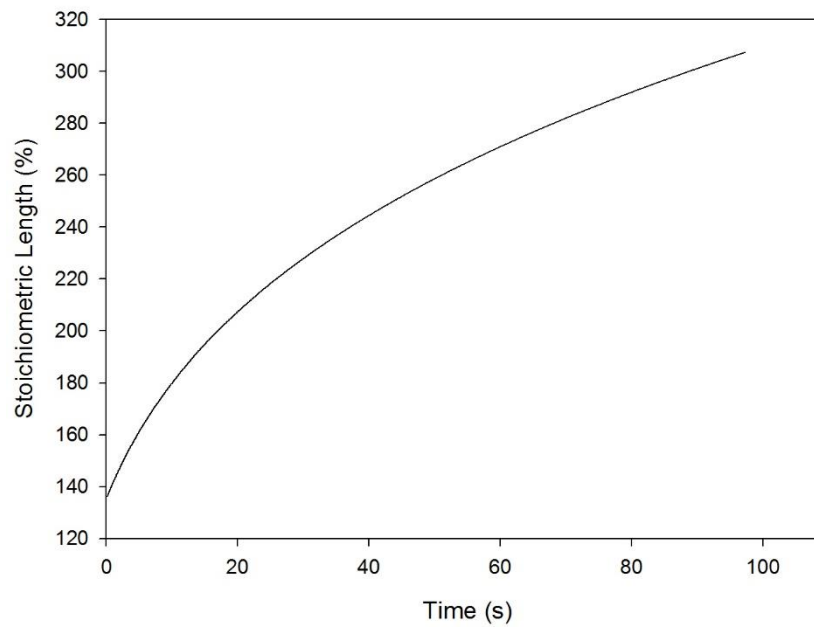


Figure 18: Stoichiometric Length vs. Time for 150% Scale Up HRE for 40% Fuel Consumption

Parameter	Value
Mass of Unconsumed Fuel (kg)	5.2337
Total Impulse (N·s)	127250.3
Average Specific Impulse (s)	216.52
$c_{theo}^*$ (m/s)	1459.1
$c_{act}^*$ (m/s)	1457.5
Combustion Efficiency, $\eta_c$	99.8%

Table 6: 150% Scale-Up HRE Post-Firing Performance Values of Interest, for 40% Fuel Burn

### 3.3.4 200% Scale Up

Parameter	Value
Fuel Grain Length (m)	0.48
Initial Fuel Port Diameter (m)	0.07
Chamber Wall Diameter (m)	0.254
Oxidizer Mass Flow Rate (kg/s)	0.775
Nozzle Throat Diameter (m)	0.0182
Nozzle Exit Diameter (m)	0.0575

Table 7: Parameters for 200% HRE Scale Up

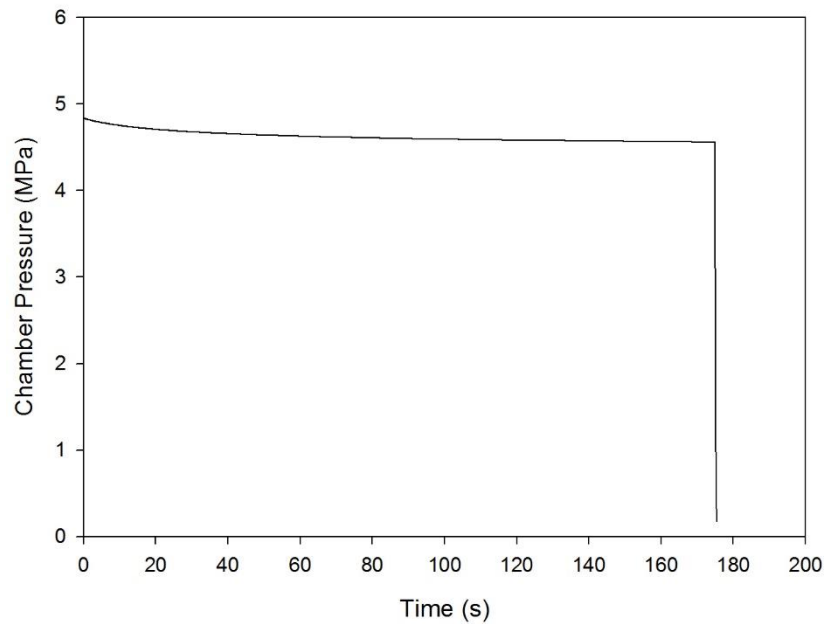


Figure 19: Chamber Pressure vs. Time for 200% Scale Up HRE for 40% Fuel Consumption

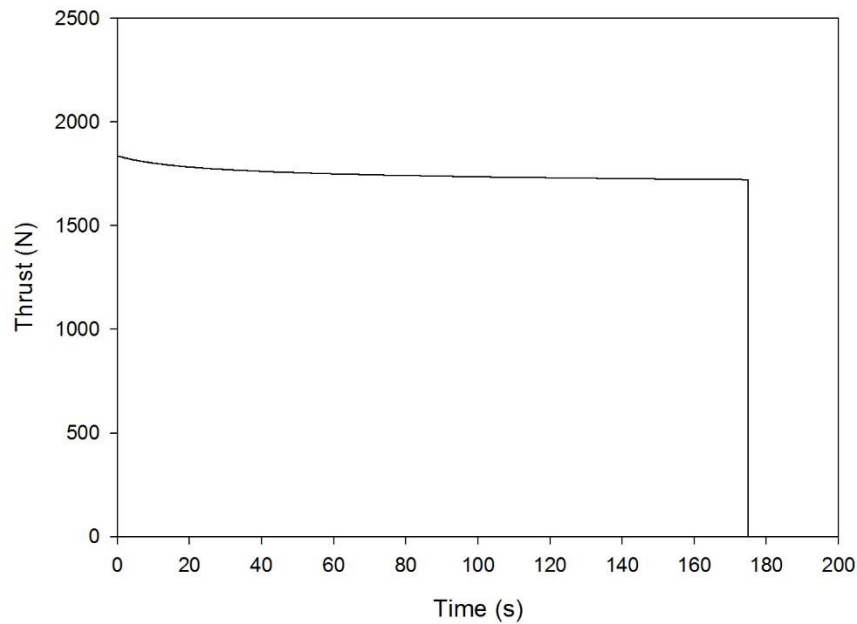
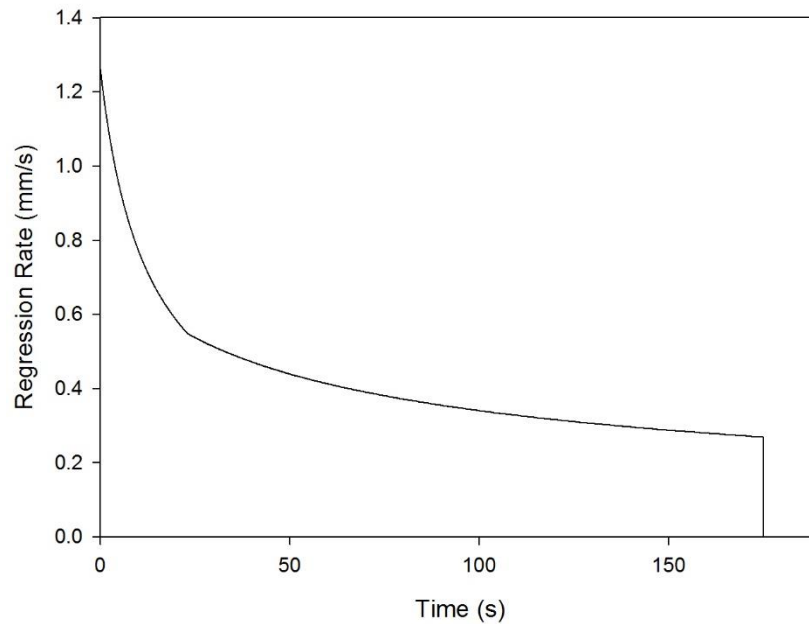


Figure 20: Thrust (Sea Level) vs. Time for 200% Scale Up HRE for 40% Fuel Consumption

At this point in the sizing process, it has become clear that so far, thrust is scaling linearly with size. In Figure 20 above, the curve begins at thrust of 1835 N and plateaus at roughly 1750N. Compared to the IAC HRE's starting and plateau thrust of 919 N and 855 N, respectively, the thrust results for the 200% scale-up are very close to being double that of the IAC HRE's. The 125% and 150% HREs are also consistent with this linear trend. Going back the chapter 1, thrust for a rocket is typically a function of thrust coefficient, chamber pressure, and nozzle throat area ( $F \cong C_F p_c A_t$ ). This linearity observed so far result should come as little surprise considering the chamber pressure is being held constant for all scale up HREs, and that the nozzle throat area is being scaled up alongside all of the other parameters. With that in mind, thrust can be approximated to be mostly a function of nozzle throat area,  $F \sim f(A_t)$ .



*Figure 21: Regression Rate vs. Time, at the Head-End Fuel Port, for 200% Scale Up HRE for 40% Fuel Consumption*

Looking at the beginning of the firings for the IAC (Figure 9) and 200% scale up HRE (above), the regression rate is beginning to show the start of a non-linear trend (one should not expect any linearity to retain in such a highly coupled model). Whereas the IAC HRE's head-end fuel port began with a regression rate of 2.4 mm/s, the 200% scale-up HRE begins at 1.26 mm/s, being almost half of the IAC regression rate at the start of firing. Of course, the regression rate has been reduced in most part due to the doubling of the fuel port diameter, thereby reducing the mass flux  $G$  the fuel port would see relative to the original IAC case.

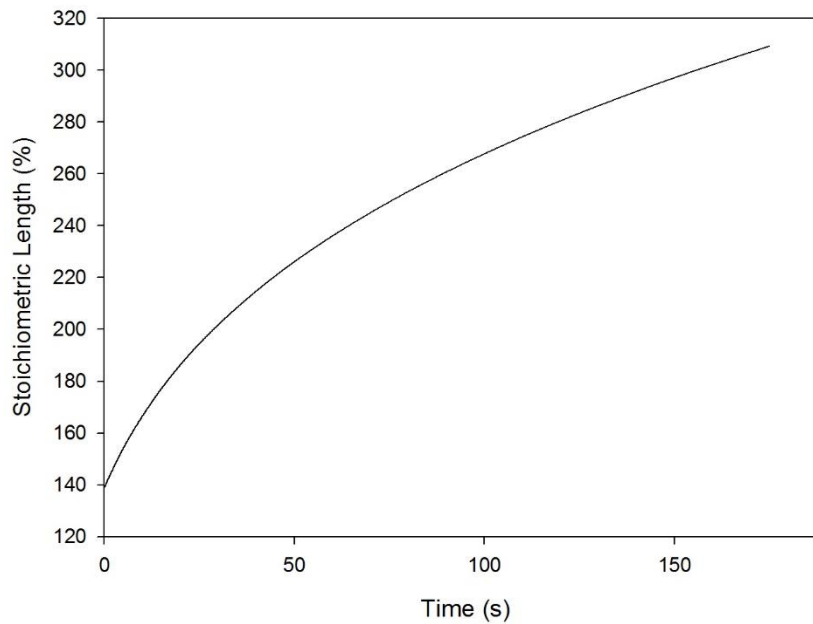


Figure 22: Stoichiometric Length vs. Time for 200% Scale Up HRE for 40% Fuel Consumption

As expected, the IAC HRE’s design feature of having a fuel grain length smaller than the stoichiometric length has carried over into the scaled-up HRE. For this HRE, the increase over the IAC has been marginal, on the order of a 5% difference between the two at the end of firing. In the QSHYB program, as previously mentioned, a HRE with a fuel grain length smaller than the stoichiometric length will have an extrapolation applied. This does not take into account the effect the oxidizer-rich core flow has on cooling the core flow, and thus the values provided are not fully indicative of how far  $L_{st}$  goes beyond the fuel grain length. Therefore, curves such as those in Figure 22 are conservative, but still illustrative of what kind of increases in stoichiometric length one would expect over the course of a firing.

Parameter	Value
Mass of Unconsumed Fuel (kg)	12.3878
Total Impulse (N·s)	305717.5
Average Specific Impulse (s)	216.55
$c_{theo}^*$ (m/s)	1459.1
$c_{act}^*$ (m/s)	1457.5
Combustion Efficiency, $\eta_c$	99.8%

Table 8: 200% Scale-Up HRE Post-Firing Performance Values of Interest, for 40% Fuel Burn

### 3.3.5 400% Scale Up

Parameter	Value
Fuel Grain Length (m)	0.96
Initial Fuel Port Diameter (m)	0.14
Chamber Wall Diameter (m)	0.508
Oxidizer Mass Flow Rate (kg/s)	1.558
Nozzle Throat Diameter (m)	0.0257
Nozzle Exit Diameter (m)	0.0813

Table 9: Parameters for 400% HRE Scale Up

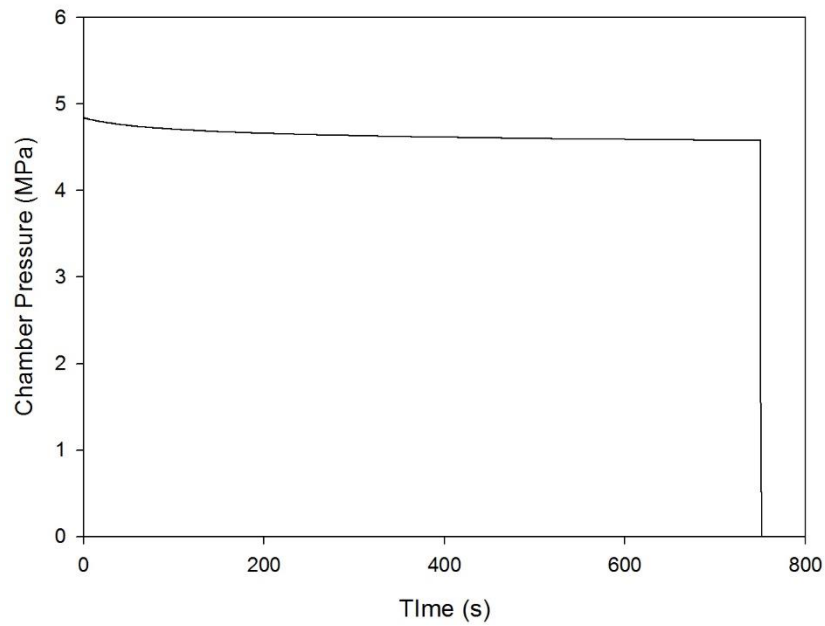


Figure 23: Chamber Pressure vs. Time for 400% Scale Up HRE for 40% Fuel Consumption

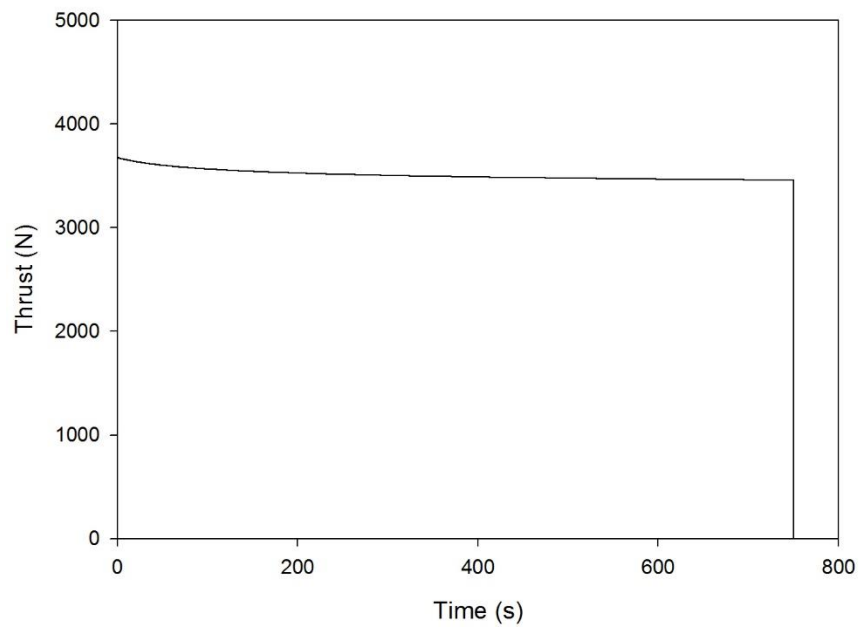


Figure 24: Thrust (Sea Level) vs. Time for 400% Scale Up HRE for 40% Fuel Consumption

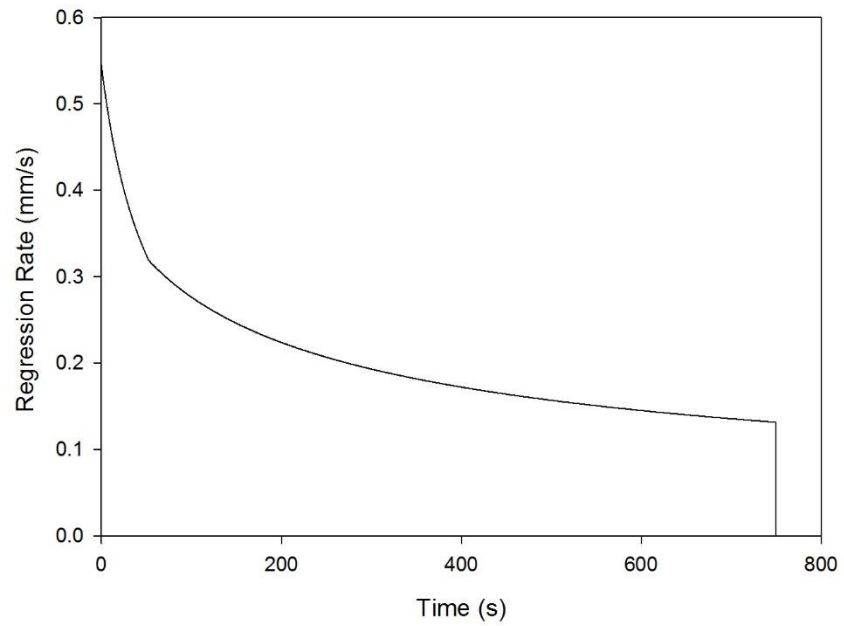


Figure 25: Regression Rate vs. Time, at the Head-End Fuel Port, for 400% Scale Up HRE for 40% Fuel Consumption

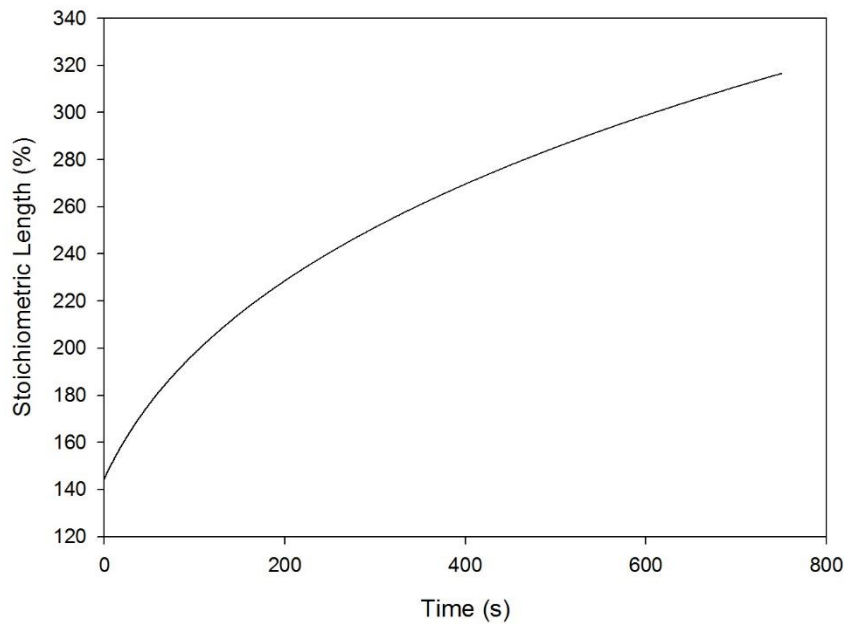


Figure 26: Stoichiometric Length vs. Time for 400% Scale Up HRE for 40% Fuel Consumption

Parameter	Value
Mass of Unconsumed Fuel (kg)	96.06
Total Impulse (N·s)	2630213.5
Average Specific Impulse (s)	216.60
$c_{theo}^*$ (m/s)	1459.1
$c_{act}^*$ (m/s)	1457.5
Combustion Efficiency, $\eta_c$	99.8%

Table 10: 400% Scale-Up HRE Post-Firing Performance Values of Interest, for 40% Fuel Burn

### 3.3.6 600% Scale Up

Parameter	Value
Fuel Grain Length (m)	1.44
Initial Fuel Port Diameter (m)	0.21
Chamber Wall Diameter (m)	0.762
Oxidizer Mass Flow Rate (kg/s)	2.340
Nozzle Throat Diameter (m)	0.0315
Nozzle Exit Diameter (m)	0.01

Table 11: Parameters for 600% HRE Scale Up

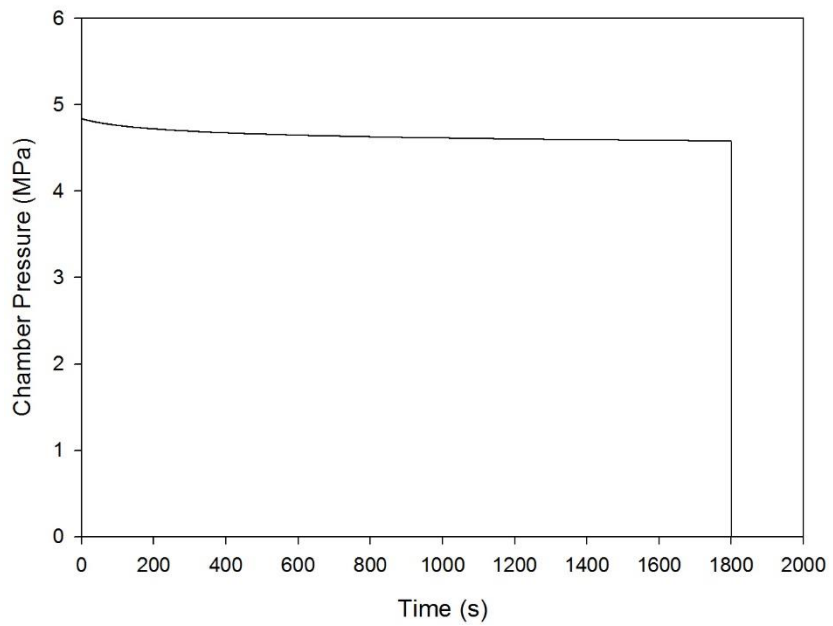


Figure 27: Chamber Pressure vs. Time for 600% Scale Up HRE for 40% Fuel Consumption

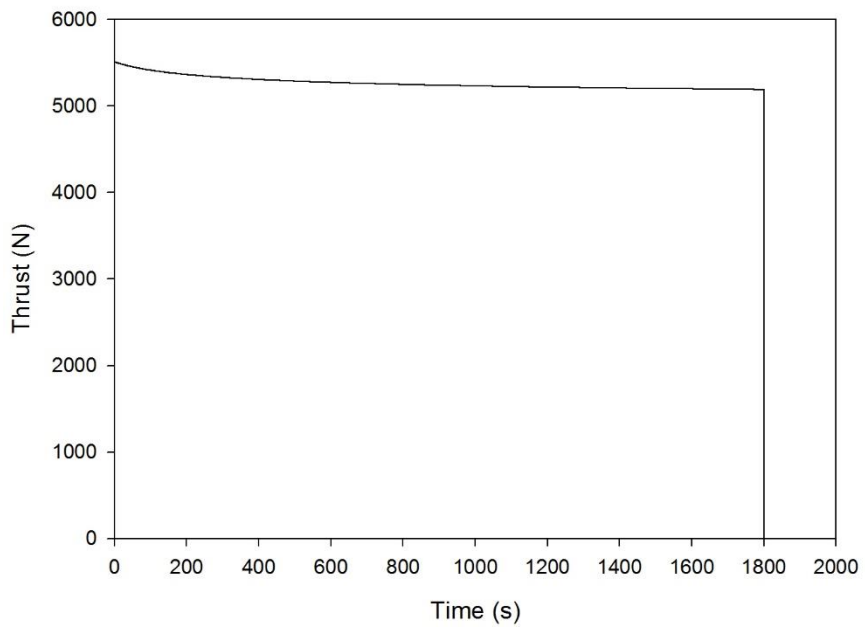


Figure 28: Thrust (Sea Level) vs. Time for 600% Scale Up HRE for 40% Fuel Consumption

Once again, the thrust for a rocket six times larger than the reference model is very close to being about 6 times larger in magnitude. Compared to the IAC HRE's starting and plateau thrust of 919 N and 855 N, respectively, the thrust results for the 600% scale-up are very close to being six times that of the IAC HRE's, with 5500 N at the peak and roughly 5250 N at in the plateau in Figure 28.

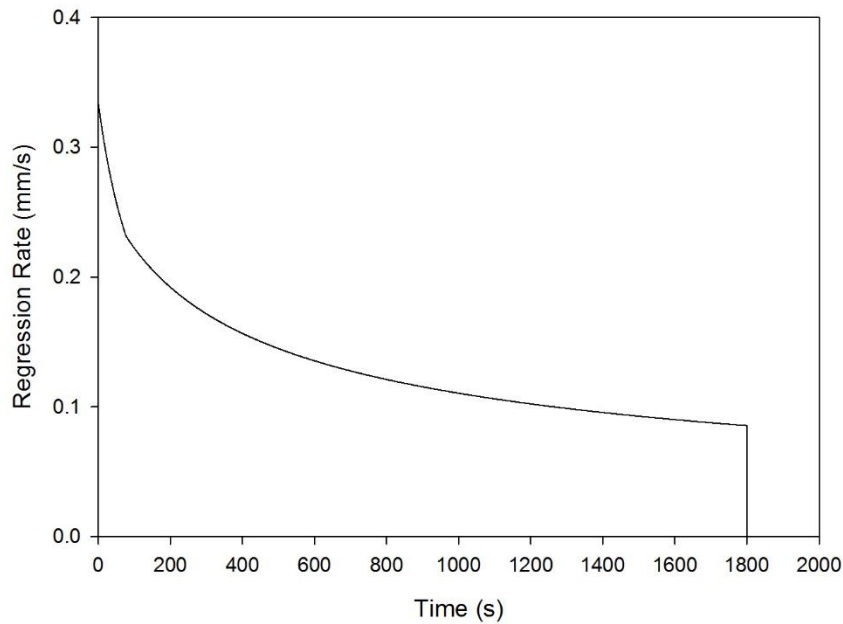


Figure 29: Regression Rate vs. Time, at the Head-End Fuel Port, for 600% Scale Up HRE for 40% Fuel Consumption

At this HRE size, the linearity observed in the head-end fuel port regression rate at the 200% scale has broken down, expectedly. Comparing the regression rate chart data between the IAC (Figure 9) and the 600% scale HRE (above), the regression rate for this HRE is almost nine times smaller in magnitude between the two at the start of firing, and roughly eight times less at the end. Looking back at the transpiration equations in section 2.1.4, it is very clear that port diameter plays a crucial role in the convective heat feedback model. However, for the 600% scale up, this diameter has only increased six-fold. A compounding effect from the Reynolds number for this port will also decrease, along with the mass flux, further compounding a reduction in friction factor, and hence a reduction in convective heat transfer.

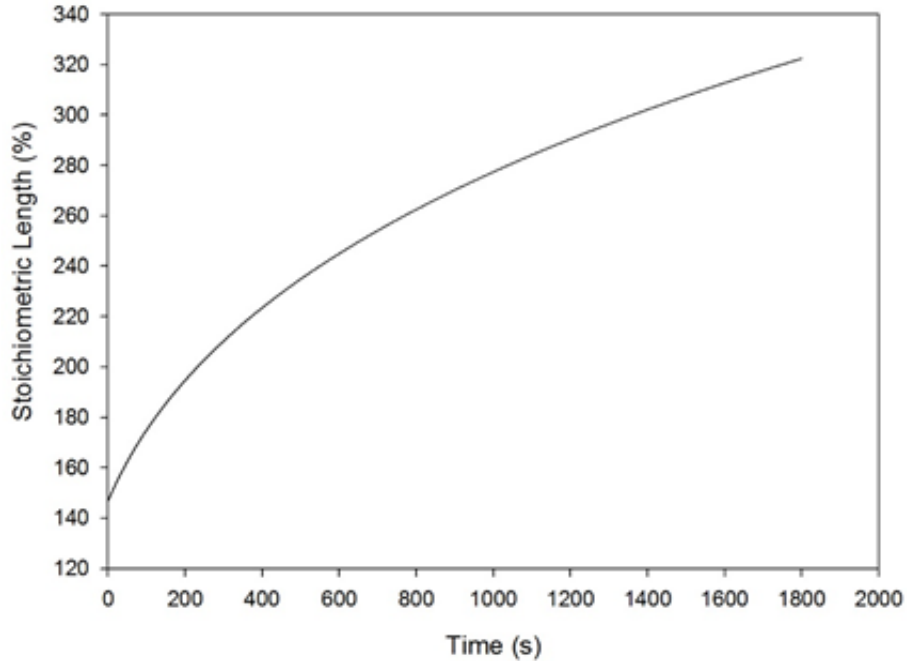


Figure 30: Stoichiometric Length vs. Time for 600% Scale Up HRE for 40% Fuel Consumption

As the HREs are increasing in size, their fuel port cross section area is increasing exponentially (since it is their *diameter* that is being scaled up). As all of the HREs are running with more oxidizer than they require (the fuel grain lengths are longer than the stoichiometric length) a portion of that oxidizer is not reacting, but eventually travels to the end of the HRE and is exhausted. This unreacted portion of oxidizer, a component of the core flow, is cooler than the combustion gases; at the smaller HRE scales, it is thought that its contribution in lower core flow temperature, and hence, the temperature available to drive the transpiration process further down the core, was not as significant as it may be at this scale. However, with a much larger fuel core, it is evident that as the port widens relatively quickly in the initial part of the firing, there comes a point where this cooler central axial core flow of oxidizer begins contributing in slowing down the regression rate further. Combined with a larger zone in the central core to have a mass flow of cooler oxidizer, of which there is an abundance all the way through the 600% scaled up HRE, confirmed via Figure 30, there are several coupled processes at play lowering the regression rate.

As a quick summary, driven by the port diameter increase, the regression rate at the 600% scale has lost its linearity in scaling possibly due a coupled effect of cooler unreacted oxidizer in the fuel port flow that is removing energy that is driving the transpiration process, further reducing mass generation from the burning fuel surface below, and hence not contributing as much to the overall mass flux within the fuel port as it would have at the smaller scales. One way to correct for this trend has so far been to slightly increase the oxidizer mass flow rate. More of this will be discussed in section 3.4.1.

Parameter	Value
Mass of Unconsumed Fuel (kg)	334.8
Total Impulse (N·s)	9211541.9
Average Impulse (s)	216.60
$c_{theo}^*$ (m/s)	1459.1
$c_{act}^*$ (m/s)	1457.5
Combustion Efficiency, $\eta_c$	99.8%

Table 12: 600% Scale-Up HRE Post-Firing Performance Values of Interest, for 40% Fuel Burn

### 3.3.7 800% Scale Up

Parameter	Value
Fuel Grain Length (m)	1.92
Initial Fuel Port Diameter (m)	0.28
Chamber Wall Diameter (m)	1.016
Oxidizer Mass Flow Rate (kg/s)	3.122
Nozzle Throat Diameter (m)	0.0364
Nozzle Exit Diameter (m)	0.115

Table 13: Parameters for 800% HRE Scale Up

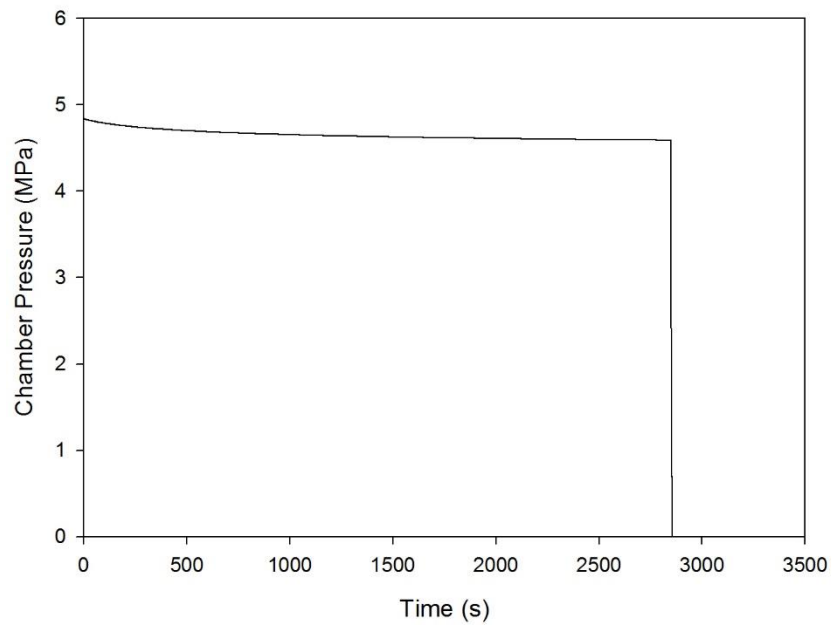


Figure 31: Chamber Pressure vs. Time for 800% Scale Up HRE for 40% Fuel Consumption

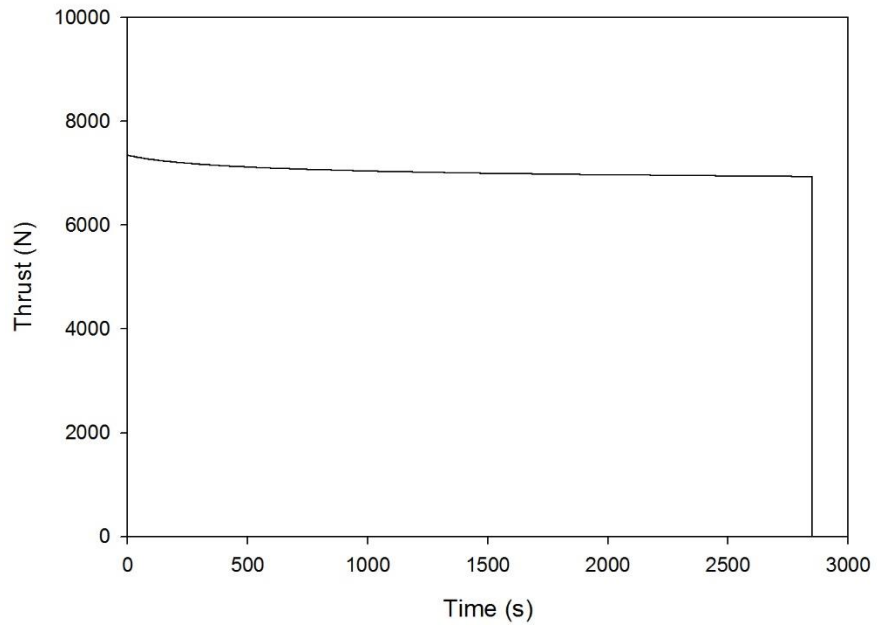


Figure 32: Thrust (Sea Level) vs. Time for 800% Scale Up HRE for 40% Fuel Consumption

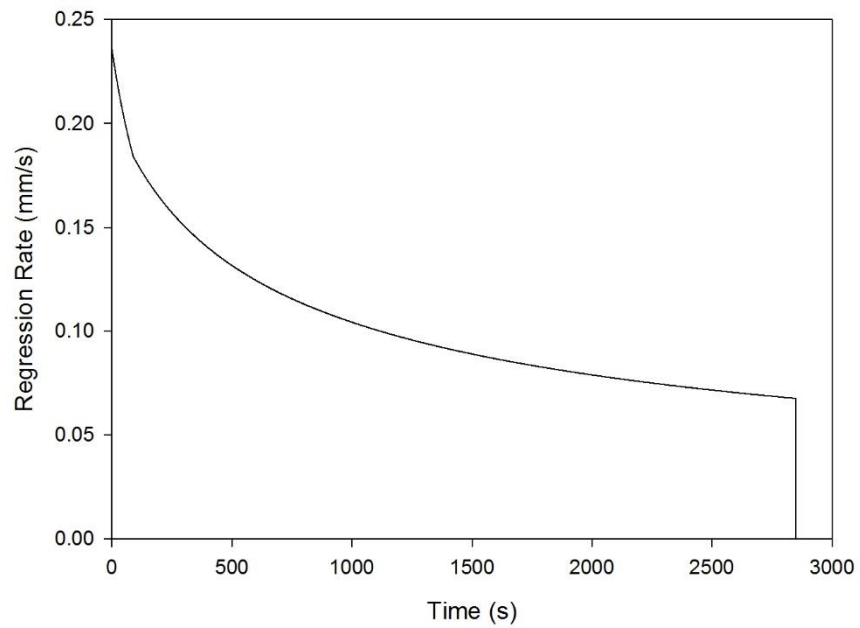


Figure 33: Regression Rate vs. Time, at the Head-End Fuel Port, for 800% Scale Up HRE for 40% Fuel Consumption

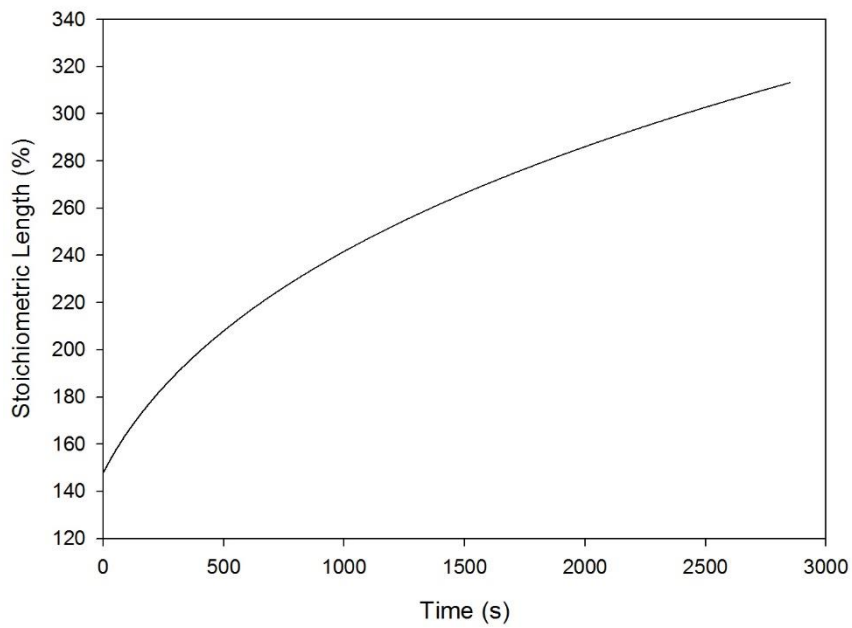


Figure 34: Stoichiometric Length vs. Time for 800% Scale Up HRE for 40% Fuel Consumption

Parameter	Value
Mass of Unconsumed Fuel (kg)	792.47
Total Impulse (N·s)	20038270.1
Average Specific Impulse (s)	216.64
$c_{theo}^*$ (m/s)	1459.1
$c_{act}^*$ (m/s)	1457.5
Combustion Efficiency, $\eta_c$	99.8%

Table 14: 800% Scale-Up HRE Post-Firing Performance Values of Interest, for 40% Fuel Burn

### 3.3.8 1000% Scale Up

Parameter	Value
Fuel Grain Length (m)	2.4
Initial Fuel Port Diameter (m)	0.35
Chamber Wall Diameter (m)	1.27
Oxidizer Mass Flow Rate (kg/s)	3.9
Nozzle Throat Diameter (m)	0.0406
Nozzle Exit Diameter (m)	0.1285

Table 15: Parameters for 1000% HRE Scale Up

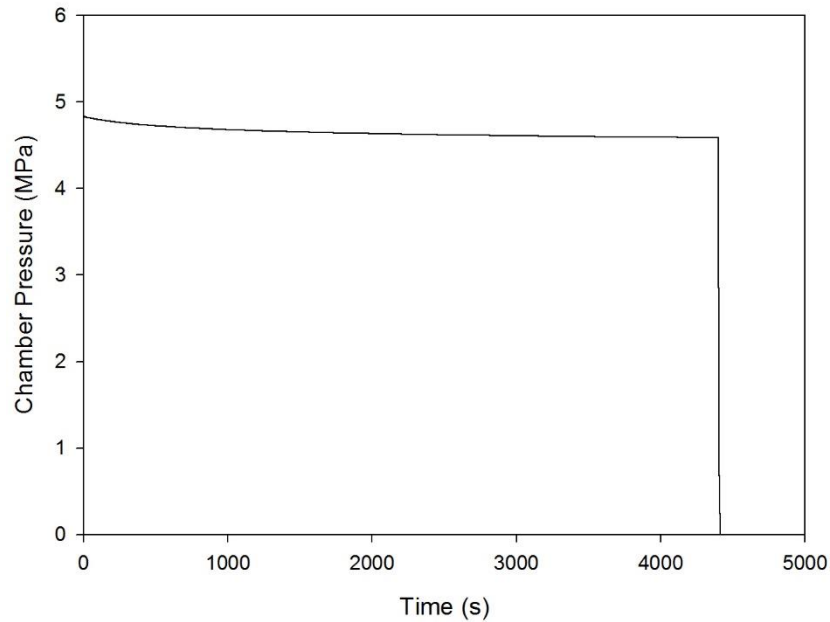


Figure 35: Chamber Pressure vs. Time for 1000% Scale Up HRE for 40% Fuel Consumption

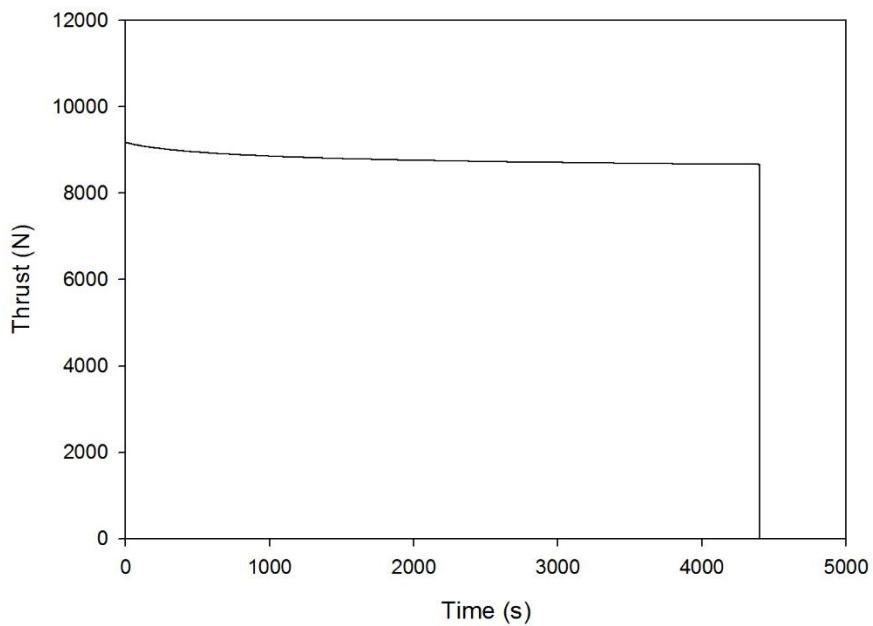


Figure 36: Thrust (Sea Level) vs. Time for 1000% Scale Up HRE for 40% Fuel Consumption

The thrust results in Figure 36 above confirm that, for the IAC HRE, scaling it up to at least ten times its original size, while retaining the same chamber pressure profile and nozzle scaling, will yield a ten-fold increase in thrust. A conclusion can be made that, with these restrictions in mind for the case of the IAC HRE being scaled up, thrust increases linearly with scale.

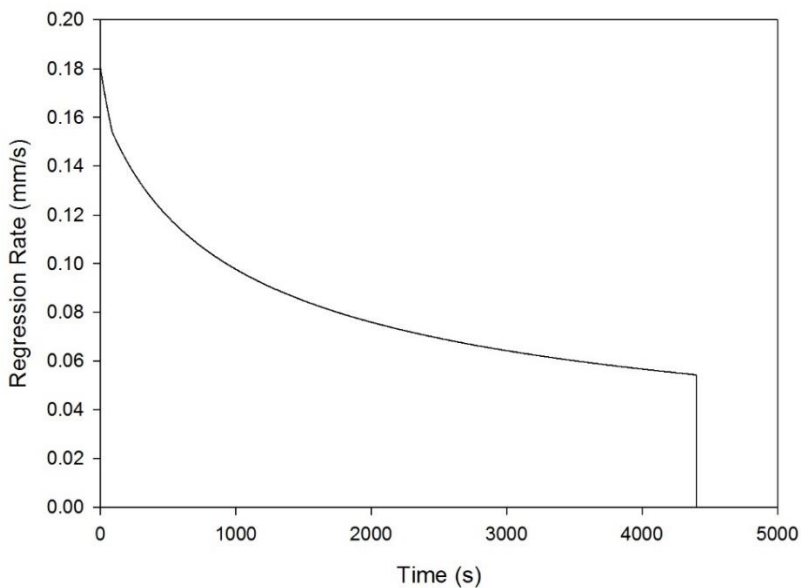


Figure 37: Regression Rate vs. Time, at the Head-End Fuel Port, for 1000% Scale Up HRE for 40% Fuel Consumption

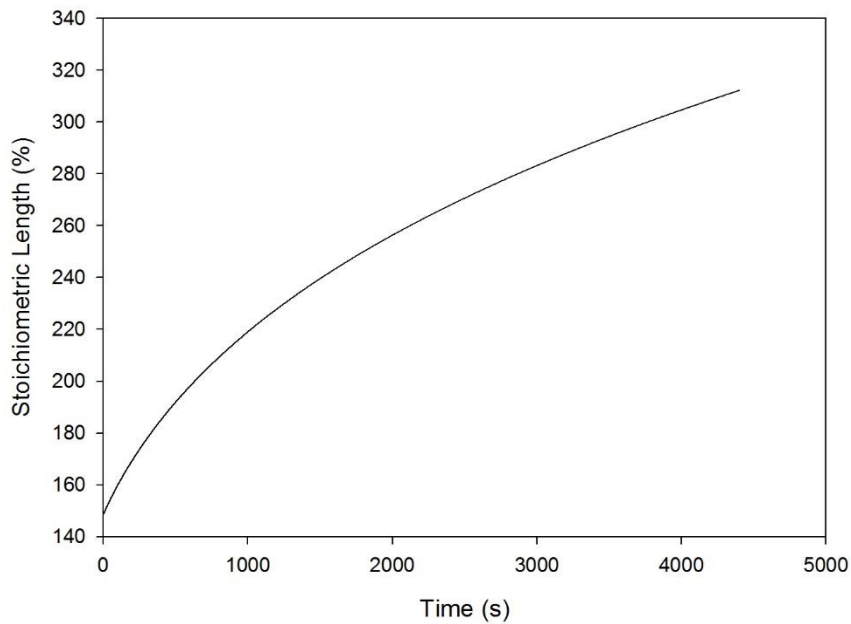


Figure 38: Stoichiometric Length vs. Time for 1000% Scale Up HRE for 40% Fuel Consumption

Overall, scaling the IAC HRE to ten times its original size yields an increase in stoichiometric length percentage of about 10% (305% for the small IAC HRE, versus about 315% observed in Figure 38). Again, this increase is expected, but as discussed for the 200% scale up stoichiometric length results, conservative given it is an extrapolation.

Parameter	Value
Mass of Unconsumed Fuel (kg)	1558.9927
Total Impulse (N·s)	38647504.4
Average Specific Impulse (s)	216.64
$c_{theo}^*$ (m/s)	1459.1
$c_{act}^*$ (m/s)	1457.5
Combustion Efficiency, $\eta_c$	99.8%

Table 16: 1000% Scale-Up HRE Post-Firing Performance Values of Interest, for 40% Fuel Burn

### 3.3.9 Combined Results for all Scales

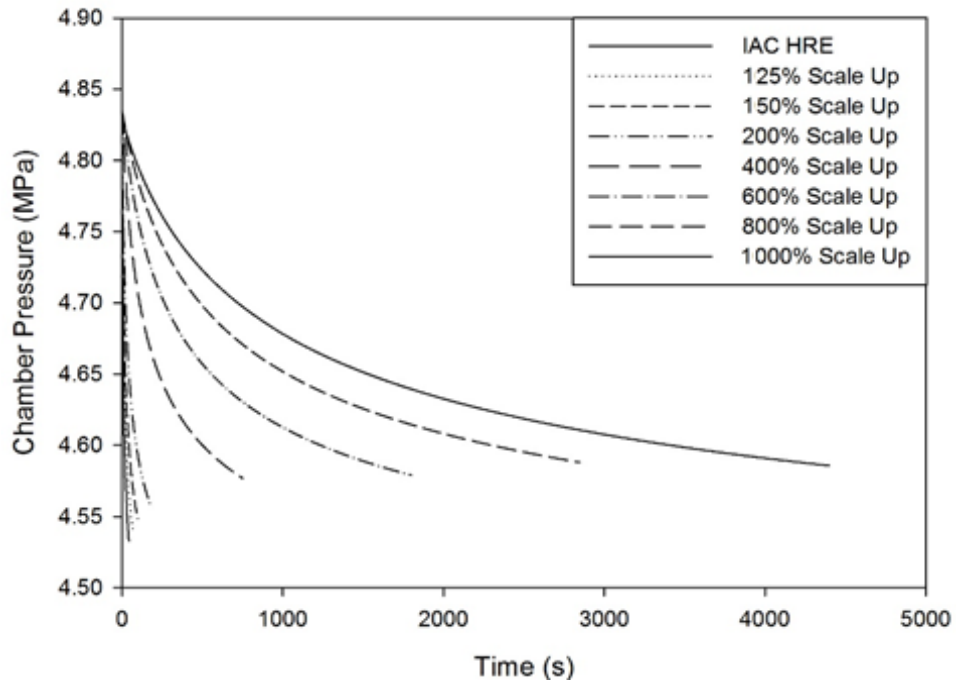


Figure 39: Chamber Pressure vs. Time for All HRE Scales for 40% Fuel Consumption

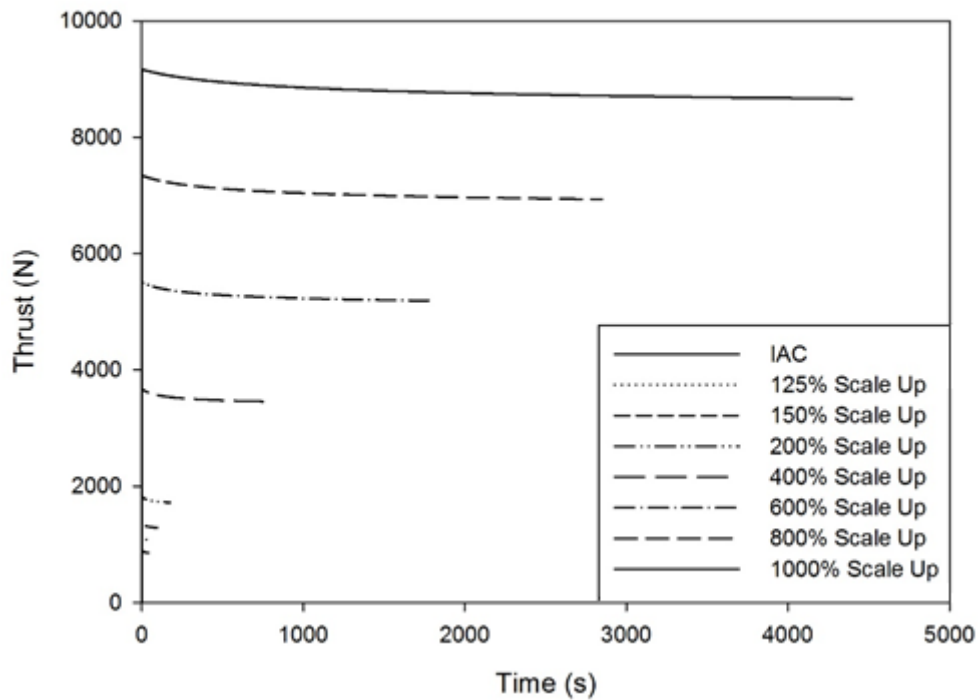


Figure 40: Thrust (Sea Level) vs. Time for all HRE Scales for 40% Fuel Consumption

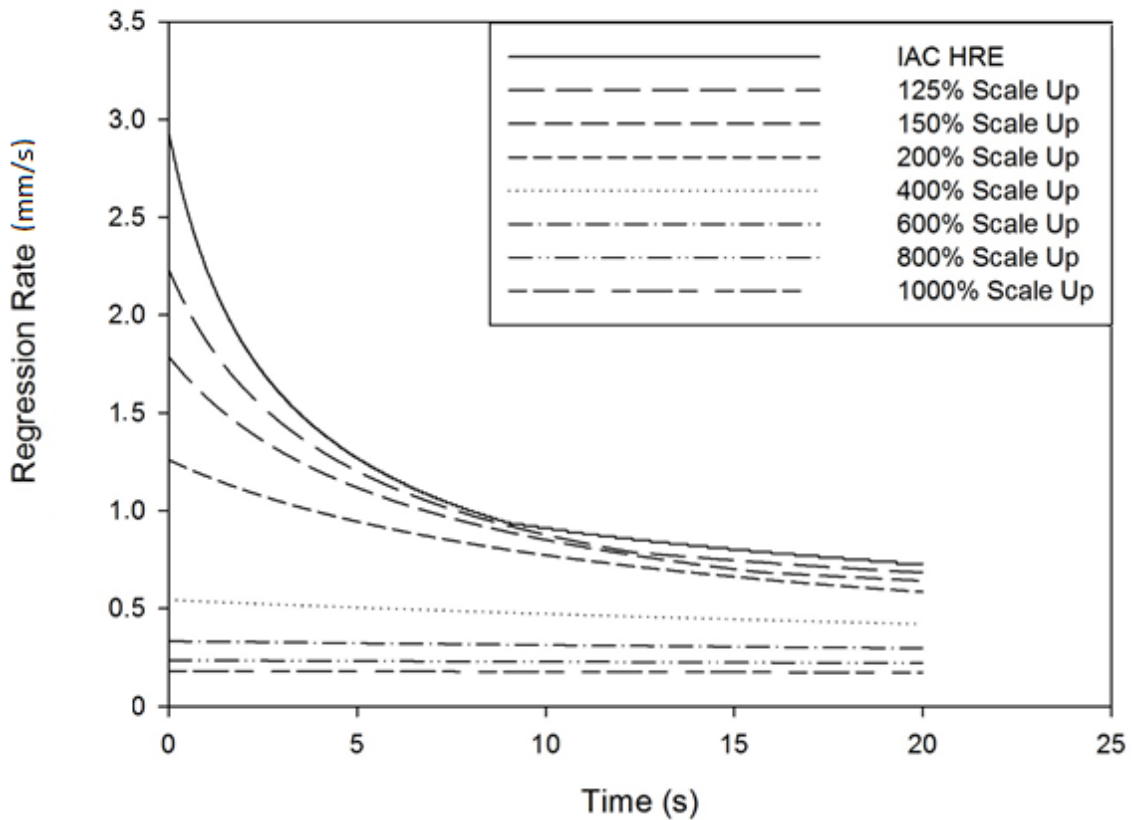


Figure 41: Regression Rate vs. Time, at the head-end fuel port, for all HRE Scales for 40% Fuel Consumption, here shown for the first 20 seconds of firing to better show trends

Figure 40 clearly shows a linear scaling of thrust for the HREs as they are scaled up, thereby confirming that for this study, thrust for the HRE's is predominantly a function of nozzle throat area. Seeing all of the HRE scale regression rate trends in Figure 41 shows the regression rates breaking down in linearity initially, especially between the 150% and 400% scales, however the all tend to being to converge towards each other well into their firings.

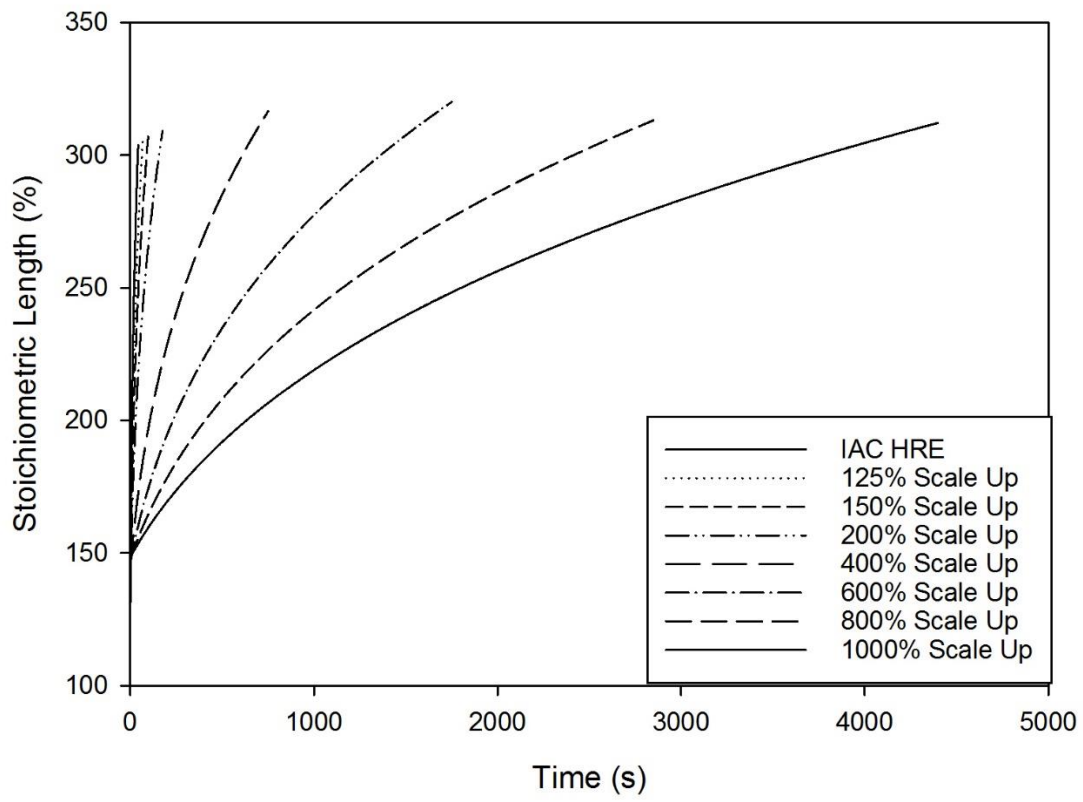


Figure 42: Stoichiometric Length vs. Time, for all HRE Scales for 40% Fuel Consumption

## 4. Discussion of Results

### 4.1 Pressure-Time Curves and Required Oxidizer Mass Flow Rate

As the goal of this study is to benchmark scaled HREs, there needed to be one constant value held throughout all of the firings. Chamber pressure was chosen to be this control variable, however chamber pressure is not a constant value over the course of a firing. For these simulations, as the firing progresses, the chamber pressure of a HRE decreases gradually since the oxidizer mass flow rate is constant<sup>1</sup>. The first point of comparison was the beginning of the firings. At this starting point, the chamber pressure for the reference HRE was about 4.833 MPa. In this case, the other HREs needed to also begin their firings at this chamber pressure. The comparison point was taken at 0.3 seconds into the firing, since the first entry in the results was an initial guess in the program, and the second the result of that guess. This was due to the fact that the program initially needs a chamber pressure starting point estimate (provided in an input file) to begin its iterations. Chamber pressure did not remain exactly the same as the HREs were scaled up, and so a parameter that could be changed without violating relative physical scaling needed to be chosen.

Looking back at what was changed as the engines were scaled up, most of the parameters needed to stay fixed in order to retain geometric similarity and scale. Technically, the nozzle throat could be adjusted in order to adjust chamber pressure; however, that would have a domino effect on mass flux, thrust, and expansion ratio. The answer to this issue was the oxidizer mass flow rate, as chamber pressure depends on it. Initially, changing the oxidizer mass flow rate from the scaled value raised some concern. The fear was that it would deviate too much from its scaled value, and then cause larger deviations on the regression rate, especially at the head end where the data was being recorded. However, in the end it was discovered that changes required were rather small. For all HRE scaled up HREs, it was found that slight *increases*, on the order of less than 2% relative to the calculated value, in the oxidizer mass flow rate from the nominal scaled up variant were required to keep the starting chamber pressure close to 4.833 MPa.

---

<sup>1</sup> The oxidizer mass flow rate is scaled accordingly as the HRE sizes move up, however it is not dynamic during the firing

<b>Oxidizer Mass Flow Rate (kg/s)</b>	<b>Calculated Value</b>	<b>Actual Value Used</b>	<b>% Difference Between Calculated and Actual Oxidizer Mass Flow Rate</b>
<b>125% Scale Up</b>	0.4812	0.4823	0.228%
<b>150% Scale Up</b>	0.5775	0.5798	0.397%
<b>200% Scale Up</b>	0.77	0.7750	0.647%
<b>400% Scale Up</b>	1.54	1.558	1.162%
<b>600% Scale Up</b>	2.31	2.340	1.290%
<b>800% Scale Up</b>	3.08	3.122	1.354%
<b>1000% Scale Up</b>	3.85	3.9	1.291%
<b>HRE Size</b>	<b>Chamber Pressure (MPa) at 40% Fuel Consumption</b>		<b>% Difference Relative to Reference HRE</b>
<b>Reference HRE</b>	4.5327		-
<b>125% Scale Up</b>	4.5407		0.176%
<b>150% Scale Up</b>	4.5483		0.344%
<b>200% Scale Up</b>	4.4579		1.650%
<b>400% Scale Up</b>	4.5769		0.970%
<b>600% Scale Up</b>	4.5789		1.014%
<b>800% Scale Up</b>	4.5879		1.210%
<b>1000% Scale Up</b>	4.5856		1.160%

*Table 17: Error percentage table for calculated versus required oxidizer mass flow rates and chamber pressure at 40% fuel consumption relative to reference HRE, for all HREs*

It is interesting to note that despite these changes to oxidizer mass flow rate being on the order of very small percentages from their scaled calculated value (less than 2% in the most extreme cases), they did manage to have a more significant effect on the chamber pressure. Without these seemingly miniscule increases to oxidizer mass flow rate, chamber pressures typically started at around 4% below the 4.833 MPa mark. The effect the oxidizer flow in the central part of the core had on the overall ballistic performance was the main reason the oxidizer mass flow rate had to be slightly increased for all HRE scales. As the HREs were shorter than

required to reach stoichiometric length, the unreacted oxidizer in the core flow would tend to slow down the transpiration process via its cooler temperature. The oxidizer in the QSHYB program was modelled very conservatively to enter the port at a temperature slightly below that of the flame. A mitigation to account for a cooler injection is to increase the oxidizer mass flow rate, as discussed. As all HREs had stoichiometric lengths larger than their fuel grain lengths, all would need a slight oxidizer mass flow rate increase (as they did) and would need larger ones for the larger scales (as observed). In this thesis however, this conservative reduction in incoming oxidizer temperature did not affect specific impulse values significantly.

Regardless, one would presume that the real case would have other effects acting on stoichiometric length; for example, the injection gas temperature in practice being lower, versus the conservative reduction in the model used. Lower gas temperatures downstream in a real case would take away from the temperature difference required to drive the transpiration process, and this would in effect lower  $I_{sp}$  more significantly.

There is also the higher operating oxidizer-fuel mixture ratio,  $r(x)$ , at a given position within the fuel port, of which is due to the fact that there is more oxidizer than required throughout the length of all HREs in this thesis (i.e. going from  $1.3r_{st}$  to  $3.1r_{st}$  in the IAC HRE, a gap widened to  $3.15r_{st}$  for the largest HRE). This reduces the effect of a lower fuel burning rate, at higher engines sizes, on internal ballistic performance. The HREs are being run at  $r = \frac{m_o}{m_f} \geq r_{st} = 6.5$ .

## 5. Conclusion

### 5.1 Concluding Remarks and Recommendations for Future Work

The results presented within this thesis have shown results that to some degree concur with observed trends (especially with respect to  $F \sim f(A_t)$ ); however, the results are only for one rocket engine. The main conclusion of this thesis is that the drop-off in performance, in going up in size, was not as much as expected.  $I_{sp}$  values remained relatively constant as the HREs were increased in size, however the regression rates of the fuels fell dramatically. Idealized higher temperature for oxidizer injection, and a higher mixture ratio influence, likely contributed to this lack of a more significant drop off. However, the HRE geometric sizing methodology used in this thesis did agree with one publication [28].

Future work should perhaps go towards extending this study into exploring what occurs in a different HRE altogether. It would do well to also explore how different fuel and oxidizer combinations behave as they are scaled up. The fuel used in this paper, HTPB, has been shown to more favourably work in a multiport setting for larger engines as it has a characteristically low regression rate. Another fuel configuration that has been of some interest, paraffin with aluminum particles and liquid oxygen as the oxidizer, could be something to consider in the future as well. This fuel and oxidizer combination has been proven to give much larger regression rates while still using a traditional single cylindrical port [9,14], which is more efficient versus using multiple ports.

Then there is the actual size of the HRE itself. Although the largest HRE in this paper grew to a diameter of 1.24 meters, of which one could argue puts one in the area of larger sounding rockets, it would still not be large enough for orbital applications. At this size for the HRE in this thesis however, the predicted data for burn time and regression rate likely became more illustrative, rather than realistic, due to limitations of this idealized 1D model (QSHYB). More realistic 3D CFD simulations would certainly be helpful in moving to the study of larger HREs, where performance drop-offs are expected to be more significant (i.e. lower  $I_{sp}$ , lower  $I_{tot}$ ).

## Appendices

### Appendix A: Performance Results for all Scales up to Propellant Burn-Out IAC HRE Full Firing Charts

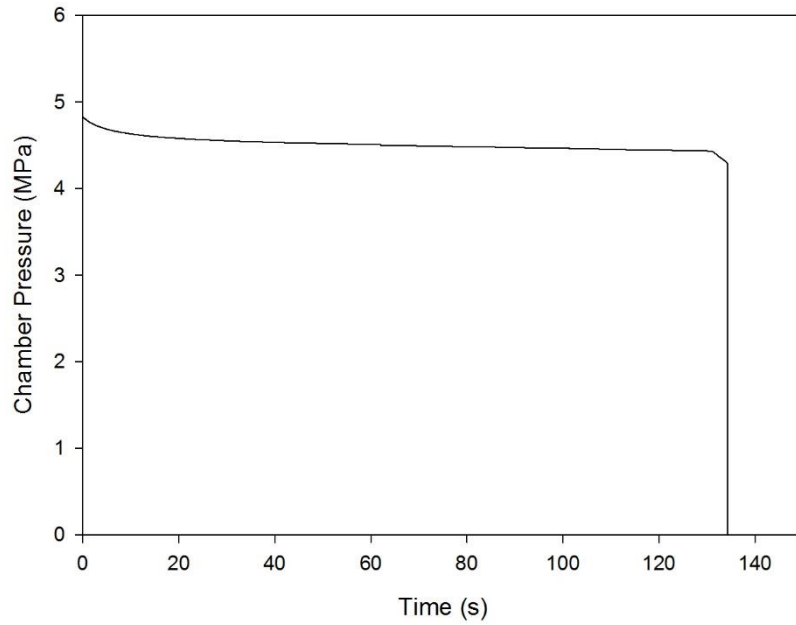


Figure 43: Chamber Pressure vs. Time for IAC HRE Up to Burn-Out

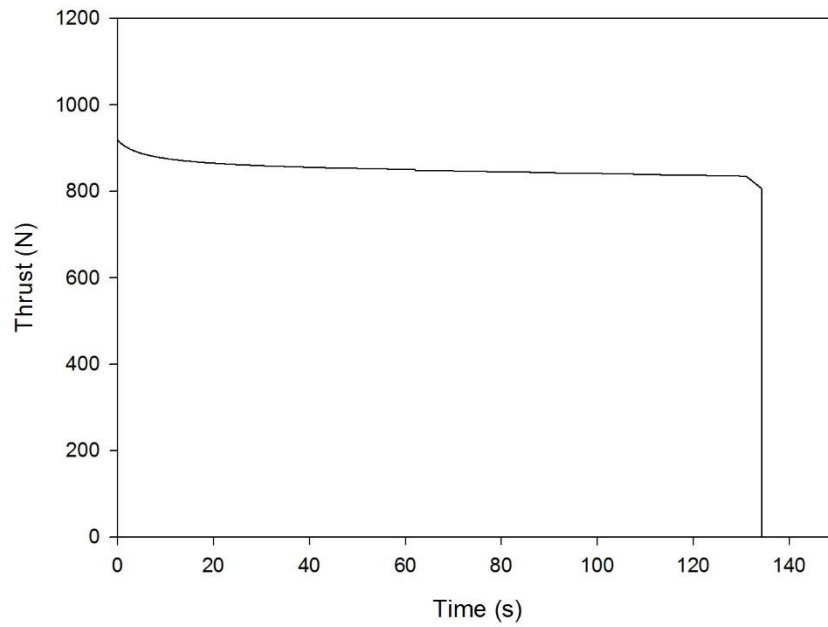


Figure 44: Thrust (Sea Level) vs. Time for IAC HRE Up to Burn-Out

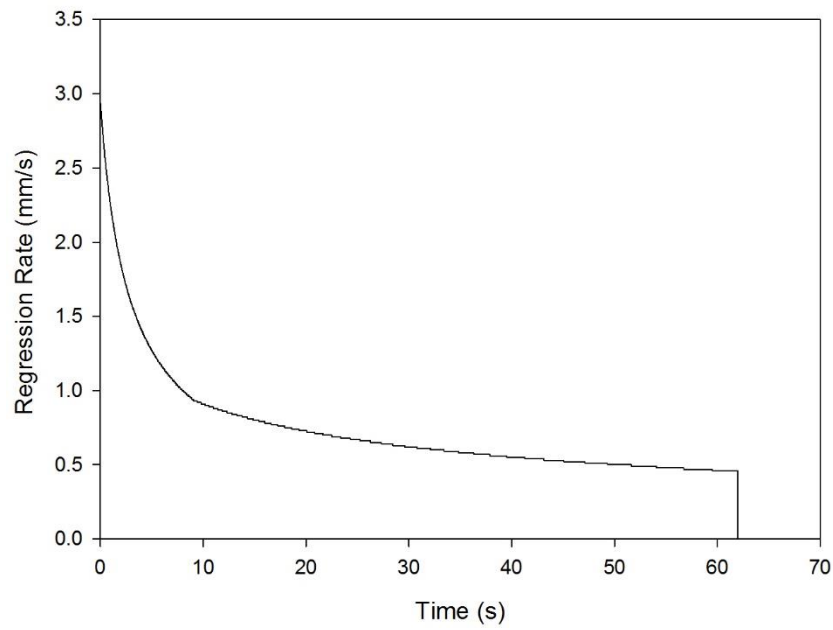


Figure 45: Regression Rate vs. Time, at the Head-End Fuel Port, for IAC HRE Up to Burn-Out

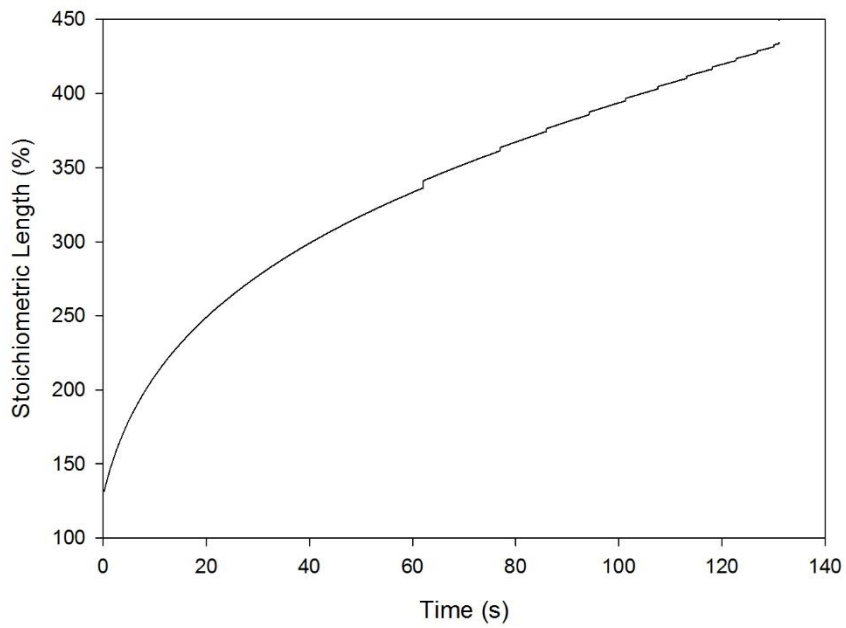


Figure 46: Stoichiometric Length vs. Time for IAC HRE Up to Burn-Out

## 125% HRE Scale Up Full Firing Charts

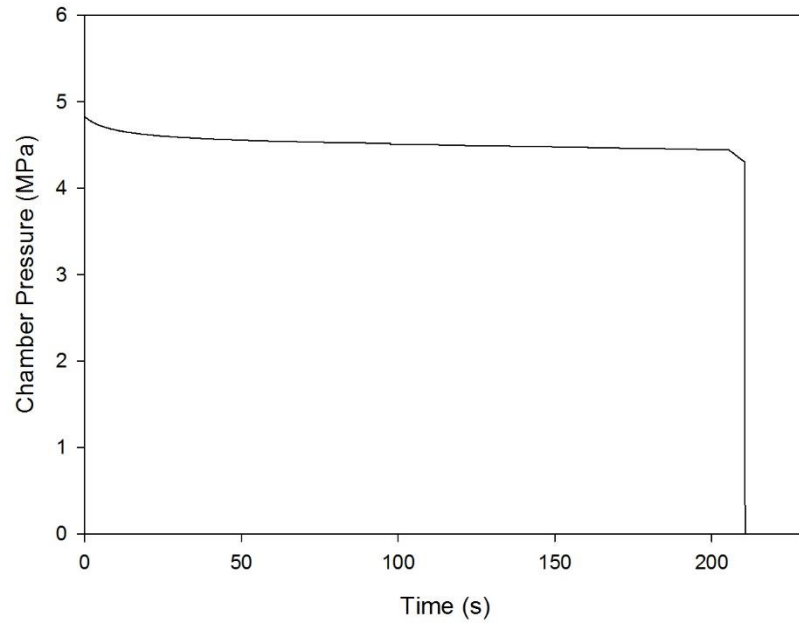


Figure 47: Chamber Pressure vs. Time for 125% Scale Up HRE Up to Burn-Out

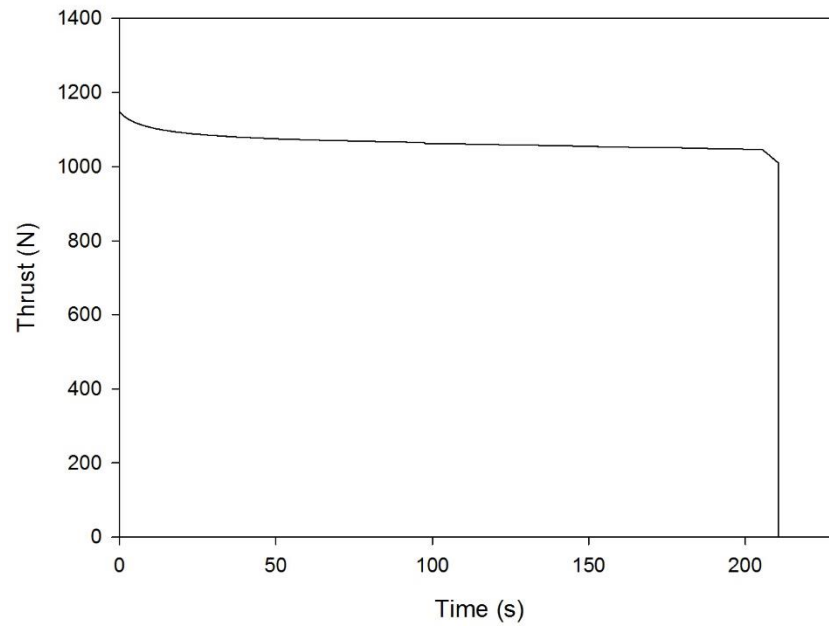


Figure 48: Thrust (Sea Level) vs. Time for 125% Scale Up HRE Up to Burn-Out

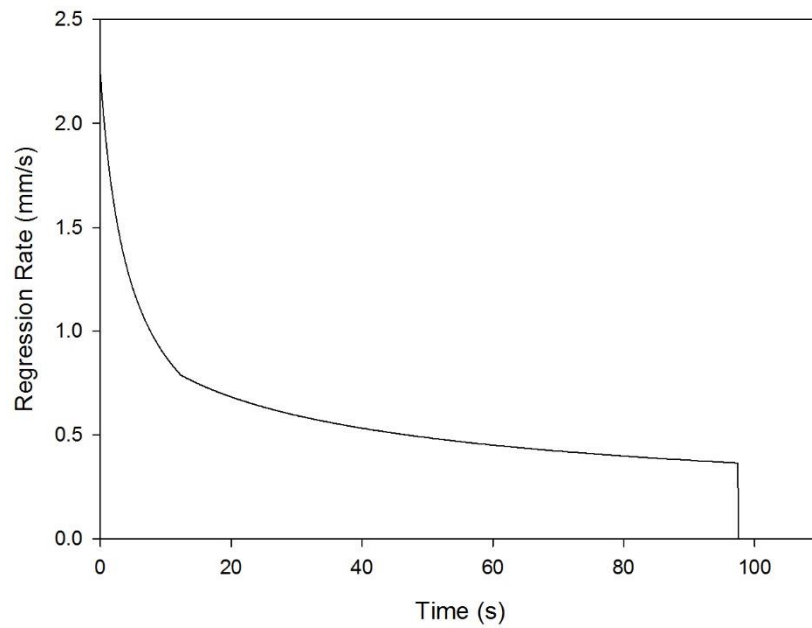


Figure 49: Regression Rate vs. Time, at the Head-End Fuel Port, for 125% Scale Up HRE Up to Burn-Out

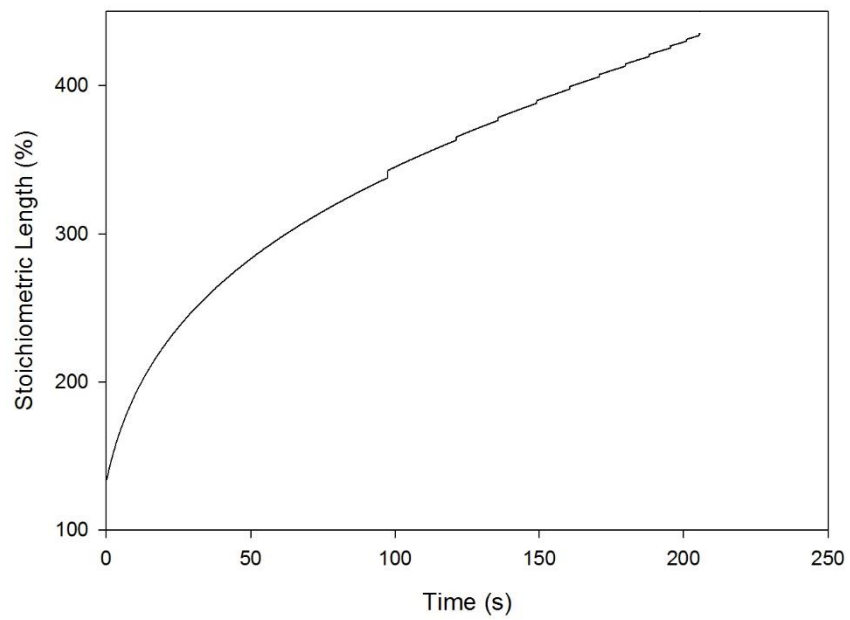


Figure 50: Stoichiometric Length vs. Time for 125% Scale Up HRE Up to Burn-Out

## 150% HRE Scale Up Full Firing Charts

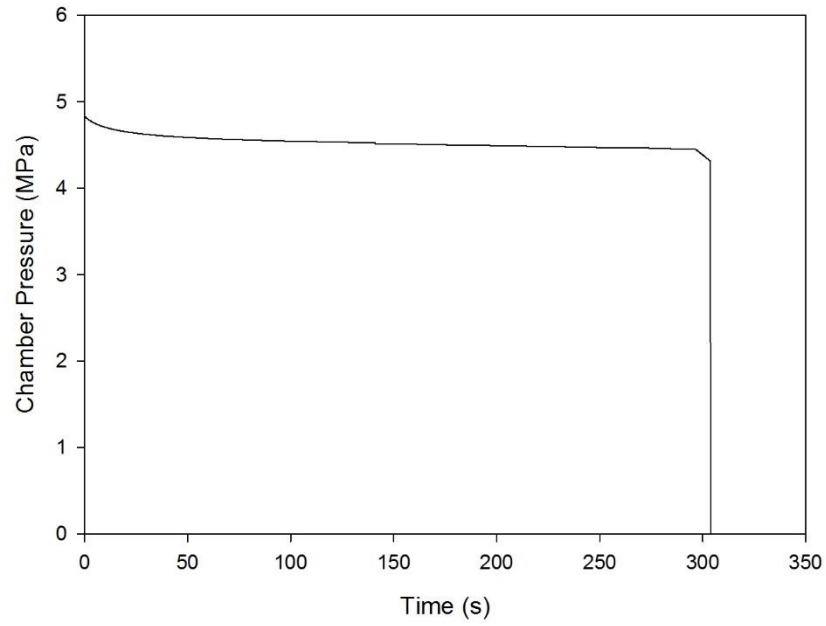


Figure 51: Chamber Pressure vs. Time for 150% Scale Up HRE Up to Burn-Out

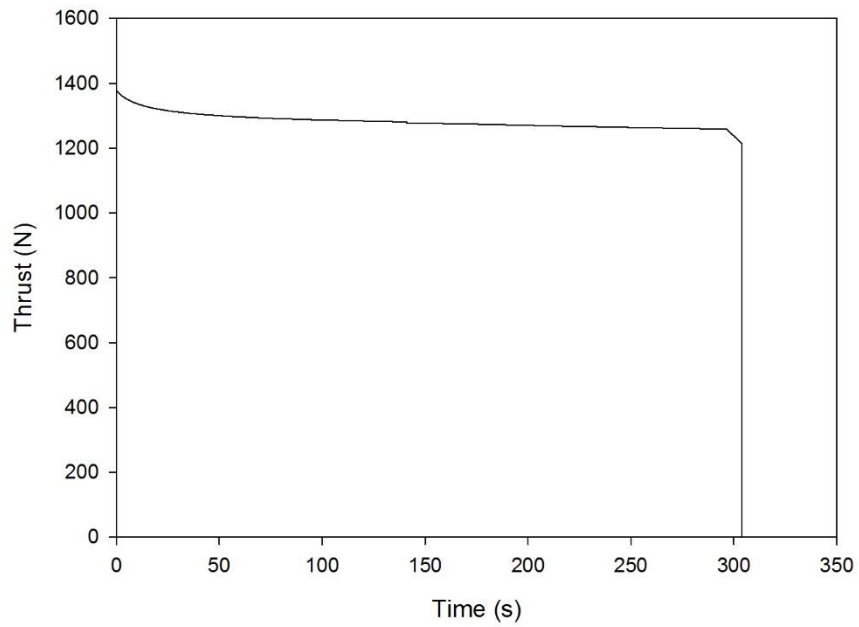


Figure 52: Thrust (Sea Level) vs. Time for 150% Scale Up HRE Up to Burn-Out

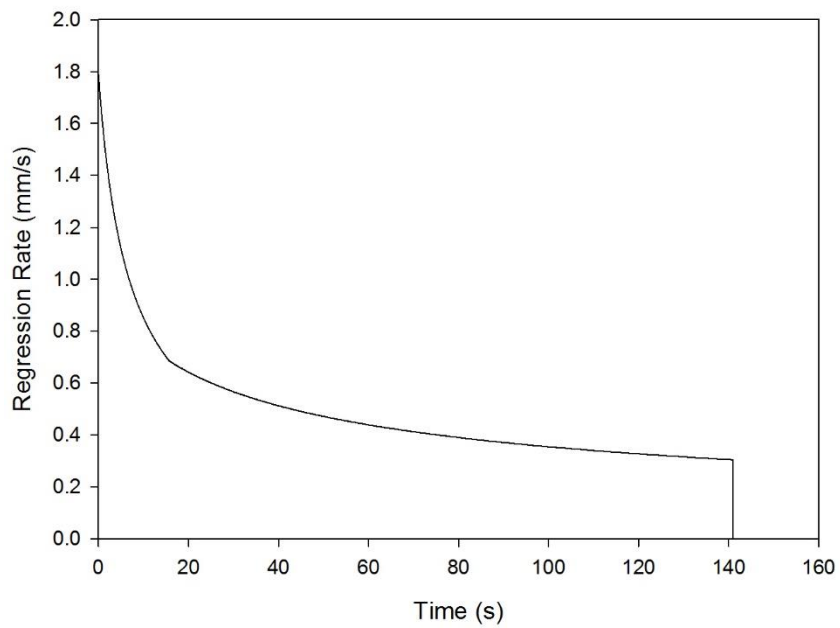


Figure 53: Regression Rate vs. Time, at the Head-End Fuel Port, for 150% Scale Up HRE Up to Burn-Out

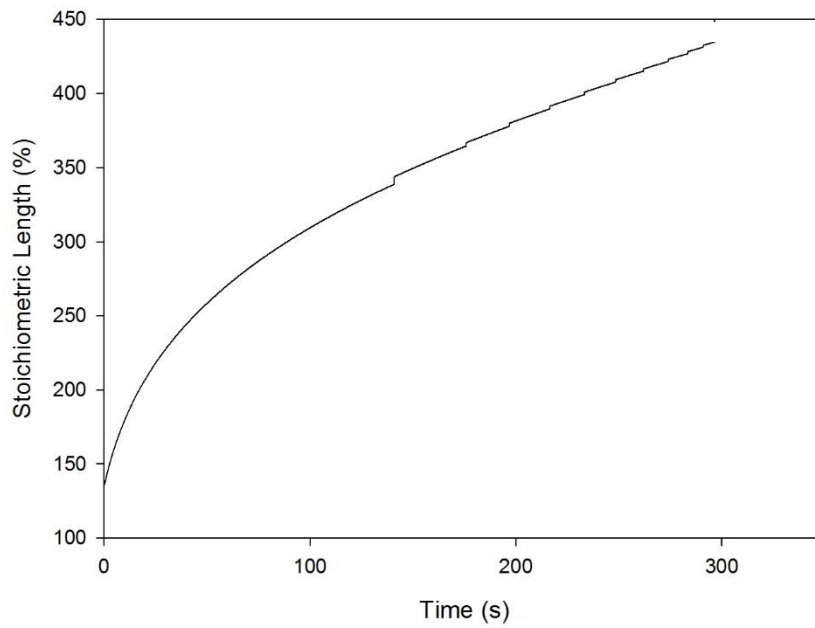


Figure 54: Stoichiometric Length vs. Time for 150% Scale Up HRE Up to Burn-Out

## 200% HRE Scale Up Full Firing Charts

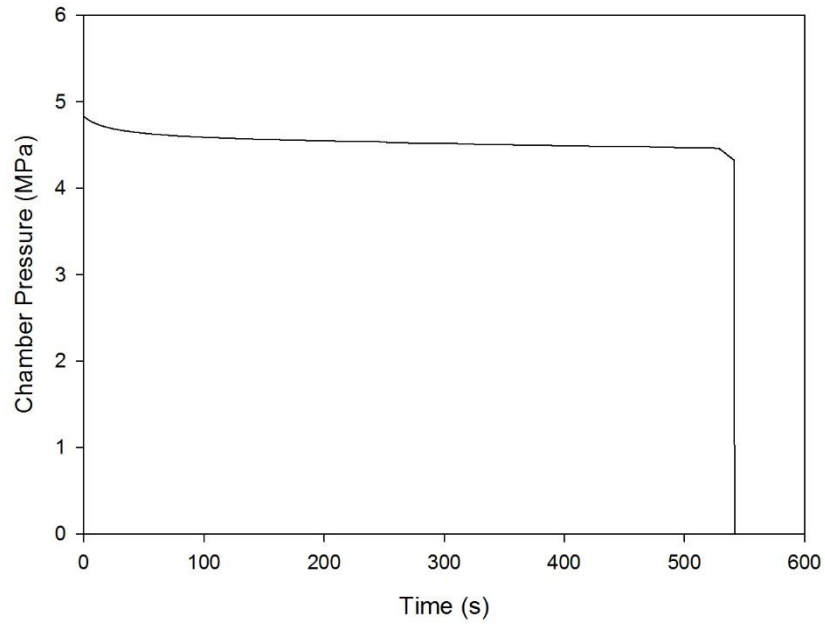


Figure 55: Chamber Pressure vs. Time for 200% Scale Up HRE Up to Burn-Out

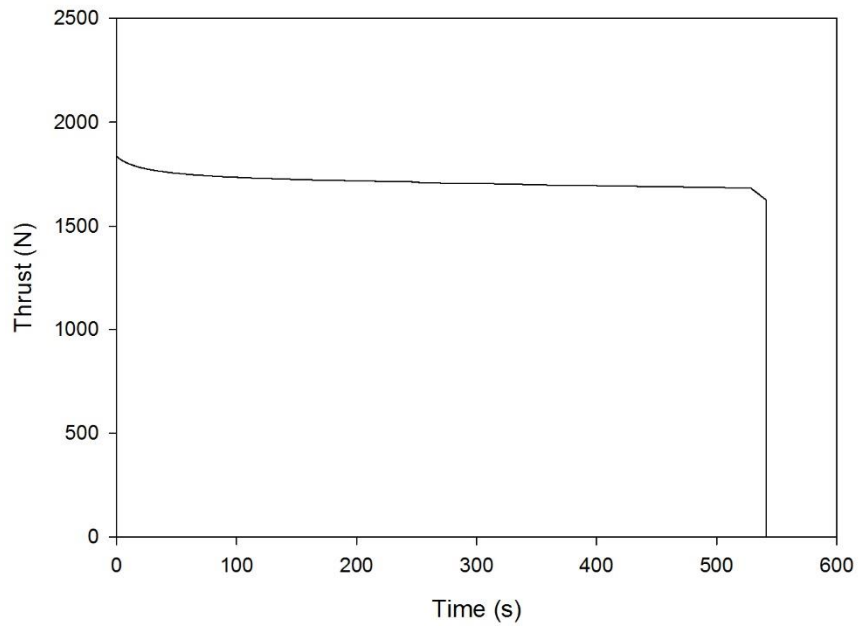


Figure 56: Thrust (Sea Level) vs. Time for 200% Scale Up HRE Up to Burn-Out

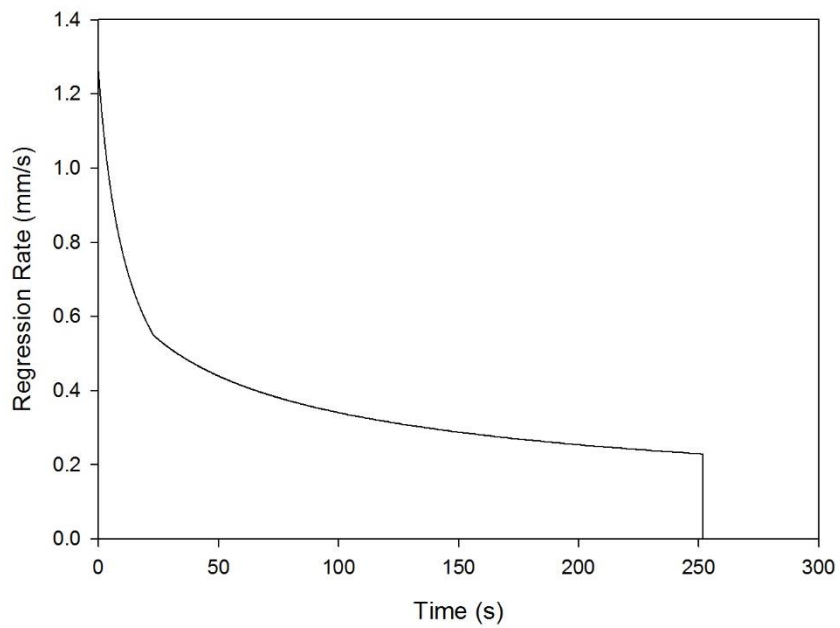


Figure 57: Regression Rate vs. Time, at the Head-End Fuel Port, for 200% Scale Up HRE Up to Burn-Out

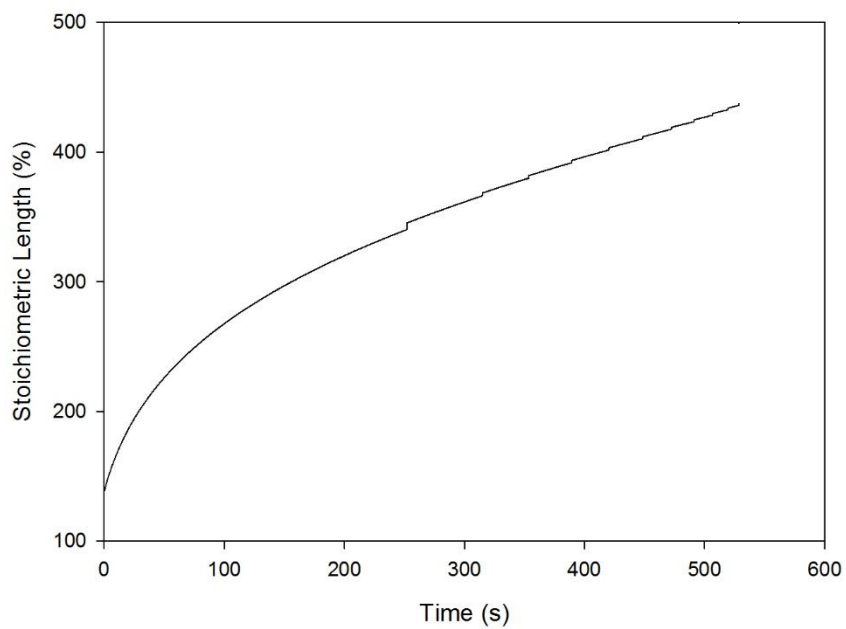


Figure 58: Stoichiometric Length vs. Time for 200% Scale Up HRE Up to Burn-Out

## 400% HRE Scale Up Full Firing Charts

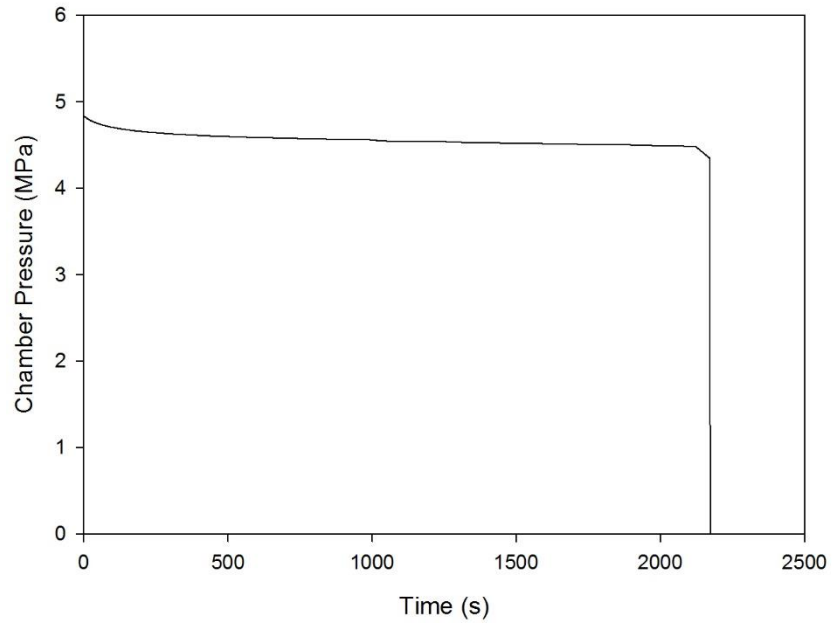


Figure 59: Chamber Pressure vs. Time for 400% Scale Up HRE Up to Burn-Out

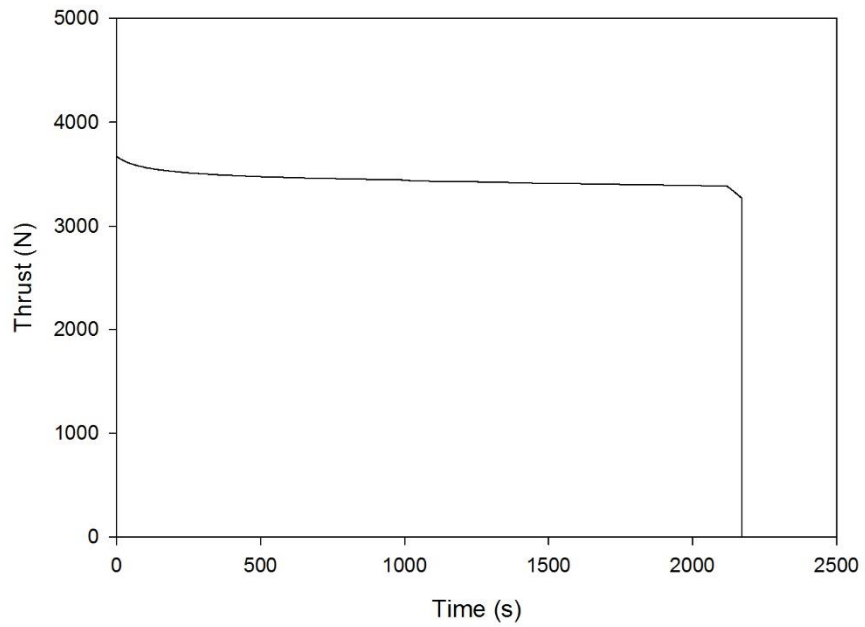


Figure 60: Thrust (Sea Level) vs. Time for 400% Scale Up HRE Up to Burn-Out

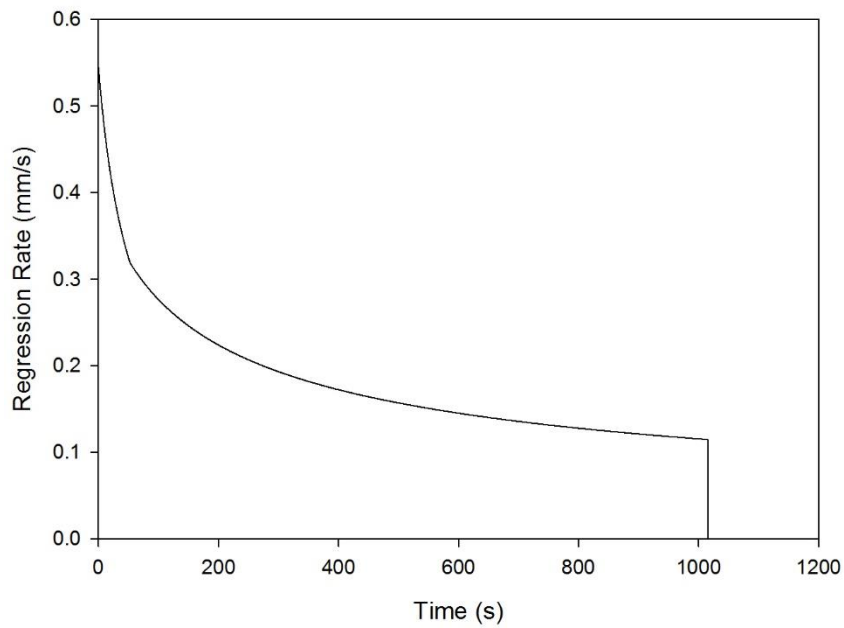


Figure 61: Regression Rate vs. Time, at the Head-End Fuel Port, for 400% Scale Up HRE Up to Burn-Out

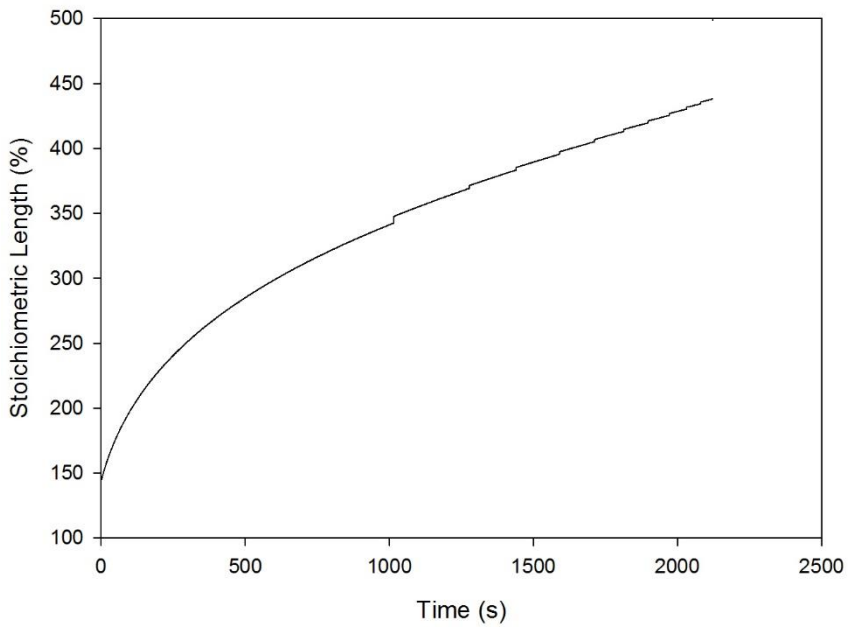


Figure 62: Stoichiometric Length vs. Time for 400% Scale Up HRE Up to Burn-Out

## 600% HRE Scale Up Full Firing Charts

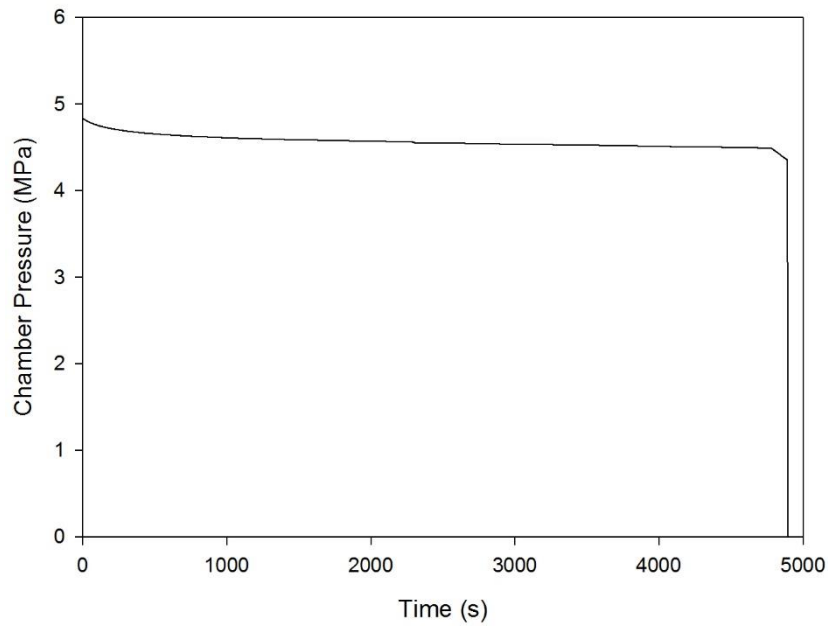


Figure 63: Chamber Pressure vs. Time for 600% Scale Up HRE Up to Burn-Out

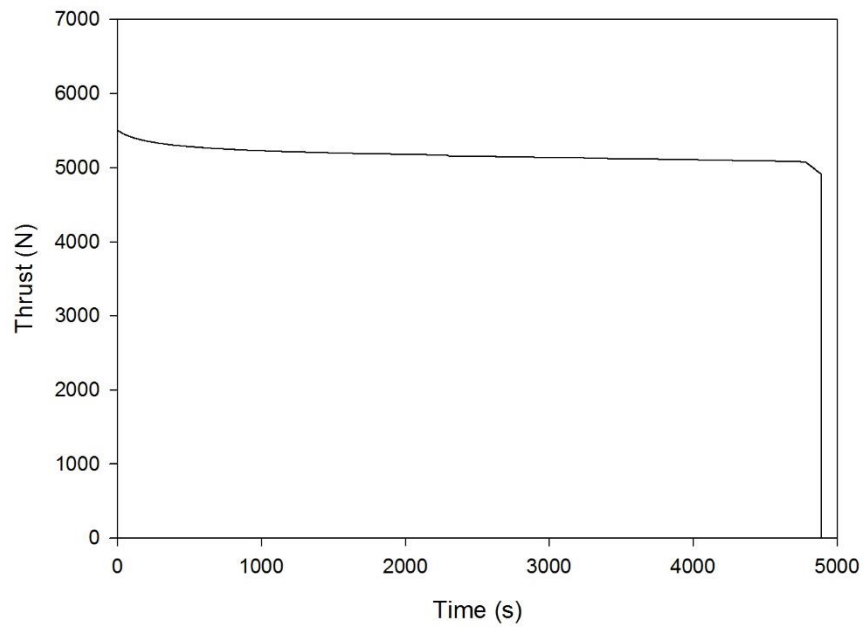


Figure 64: Thrust (Sea Level) vs. Time for 600% Scale Up HRE Up to Burn-Out

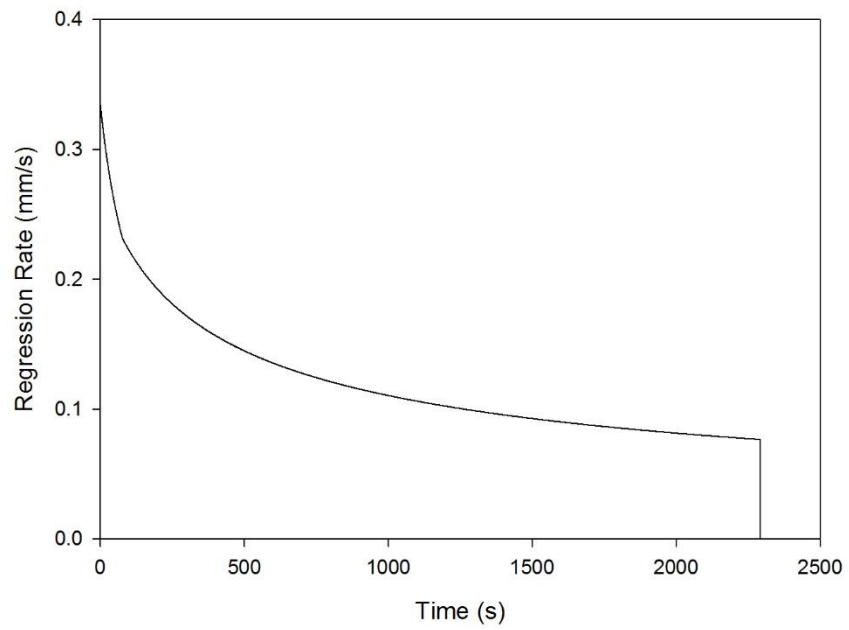


Figure 65: Regression Rate vs. Time, at the Head-End Fuel Port, for 600% Scale Up HRE Up to Burn-Out

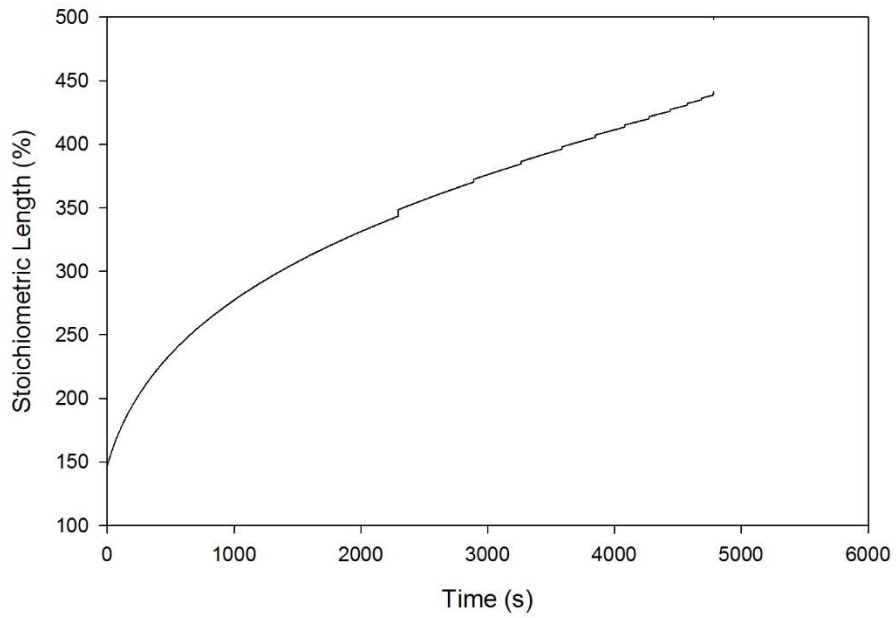


Figure 66: Stoichiometric Length vs. Time for 600% Scale Up HRE Up to Burn-Out

800% HRE Scale Up Full Firing Charts

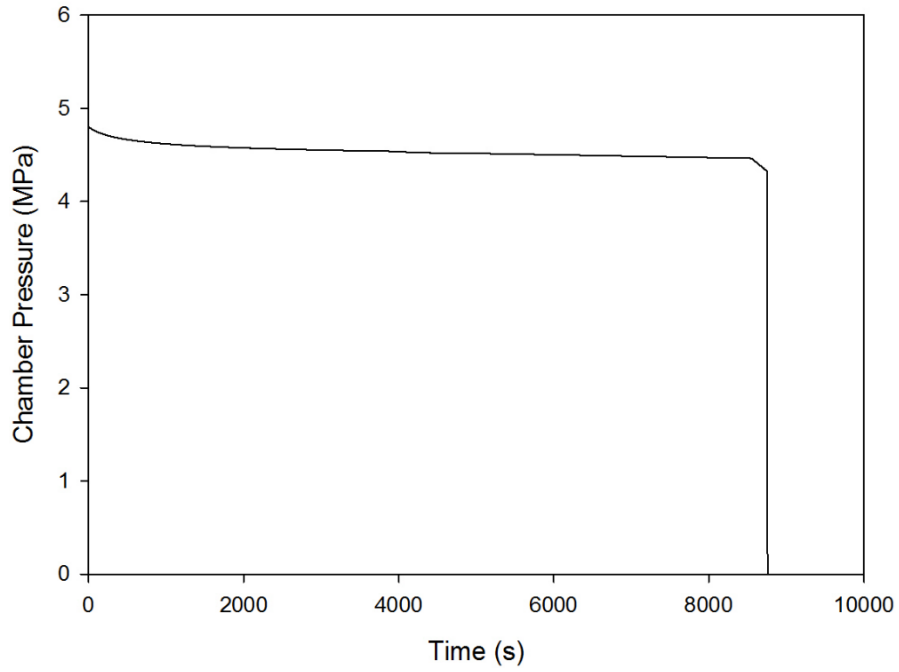


Figure 67: Chamber Pressure vs. Time for 800% Scale Up HRE Up to Burn-Out

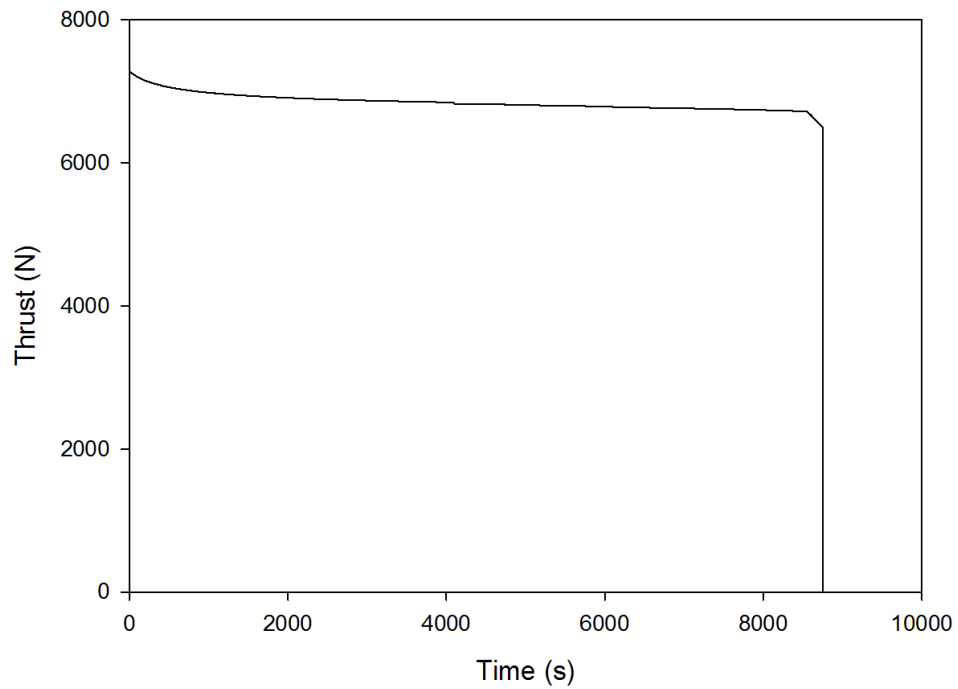


Figure 68: Thrust (Sea Level) vs. Time for 800% Scale Up HRE Up to Burn-Out

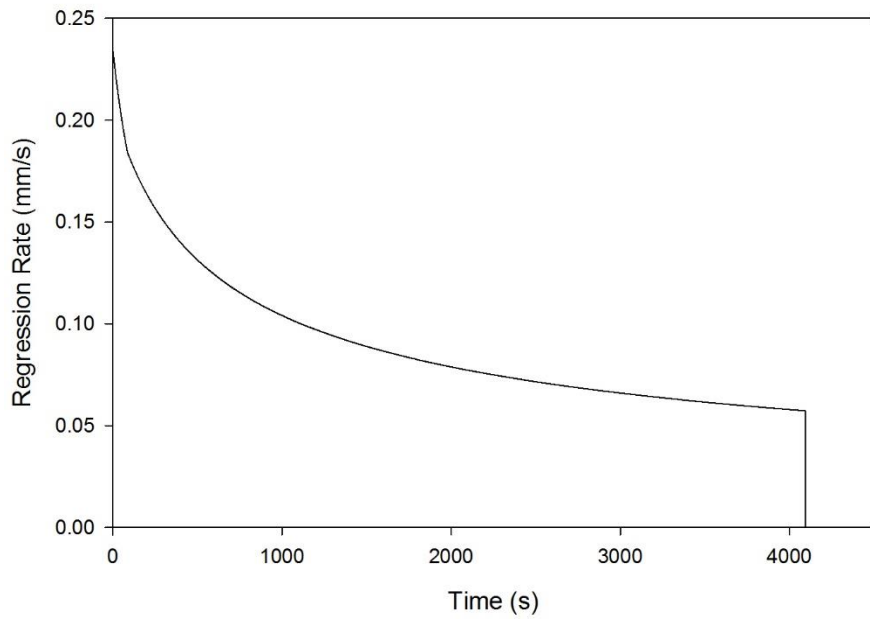


Figure 69: Regression Rate vs. Time, at the Head-End Fuel Port, for 800% Scale Up HRE Up to Burn-Out

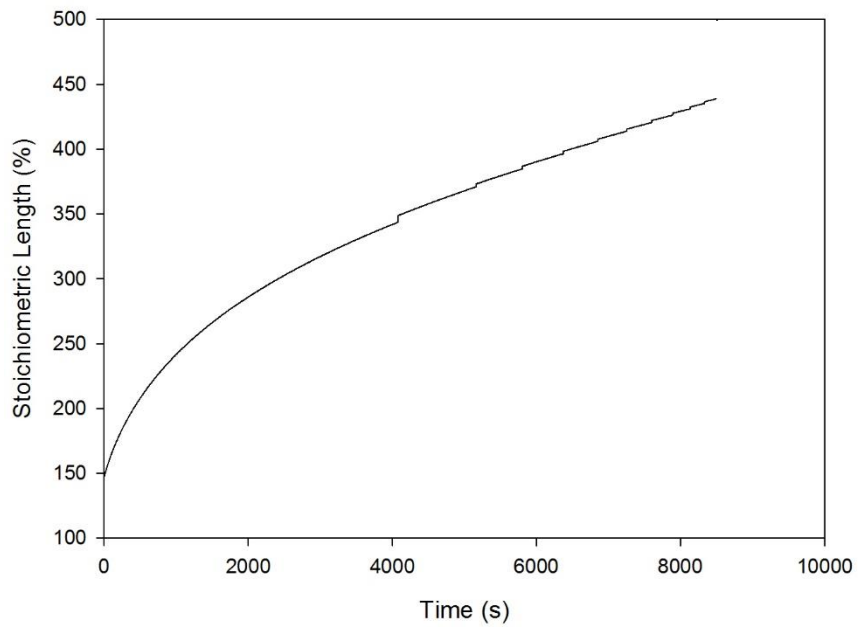


Figure 70: Stoichiometric Length vs. Time for 800% Scale Up HRE Up to Burn-Out

## 1000% HRE Scale Up Full Firing Charts

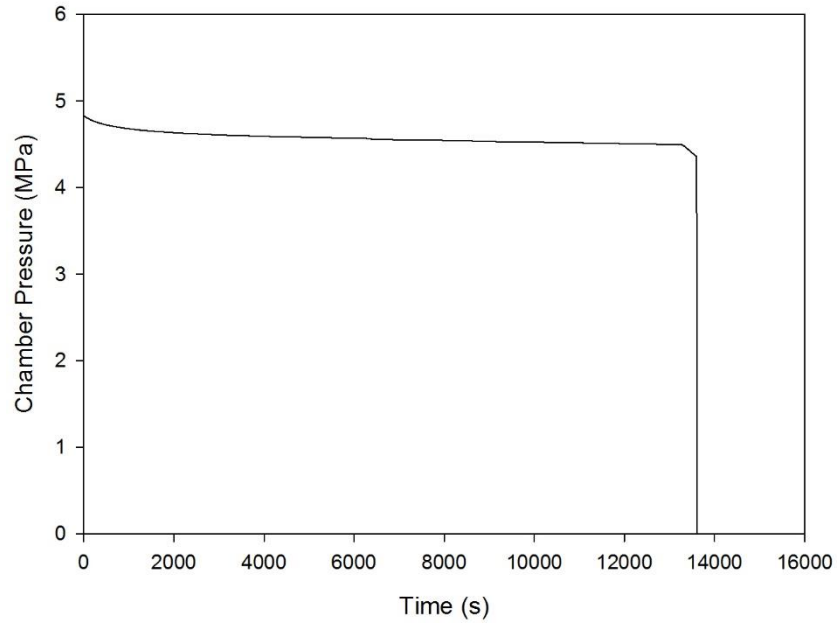


Figure 71: Chamber Pressure vs. Time for 1000% Scale Up HRE Up to Burn-Out

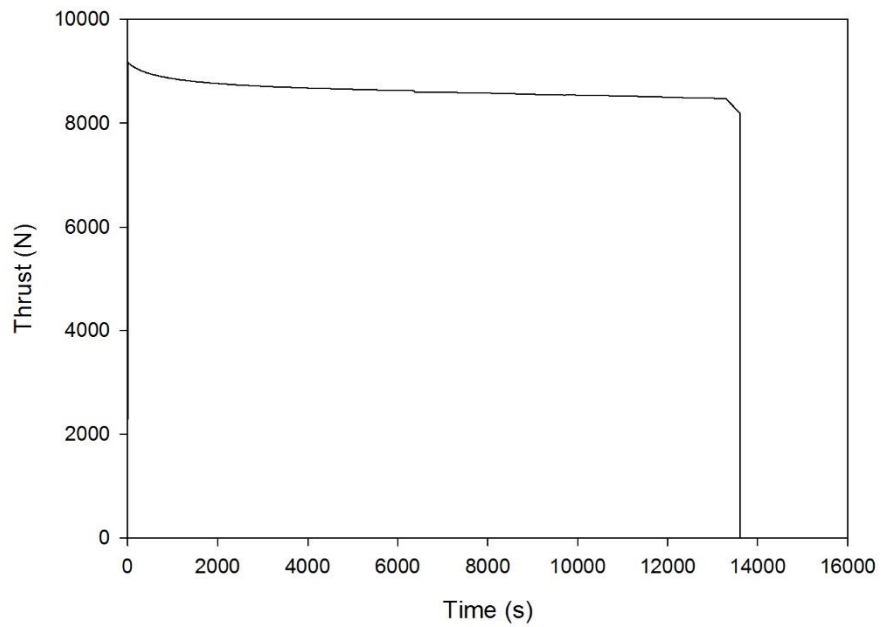


Figure 72: Thrust (Sea Level) vs. Time for 1000% Scale Up HRE Up to Burn-Out

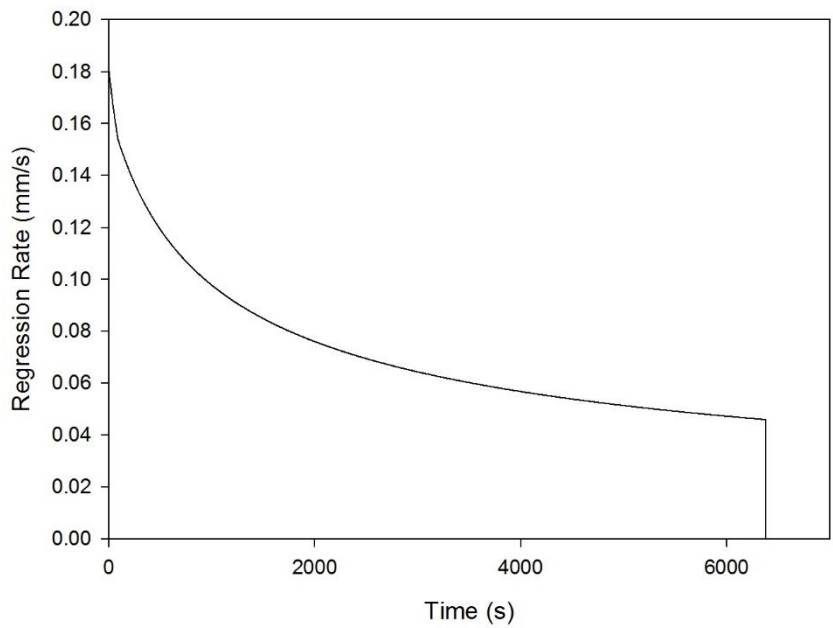


Figure 73: Regression Rate vs. Time, at the Head-End Fuel Port, for 1000% Scale Up HRE Up to Burn-Out

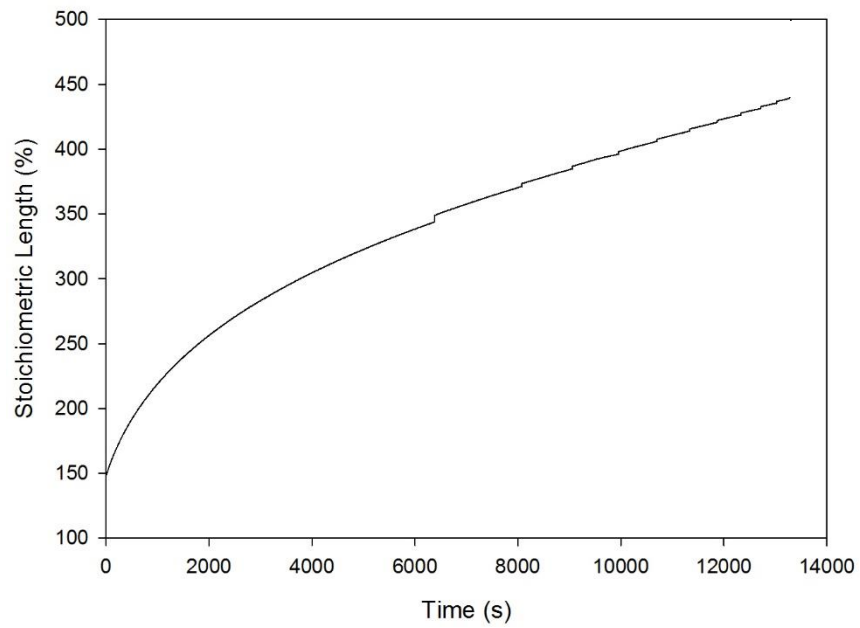


Figure 74: Stoichiometric Length vs. Time for 1000% Scale Up HRE Up to Burn-Out

## Appendix B: Nozzle Scaling Calculator (for Matlab R2015b)

```
format long
clear
clc
%nozzle throat diameter in meters
%dti = 0.01285; %IAC
dti=0.01285;

%Desired conv-div nozzle expansion ratio below (isentropic)
expansion_ratio = 10.0;

%Enter scale factor below (50% is 1.5, 100% is 2, etc)
%SF= 1.25; %base
%SF = 2; % 200% size up
%SF = 4; % 400% size up
%SF = 6; % 600% size up
%SF = 8; % 800% size up
SF = 10; % 10 times size up (big ol' rocket)
%% Get A throat base and A throat scaled
A_t_base = (pi*(dti^2))/4;
A_t_scaled = (A_t_base)*(SF)

%% Get A exit scaled
A_e_scaled = (expansion_ratio)*(A_t_scaled);

%% Get scaled nozzle throat and exit diameters

d_t_scaled = sqrt ((4*A_t_scaled)/pi)

d_e_scaled = sqrt ((4*A_e_scaled)/pi)
```

## References

- [1] Jens, E. T., Cantwell, B. J., and Hubbard, G. S., "Hybrid Rocket Propulsion Systems for Outer Planet Exploration Missions," *Acta Astronautica*, Vol. 128 (2016), November-December 2016, pp. 119–130.
- [2] Davydenko, N., Gollender, R., Gubertov, A., Mironov, V., and Volkov, N., "Hybrid Rocket Engines: The Benefits and Prospects," *Aerospace Science and Technology*, Vol. 11 (2007), December 2006, pp. 55–60.
- [3] Cantwell, B., Karabeyoglu, A., and Altman, D., "Recent Advances In Hybrid Propulsion," *International Journal of Energetic Materials and Chemical Propulsion*, Vol. 9, Issue 4, 2010, pp. 305–326.
- [4] Barato, F., Bellomo, N., and Pavarin, D., "Integrated Approach for Hybrid Rocket Technology Development," *Acta Astronautica*, Vol. 128, November-December 2016, Padova, pp. 257–261.
- [5] Lazzarin, M., Faenza, M., Barato, F., Bellomo, N., Bettella, A., and Pavarin, D., "Computational Fluid Dynamics Simulation of Hybrid Rockets of Different Scales," *Journal of Propulsion and Power*, Vol. 31, No. 5, September-October 2015, Padova, pp. 1458–1469.
- [6] Chiaverini, M.J., Serin, N., Johnson, D., Lu, Y.C., Kuo, K.K. and Risha, G.A., "Regression Rate Behavior of Hybrid Rocket Solid Fuels," *Journal of Propulsion & Power*, Vol. 16, No. 1, January-February, 2000, pp. 125-132.
- [7] Chiaverini, M.J., "Review of Solid-Fuel Regression Rate Behavior in Classical and Nonclassical Hybrid Rocket Motors," Ch. 2 in *Fundamentals of Hybrid Rocket Combustion and Propulsion*, edited by Chiaverini, M.J. and Kuo, K.K., Vol. 218, Progress in Astronautics & Aeronautics series, AIAA Publications, Reston, VA, 2007, pp. 37-125.
- [8] Karabeyoglu, A., Zilliac, G., Cantwell, B. J., Dezilwa, S., and Castellucci, P., "Scale-Up Tests of High Regression Rate Paraffin-Based Hybrid Rocket Fuels," *Journal of Propulsion and Power*, vol. 20, No. 6, November-December 2004, pp. 1037–1045.
- [9] Karabeyoglu, A., Zilliac, G., Cantwell, B., Zilwa, S. D., and Castellucci, P., "Scale-up Tests of High Regression Rate Liquefying Hybrid Rocket Fuels," *41<sup>st</sup> Aerospace Sciences Meeting and Exhibit*, AIAA Paper No. 2003-1162, Nevada, January 6-9 2003, pp. 1–19.
- [10] Karabeyoglu, M. A., Altman, D., and Cantwell, B. J., "Combustion of Liquefying Hybrid Propellants: Part 1, General Theory," *Journal of Propulsion and Power*, Vol. 18, No. 3, California, May-June, 2002, pp. 610–620.
- [11] Greatrix, D.R., "Regression Rate Estimation for Standard-Flow Hybrid Rocket Engines," *Aerospace Science & Technology*, Vol. 13, No. 7, October-November 2009, pp. 358-363.

- [12] Greatrix, D.R., "Model for Predicting Fuel Regression Rate in Hybrid Rocket Engines", *43<sup>rd</sup> AIAA/ASME/SAE/ASEE Joint Propulsion Conference & Exhibit*, AIAA Paper No. 2007-5346, Ohio, July 8-11, 2007.
- [13] Sutton, G. P., and Biblarz, O., *Rocket Propulsion Elements*, 8<sup>th</sup> Edition, New York: Wiley, 2010.
- [14] Daisuke, S., Yuasa, S., Hirata, K., Sakurai, T. and Shiraishi, N., "Combustion Characteristics of Paraffin-Fueled Swirling Oxidizer-Flow-Type Hybrid Rocket Engines," *48<sup>th</sup> AIAA/ASME/SAE/ASEE Joint Propulsion Conference*, AIAA Paper No. 2012-3904, Atlanta, July 30 – Aug. 1, 2012.
- [15] Bockelt, M.W. and Greatrix, D.R., "Application of Swirl and Spin for In-Flight Thrust Modulation of Hybrid Rocket Engines," *6<sup>th</sup> European Conference for Aeronautics and Space Sciences (EUCASS)*, Krakow, June 29 – July 3, 2015.
- [16] Greatrix, D.R., *Powered Flight– The Engineering of Aerospace Propulsion*, Springer-Verlag London Limited, 2012, pp. 293-434.
- [17] Marxman, G. A., "Boundary-Layer Combustion in Propulsion," *Symposium (International) on Combustion*, vol. 11, Issue 1, January 1967, pp. 269–289.
- [18] Marxman, G. A., "Combustion in the Turbulent Boundary Layer on a Vaporizing Surface," *Tenth Symposium (International) on Combustion*, vol. 10, Issue 1, January 1965, pp. 1337–1349.
- [19] Marxman, G., and Gilbert, M., "Turbulent Boundary Layer Combustion in the Hybrid Rocket," *Symposium (International) on Combustion*, Vol. 9, Issue 1, Jan. 1963, pp. 371–383.
- [20] Marxman, G., Muzzy, R., and Wooldridge, C., "Fundamentals of Hybrid Boundary Layer Combustion," *AIAA Heterogeneous Combustion Conference*, Florida, December 11-13, 1963.
- [21] Muzzy, R., and Wooldridge, C., "Internal Ballistic Considerations in Hybrid Rocket Design," *AIAA 2<sup>nd</sup> Propulsion Joint Specialist Conference*, AIAA Paper No. 66-628, Colorado, June 13-17 1966, pp. 5–39.
- [22] Netzer, D. W., "Hybrid Rocket Internal Ballistics," *Chemical Propulsion Information Agency*, January 1972, pp. 6–20.
- [23] Estey, P., Altman, D., and Mcfarlane, J., "An Evaluation of Scaling Effects for Hybrid Rocket Motors," *AIAA/ASME/SAE 27<sup>th</sup> Joint Propulsion Conference*, AIAA Paper No. 91-2517, California, June 24-26, 1991.
- [24] Greatrix, D.R. and Gottlieb, J.J., "Erosive Burning Model for Composite-Propellant Rocket Motors with Large Length-to-Diameter Ratios," *Canadian Aeronautics and Space Journal* 33 (3) (Sept.1987) 133-142.

[25] Mickley H.S., Ross R.C., Squyer A.L. and Stewart W.F., "Heat, Mass, and Momentum Transfer for Flow Over a Flat Plate with Blowing or Suction," *NACA*, TN3208, July, 1954.

[26] Moffat RJ, Kays WM, "The Turbulent Boundary Layer on a Porous Plate: Experimental Heat Transfer with Uniform Blowing and Suction," *International Journal of Heat and Mass Transfer*, Vol. 10, Issue 10, October, 1968, California, pp. 1547–1566.

[27] Greatrix DR, Gottlieb JJ, Constantinou T (1987), "Quasi-Steady Analysis of the Internal Ballistics of Solid-Propellant Rocket Motors". *Can Aeronaut Space J* 33:61–70

[28] Gany, A., "Scale Effects in Hybrid Motors Under Similarity Conditions," *AIAA/ASME/SAE/ASEE 32<sup>nd</sup> Joint Propulsion Conference and Exhibit*, AIAA Paper No. 96-2846, Florida, July 1-3, 1996.